

2003

# Phosphoproteomic studies of smooth muscle contraction: investigation of differential phosphorylation in relaxed/contracted rat aortic smooth muscle tissue using MALDI-TOF MS

Tonya M. Pekar

Follow this and additional works at: <http://mds.marshall.edu/etd>

 Part of the [Amino Acids, Peptides, and Proteins Commons](#), [Biochemistry, Biophysics, and Structural Biology Commons](#), [Other Chemistry Commons](#), and the [Other Life Sciences Commons](#)

---

## Recommended Citation

Pekar, Tonya M., "Phosphoproteomic studies of smooth muscle contraction: investigation of differential phosphorylation in relaxed/contracted rat aortic smooth muscle tissue using MALDI-TOF MS" (2003). *Theses, Dissertations and Capstones*. Paper 781.

**PHOSPHOPROTEOMIC STUDIES OF SMOOTH MUSCLE  
CONTRACTION**

Investigation of Differential Phosphorylation in  
Relaxed/Contracted Rat Aortic Smooth Muscle Tissue  
using MALDI-TOF MS

**Thesis submitted to  
The Graduate College of  
Marshall University**

**In partial fulfillment of the  
Requirements for the degree of  
Master of Science  
Chemistry**

**by**

**Tonya M. Pekar**

**Dr. William Price, Committee Chairperson  
Dr. Leslie Frost  
Dr. Seth Bush**

**Marshall University**

**Huntington, WV**

**December, 2003**

## **DEDICATION**

I would like to dedicate this thesis to all the hard-working students at Marshall University who I have come to know, respect, and love. I wish the best for them all, and will not forget the challenges that were overcome in their aid.

## **ACKNOWLEDGEMENTS**

I would like to thank Dr. William Price, my research advisor, Dr. Leslie Frost, Dr. Seth Bush, and Bin Schmitz for their great assistance and guidance in this and other endeavors. I would also like to thank Dr. Gary Wright and Dr. William McCumbee for their guidance and assistance at MUSOM. Finally, I would like to thank my parents for their support, and more importantly, their faith in me, which far surpassed the faith I had in myself.

## TABLE OF CONTENTS

<b>ABSTRACT</b> .....	<b>x</b>
<b>DEDICATION</b> .....	<b>ii</b>
<b>TABLE OF CONTENTS</b> .....	<b>iv</b>
<b>LIST OF FIGURES</b> .....	<b>vii</b>
<b>LIST OF TABLES</b> .....	<b>vi</b>
<b>ABBREVIATIONS/ACRONYMS</b> .....	<b>xi</b>
<b>INTRODUCTION</b> .....	<b>1</b>
SMOOTH MUSCLE .....	1
SMOOTH VS. SKELETAL: SIMILARITIES .....	2
<i>Composition</i> .....	2
<i>Regulation of Contraction</i> .....	2
<i>Mechanism of Contraction</i> .....	3
SMOOTH VS. SKELETAL: DIFFERENCES .....	4
<i>Ultrastructure and Composition</i> .....	4
<i>Mechanism of Contraction</i> .....	5
<i>Regulation of Contraction</i> .....	6
<i>Mechanical Properties</i> .....	8
<i>SM Heterogeneity</i> .....	9
SMOOTH MUSCLE MECHANICS.....	9
SIGNAL TRANSDUCTION PATHWAYS.....	10
<i>Ca<sup>2+</sup> Influx</i> .....	10
<i>Calcium Sensitization/Desensitization</i> .....	12
<i>IP<sub>3</sub>/DAG Signaling</i> .....	17
<i>cAMP/cGMP Signaling</i> .....	19
<i>RhoA/Rho Kinase Signaling</i> .....	21
<i>MAPK Signaling</i> .....	24
<i>Other Regulatory Proteins</i> .....	25
CAVEOLAE .....	25
STUDY OF SM .....	26
PROTEOMICS .....	27
PHOSPHOPROTEOMICS.....	28
<b>MATERIALS</b> .....	<b>34</b>
MATERIALS.....	34
REAGENTS.....	34
INSTRUMENTATION.....	37
BUFFERS AND SOLUTIONS.....	39

<b>METHODS .....</b>	<b>45</b>
<b>SAMPLE PREPARATION.....</b>	<b>45</b>
<i>Dissection/Tissue Extraction.....</i>	<i>45</i>
<i>Radioactive Phosphorous Labeling.....</i>	<i>45</i>
<i>Phorbol Incubation.....</i>	<i>45</i>
<i>Cell Lysis.....</i>	<i>46</i>
<i>Solubilization of Membrane Proteins.....</i>	<i>46</i>
<b>SAMPLE PURIFICATION.....</b>	<b>47</b>
<i>Acetone Precipitation.....</i>	<i>47</i>
<i>Dialysis.....</i>	<i>47</i>
<b>SEPARATION/ISOLATION OF PROTEINS.....</b>	<b>47</b>
<i>1D SDS-PAGE.....</i>	<i>47</i>
<i>2D SDS-PAGE.....</i>	<i>48</i>
<b>ANALYSIS.....</b>	<b>50</b>
<i>Visualization of Protein Bands.....</i>	<i>50</i>
<i>Gel Imaging.....</i>	<i>51</i>
<i>Proteolytic Digest of Proteins (Tryptic Digest).....</i>	<i>51</i>
<i>Desalting.....</i>	<i>52</i>
<i>MALDI-TOF MS.....</i>	<i>53</i>
<i>Protein Database Searching (MASCOT).....</i>	<i>55</i>
<b>RESULTS AND DISCUSSION .....</b>	<b>57</b>
<b>2D GEL ELECTROPHORESIS.....</b>	<b>57</b>
<b>MALDI-TOF MS ANALYSIS.....</b>	<b>80</b>
<i>PSD Analysis.....</i>	<i>100</i>
<b>MASCOT SEARCH RESULTS.....</b>	<b>101</b>
<b>PHOSPHOPROTEOMIC ANALYSIS.....</b>	<b>105</b>
<b>CONCLUSIONS .....</b>	<b>110</b>
<b>APPENDIX I: Mass Spectrometry.....</b>	<b>112</b>
<b>APPENDIX II: MALDI-TOF MS and PSD.....</b>	<b>117</b>
<b>APPENDIX III: Proteomic Analysis.....</b>	<b>122</b>
<b>APPENDIX IV: Important Proteins in SM.....</b>	<b>123</b>
<b>APPENDIX V: Common Amino Acids.....</b>	<b>128</b>
<b>REFERENCES.....</b>	<b>131</b>

## LIST OF TABLES

<b>TABLE 1:</b> Agonists/Relaxants of SM Contraction .....	<b>7</b>
<b>TABLE 2:</b> MALDI-TOF Calibration Standards .....	<b>54</b>
<b>TABLE 3:</b> MASCOT Search Parameters .....	<b>55</b>
<b>TABLE 4:</b> 1D Gel MASCOT Search Results.....	<b>77</b>
<b>TABLE 5:</b> 2D Gel MASCOT Search Results.....	<b>86</b>
<b>TABLE 6:</b> Theoretical Autolytic Trypsin Peaks.....	<b>98</b>
<b>TABLE 7:</b> Experimental Autolytic Trypsin Peaks .....	<b>99</b>
<b>TABLE 8:</b> MASCOT Search Results--Band 1P .....	<b>102</b>
<b>TABLE 9:</b> Peak comparisons for Band 1P to Actinin Peaks .....	<b>103</b>
<b>TABLE 10:</b> Unmatched Peaks for Band 1P.....	<b>104</b>
<b>TABLE 11:</b> MALDI Matrices .....	<b>117</b>

## LIST OF FIGURES

<b>FIGURE 1:</b> Sliding Filament Model I .....	3
<b>FIGURE 2:</b> Sliding Filament Model II .....	4
<b>FIGURE 3:</b> Sarcomere .....	5
<b>FIGURE 4:</b> Crossed Filament Model .....	5
<b>FIGURE 5:</b> Thin Filament and Associated Proteins in Contraction.....	6
<b>FIGURE 6:</b> Legend for Signal Transduction Diagrams .....	10
<b>FIGURE 7:</b> Ca <sup>2+</sup> Flux.....	11
<b>FIGURE 8:</b> Contraction Pathways.....	14
<b>FIGURE 9:</b> Relaxation Pathways .....	16
<b>FIGURE 10:</b> IP <sub>3</sub> /DAG Signaling .....	17
<b>FIGURE 11:</b> Structure of IP <sub>3</sub> /DAG .....	18
<b>FIGURE 12:</b> Conversion of ATP to cAMP .....	19
<b>FIGURE 13:</b> cGMP .....	20
<b>FIGURE 14:</b> cAMP/cGMP Signaling.....	20
<b>FIGURE 15:</b> Rho Signaling .....	22
<b>FIGURE 16:</b> MAPK Signaling .....	24
<b>FIGURE 17:</b> Phosphorylation of Serine .....	28
<b>FIGURE 18:</b> Beta-Elimination.....	30
<b>FIGURE 19:</b> Michael Addition.....	31
<b>FIGURE 20:</b> Oxidation of Lysine-Like Residue.....	32
<b>FIGURE 21:</b> Phorbol Structure.....	33
<b>FIGURE 22:</b> 2D Gel 7_24_01_Phorbol_sup.....	58
<b>FIGURE 23:</b> 2D Gel 7_30_02_Control .....	58
<b>FIGURE 24:</b> 2D Gel 10_09_02_Control.....	59
<b>FIGURE 25:</b> 2D Gel 10_09_02_Phorbol .....	60
<b>FIGURE 26:</b> 2D Gel 10_09_02_Control_Pell.....	61
<b>FIGURE 27:</b> 2D Gel 10_09_02_Phorbol_Pell .....	62
<b>FIGURE 28:</b> 2D Gel 6_18_02_Control.....	62
<b>FIGURE 29:</b> 2D Gel 6_18_02_Phorbol .....	63
<b>FIGURE 30:</b> 2D Gel 7_12_02_Control.....	63
<b>FIGURE 31:</b> 2D Gel 7_12_02_Phorbol .....	64



<b>FIGURE 32:</b> 2D Gel 7_30_02_Phorbol .....	<b>65</b>
<b>FIGURE 33:</b> MALDI Spectrum of Band 8C.....	<b>67</b>
<b>FIGURE 34:</b> MALDI Spectrum of Band 4P .....	<b>67</b>
<b>FIGURE 35:</b> MALDI Spectrum of Band 5C.....	<b>68</b>
<b>FIGURE 36:</b> MALDI Spectrum of Band 2P .....	<b>68</b>
<b>FIGURE 37:</b> MALDI Spectrum of Band 2C.....	<b>69</b>
<b>FIGURE 38:</b> MALDI Spectrum of Band 3C.....	<b>69</b>
<b>FIGURE 39:</b> MALDI Spectrum of Band 1P .....	<b>70</b>
<b>FIGURE 40:</b> MALDI Spectrum of Band 2P .....	<b>70</b>
<b>FIGURE 41:</b> MALDI Spectrum of Band 18C.....	<b>71</b>
<b>FIGURE 42:</b> MALDI Spectrum of Band 24P .....	<b>71</b>
<b>FIGURE 43:</b> MALDI Spectrum of Band 15P .....	<b>72</b>
<b>FIGURE 44:</b> MALDI Spectrum of Band 7CP .....	<b>72</b>
<b>FIGURE 45:</b> MALDI Spectrum of Band 6CP .....	<b>73</b>
<b>FIGURE 46:</b> 2D Gel 7_12_01_Phorbol_pell .....	<b>74</b>
<b>FIGURE 47:</b> 1D Gel 6_13_02 .....	<b>75</b>
<b>FIGURE 48:</b> MALDI Spectrum of Band 1C.....	<b>76</b>
<b>FIGURE 49:</b> MALDI Spectrum of Band 2C.....	<b>76</b>
<b>FIGURE 50:</b> MALDI Spectrum of Band 2P .....	<b>77</b>
<b>FIGURE 51:</b> 2D Gel 9_26_03_Control.....	<b>78</b>
<b>FIGURE 52:</b> 2D Gel 9_26_03_Phorbol .....	<b>79</b>
<b>FIGURE 53:</b> MALDI Spectrum of Band 1C.....	<b>81</b>
<b>FIGURE 54:</b> MALDI Spectrum of Band 4C.....	<b>82</b>
<b>FIGURE 55:</b> MALDI Spectrum of Band 6C.....	<b>82</b>
<b>FIGURE 56:</b> MALDI Spectrum of Band 8C.....	<b>83</b>
<b>FIGURE 57:</b> MALDI Spectrum of Band 12P .....	<b>83</b>
<b>FIGURE 58:</b> MALDI Spectrum of Band 11C.....	<b>84</b>
<b>FIGURE 59:</b> MALDI Spectrum of Band 11P .....	<b>84</b>
<b>FIGURE 60:</b> MALDI Spectrum of Band 1C.....	<b>85</b>
<b>FIGURE 61:</b> MALDI Spectrum of Band 5P .....	<b>85</b>
<b>FIGURE 62:</b> MALDI Spectrum of Band 10P-1.....	<b>87</b>
<b>FIGURE 63:</b> MALDI Spectrum of Band 10P-2.....	<b>87</b>
<b>FIGURE 64:</b> MALDI Spectrum of Band 10P-3.....	<b>88</b>

<b>FIGURE 65:</b> MALDI Spectrum of Band 1P .....	<b>89</b>
<b>FIGURE 66:</b> MALDI Spectrum of Band 4P .....	<b>89</b>
<b>FIGURE 67:</b> MALDI Spectrum of Band 6P .....	<b>90</b>
<b>FIGURE 68:</b> MALDI Spectrum of Band 2P .....	<b>91</b>
<b>FIGURE 69:</b> MALDI Spectrum of Band 14C.....	<b>92</b>
<b>FIGURE 70:</b> MALDI Spectrum of Band 11P.....	<b>92</b>
<b>FIGURE 71:</b> MALDI Spectrum of Band 16C.....	<b>93</b>
<b>FIGURE 72:</b> MALDI Spectrum of Band 26C.....	<b>93</b>
<b>FIGURE 73:</b> MALDI Spectrum of Band 9CP .....	<b>94</b>
<b>FIGURE 74:</b> MALDI Spectrum of Band 17C.....	<b>94</b>
<b>FIGURE 75:</b> MALDI Spectrum of Band 6C .....	<b>96</b>
<b>FIGURE 76:</b> MALDI Spectrum of Band 1C .....	<b>96</b>
<b>FIGURE 77:</b> MALDI Spectrum of Band 23C.....	<b>97</b>
<b>FIGURE 78:</b> MALDI Spectrum of Band of Digested Glove.....	<b>97</b>
<b>FIGURE 79:</b> MALDI Spectrum of Band of Self-Digested Trypsin.....	<b>99</b>
<b>FIGURE 80:</b> MALDI Spectrum of Band 1P .....	<b>101</b>
<b>FIGURE 81:</b> Sequence Coverage of $\alpha$ -Actinin by 1P.....	<b>102</b>
<b>FIGURE 82:</b> Autoradiograph Control--1 .....	<b>106</b>
<b>FIGURE 83:</b> Autoradiograph Phorbol--1 .....	<b>107</b>
<b>FIGURE 84:</b> Autoradiograph Phorbol--2 .....	<b>107</b>
<b>FIGURE 85:</b> Autoradiograph Phorbol--MP .....	<b>108</b>
<b>FIGURE 86:</b> Matrix Embedded Sample.....	<b>113</b>
<b>FIGURE 87:</b> Ion Trap Mass Analyzer.....	<b>114</b>
<b>FIGURE 88:</b> MS Isotope Peaks .....	<b>115</b>
<b>FIGURE 89:</b> MS Dimer Peaks.....	<b>116</b>
<b>FIGURE 90:</b> Diagram of Bruker Biflex III MALDI-TOF MS.....	<b>118</b>
<b>FIGURE 91:</b> Ionization Chamber .....	<b>119</b>
<b>FIGURE 92:</b> Reflectron Mode.....	<b>120</b>
<b>FIGURE 93:</b> Fragmentation of a Peptide Bond.....	<b>121</b>

## ABSTRACT

Many human disorders are associated with the malfunction of smooth muscle tissue, or are related to the capabilities of its proper function—asthma, glaucoma, renal inefficiency, hypertension, and cardiovascular disease. Dysfunctional proteins are frequently implicated as the source of such disorders. As the second highest cause of death in the United States, the epidemic of cardiovascular disease makes the study of smooth muscle of utmost concern.

The capabilities of proteomics and mass spectrometry allow the entire proteome complement of a cell or tissue type to be analyzed at once. This investigation employs such techniques in an effort to better understand the mechanisms of signal transduction for the contraction of smooth muscle tissue. The differential phosphorylation of proteins between resting and contracted tissue was targeted, specifically, because phosphorylation is the primary means of communication and activity modification of proteins. Much of what is known about the regulation of signal transduction in smooth muscle contraction is conducted through the activation of myosin light chain kinase (MLCK) and/or myosin light chain phosphatase (MLCP).

Protocols of analysis using phosphoproteomic techniques and MALDI-TOF MS were developed for the purposes of this investigation. The localization of the more abundant proteins actin, myosin heavy chain (MHC), and tropomyosin was determined on a 2D gel. Tropomyosin was found to be phosphorylated in phorbol-contracted tissue, indicating that this protein may play a larger role in contractile regulation than originally thought. The function of such thin-filament associated proteins should be investigated more thoroughly. A thorough understanding of contraction in normal tissue will provide the base for which dysfunctions can be compared. Continued improvements in methodology will aid the advancement of this research.

## ABBREVIATIONS AND ACRONYMS

---

<b>Proteins</b>	
AKAP86	A Kinase Anchor Protein 86
BK Channels	Ca <sup>2+</sup> activated K <sup>+</sup> channels
CaD	Calbindin
CaM	Calmodulin
CaM KII	Calmodulin Kinase II
GEFs	Guanidine Exchange Factors
GDI	Guanidine Dissociation Inhibitors
HMM	Heavy Meromyosin
HSP-20	20 kDa Heat Shock Protein
LMM	Light Meromyosin
MAPK	Mitogen-Activated Protein Kinase
MAPKK	Mitogen-Activated Protein Kinase Kinase
MHC	Myosin Heavy Chain
MLC-20	Regulatory Myosin Light Chain
MLC <sub>essential</sub>	Essential Myosin Light Chain
MLCK	Myosin Light Chain Kinase
MLCP	Myosin Light Chain Phosphatase
MYPT-1	Regulatory Subunit of MLCP
PAK	p21 Activated Protein Kinase
PKA	cAMP-Dependent Protein Kinase
PKC	Protein Kinase C
PKG	cGMP-Dependent Protein Kinase
PLA <sub>2</sub> /PKA <sub>2</sub>	Phospholipase A2
PLC-β	Phospholipase C-Beta
PP1	Catalytic Subunit of MLCP
RyaR	Ryanodine Receptors
RhoA	RhoA GTPase

ROK	Rho-Associated Protein Kinase
Tm	Tropomyosin
TnC	Troponin C

---

### Chemicals

---

AA	Arachidonic Acid
AcCN	Acetonitrile
AcOH	Acetic Acid
ADP	Adenosine Diphosphate
ATP	Adenosine Triphosphate
BaOH <sub>2</sub>	Barium Hydroxide
cAMP	Cyclic-Adenosine Monophosphate
cGMP	Cyclic-Guanosine Monophosphate
CaCl <sub>2</sub>	Calcium Chloride
DAG	Diacylglycerol
DMSO	Dimethyl Sulfoxide
DTT	Dithiothreitol
EDTA	Ethylenediamine
GDP	Guanosine Diphosphate
GTP	Guanosine Triphosphate
HCCA	$\alpha$ -cyano-4-hydroxy-cinnamic acid
HCl	Hydrochloric Acid
H <sub>2</sub> O	>17 M $\Omega$ Nanopure Water
H <sub>2</sub> O <sub>2</sub>	Hydrogen Peroxide
H <sub>3</sub> PO <sub>4</sub>	Phosphoric Acid
IPA	Isopropanol
IP <sub>3</sub>	Triphosphoinositol/Inositol-triphosphate
IP <sub>4</sub>	Tetraphosphoinositol
K <sub>3</sub> Fe(CN) <sub>6</sub>	Potassium Ferricyanide
KH <sub>2</sub> PO <sub>4</sub>	Monobasic Potassium Phosphate

K <sub>2</sub> HPO <sub>4</sub>	Dibasic Potassium Phosphate
MeOH	Methanol
MgCl <sub>2</sub>	Magnesium Chloride
NO	Nitric Oxide
NaCl	Sodium Chloride
NaOH	Sodium Hydroxide
NaHCO <sub>3</sub>	Sodium Bicarbonate
Na <sub>2</sub> PO <sub>4</sub>	Sodium Phosphate
Na <sub>2</sub> SO <sub>3</sub>	Sodium Thiosulfate
Na <sub>3</sub> VO <sub>4</sub>	Sodium Orthovanadate
NH <sub>4</sub> HCO <sub>3</sub>	Ammonium Bicarbonate
NP-40	Nonoxynol-9 (Non-ionic detergent)
PMSF	Phenylmethylsulfonyl fluoride
SDS	Sodium Dodecyl Sulfate (Ionic detergent)
TCA	Trichloroacetic Acid
TEA	Triethanolamine
TFA	Trifluoroacetic Acid
Tris	Hydroxymethyl aminomethane

---

**Other**

---

AHA	American Heart Association
BacT	Bacterial Toxins
Da/kDa	Daltons/Kilodaltons
DC	Direct Current
ESI	Electrospray Ionization
eV	Electron Volts
FAB	Fast Atom Bombardment
FT-ICR	Fourier Transform-Ion Cyclotron Resonance
FT-MS	Fourier Transform Mass Spectrometry
g/mg	Gram/Milogram

GI	Gastrointestinal
HGP	Human Genome Project
HPLC	High Pressure/Performance Liquid Chromatography
IE	Electron Ionization
IEF	Isoelectric Focusing (1 <sup>st</sup> Dimension Separation of 2D Gel Electrophoresis)
IMAC	Immobilized Metal Affinity Chromatography
KE	Kinetic Energy
LSI-MS	Liquid Secondary Ion Mass Spectrometry
MALDI	Matrix-Assisted Laser Desorption/Ionization
mL; L	Milliliter; Liter
mM; M	Millimolar; Molar
mRNA	Messenger Ribonucleic Acid
MS	Mass Spectrometry
MUSOM	Marshall University Joan C. Edwards School of Medicine
MW	Molecular Weight
m/z	Mass to Charge Ratio
Nanopure H <sub>2</sub> O	>17 MΩ Water
PBS	Phosphate Buffered Saline
PE	Potential Energy
PF <sub>2</sub>	Prostaglandin F <sub>2</sub>
pI	Isoelectric Point
PM	Plasma Membrane
PSD	Post Source Decay
Rc	C-terminal portion of a peptide/protein
rF	Radiofrequency Electromagnetic Radiation
RIPA Buffer	Radioimmunoprecipitation Buffer
Rn	N-terminal portion of a peptide/protein
RP-HPLC	Reverse Phase HPLC
RPM	Revolutions per minute
SDS-PAGE	Sodium Dodecyl Sulfate-Polyacrylamide Gel Electrophoresis

(2<sup>nd</sup> Dimension Separation of 2D Gel Electrophoresis)

SM	Smooth Muscle
SR	Sarcoplasmic Reticulum
STICs	Spontaneous Inward Ca <sup>2+</sup> Currents
STOCs	Spontaneous Outward Ca <sup>2+</sup> Currents
UI	Urointestinal
UV	Ultraviolet
WHO	World Health Organization



# INTRODUCTION

## Smooth Muscle

Smooth muscle (SM) tissue consists of the involuntary muscles found in the lining of most hollow organs, including blood vessels, and functions to produce and regulate tension and mechanical processes. The primary function of SM is contraction—tension development and maintenance. Generated force is used to regulate such processes as blood flow/circulation, movement through the gastrointestinal (GI)/urogenital (UI) tracts, retinal function (light reactions, pressure), and laboral uterine contractions (Abdel-Latif, 2001). SM tissue can be classified into six different types: vascular, respiratory, urinary, reproductive, gastrointestinal, and ocular.

Many disorders are associated with either the malfunction of SM tissue, or are related to the capabilities of its proper function. These include cardiovascular disease, hypertension (high blood pressure), glaucoma, asthma, renal inefficiency, restenosis, atherosclerosis, and cerebral vasospasm. In particular, overconstriction, or blockage of blood vessels, can cause hypertension and heart disease.

According to research conducted by the World Health Organization (WHO), approximately 16.6 million people around the world die a year from cardiovascular-associated disorders with approximately 600 million people at high risk for heart attack, stroke, and/or cardiac failure (WHO, 2002). What's more these numbers are growing (WHO 2002). To add to the weight of this problem, the age of monitored patients is decreasing. The average age of afflicted patients used to be in the 70s, but has grown to include those in their 30s or 40s (Nurseweek, 2003).

An estimated \$352 billion a year will be spent in America for the treatment and disability coverage of heart disease. As the leading cause of death in many countries, including the United States, risk factors include: hypertension, high cholesterol, obesity, diabetes, heredity, tobacco use, poor diet, increasing age, physical inactivity, and excess alcohol intake (AHA, 2003).

Treatment and prevention of this epidemic begins with an understanding of normal SM function—both its mechanical and biochemical properties. Devising how signaling pathways are

altered during the state of disease would be the next step to develop treatments for a disorder. For example, one of the primary treatments for patients enduring overconstriction of blood vessels or airways is to treat them with a vasodilator, an agonist that signals SM tissue to relax, such as nitroglycerine which produces nitric oxide (NO).

Smooth muscle can be characterized as either tonic or phasic (Somlyo 1968, 1990). Phasic SM demonstrates activation of contraction via the production of action potentials, and develops faster shortening and tension development (Somlyo 1968, 1993, 1994; Johansson 1980). Tonic SM exhibits graded polarization, or slower waves of  $\text{Ca}^{2+}$  influx (Fuglsang 1993; Somlyo 1993; Prosser 1992).

## **Smooth Vs. Skeletal: Similarities**

### ***Composition***

Both smooth and skeletal muscle have many of the same proteins related to contractile activities and/or signal transduction, although they have different isoforms. (see appendix III for protein info.) Such proteins include: actin, myosin, MgATPase, calmodulin (CaM), voltage-dependent anion channels, and myosin light chain kinase (MLCK)—though the structure of this protein in the two muscles is very different (Hartshorne 1987). Actin is made up of G-actin monomers that compose the thin filaments to make F-actin. Myosin is a hexameric protein. The six monomers that make up myosin consist of two heavy chains (MHC), two essential light chain monomers ( $\text{MLC}_{\text{essential}}$ ) and two myosin regulatory light chains (MLC-20) (See Appendix IV).

### ***Regulation of Contraction***

Both types of muscle contractions are regulated by depolarization states of the plasma membrane (PM) and cytosolic concentrations of calcium ( $[\text{Ca}^{2+}]$ ), referred to as electromechanical coupling. Electrical depolarization of the membrane from a resting potential of -70 to -40 mV (depending on the cell type) to a more positive potential causes the opening of voltage-gated calcium ( $\text{Ca}^{2+}$ ) channels in the plasma membrane (PM) and the sarcoplasmic

reticulum (SR) leading to increased levels of cytosolic  $\text{Ca}^{2+}$  (Somlyo 1989; Johansson 1980). Contraction occurs with a change to a more positive membrane potential (depolarization), relaxation occurs when the potential switches back to a more negative potential (repolarization), (Filo 1965; Somlyo 1998).

### *Mechanism of Contraction*

Both muscles use the same actomyosin molecular motor (MgATPase) to facilitate mechanical contraction via the familiar, well-researched sliding filament mechanism. Briefly, a phosphorylated myosin regulatory light chain (MLC-20) from myosin thick filaments enables the MgATPase motorized myosin head to walk along the thin filaments of actin (F-actin), shortening and contracting muscle fibers (Figures 1 and 2, below).

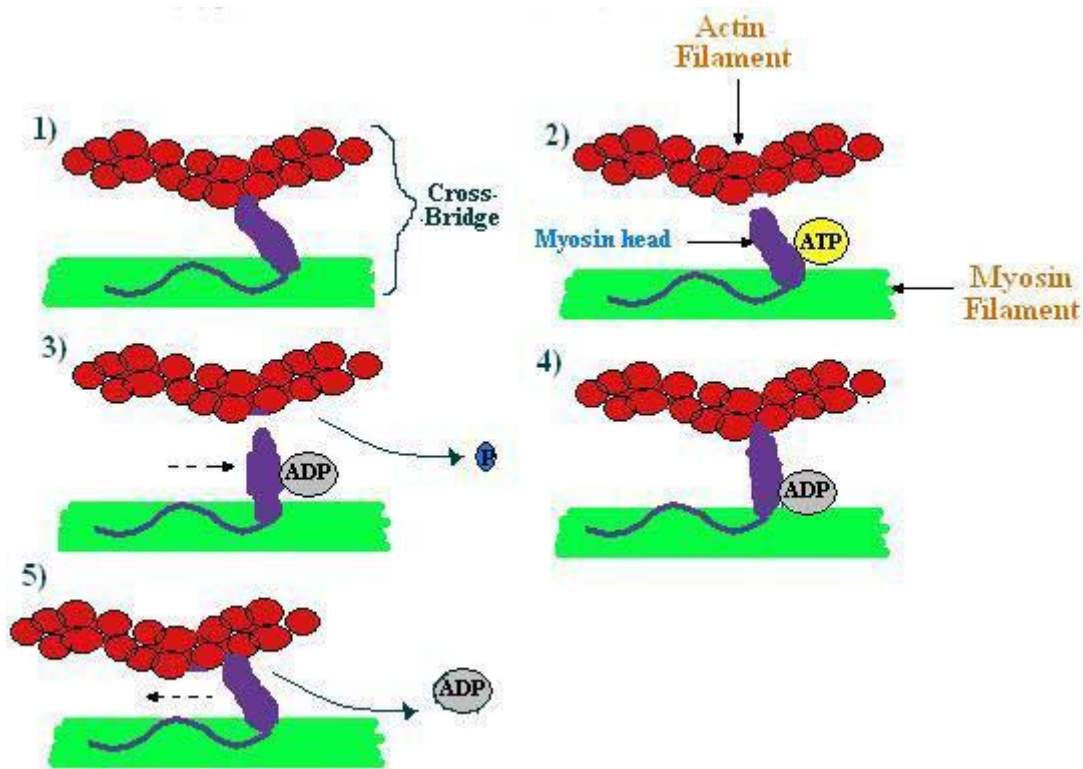


**Figure 1:** Illustration of the mechanism of the sliding filament model in a repeated 5 step operation. 1) Myosin heads are bound to actin filaments at the myosin binding site. 2) ATP binds to the regulatory light chain of myosin (MLC-20). The myosin head dissociates. 3) Hydrolysis of ATP causes a conformational change in the myosin head into a “cocked” formation. 4) The myosin head binds the actin filament again. 5) ADP is released, and the myosin head pulls the myosin filament forward in the “power stroke”.

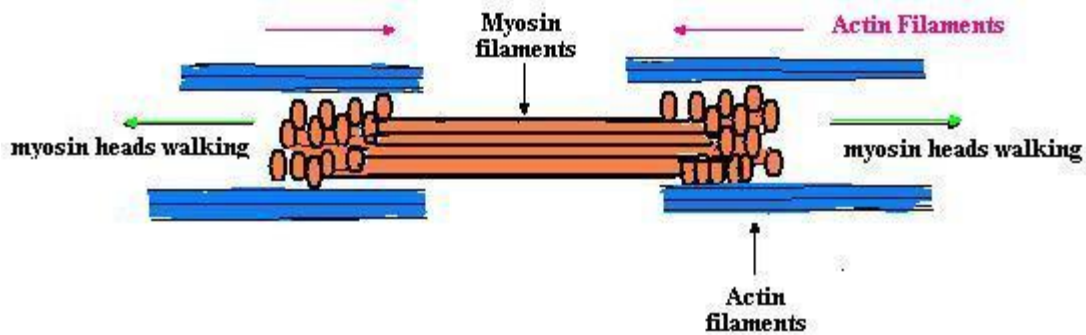


**Figure 2:** Model of the sliding filament mechanism of contraction, in which activated MgATPase myosin heads walk along actin filaments to shorten and contract fiber lengths.

These actomyosin interactions are called cross-bridges. Similarity in the behavior of force-velocity relationships in response to changes in muscle length and tension development support this theory of analogous contraction (Hibberd 1989; Somlyo 1988, Horiutu 1989; Arner 1987; Fuglsang 1993).

### **Smooth Vs. Skeletal: Differences**

#### ***Ultrastructure and Composition***

Though the two types of muscle fibers share similar components and the same general mechanism, they differ in their ultrastructural design, and consequently, many of their mechanical properties. Skeletal muscle fibers are arranged in a striated organization of stacked filaments in repeating units called sarcomeres. Smooth muscle fibers exist as ordered arrays of crossed filaments (Figures 3 and 4, below). SM also has a greater ratio of actin to myosin, with a much lower level of myosin than skeletal muscle. The abundances of actin and tropomyosin are consistent with skeletal muscle. Actin filaments are attached to dense bodies containing  $\alpha$ -actinin, assumed to be analogous to the Z-discs in skeletal muscle.

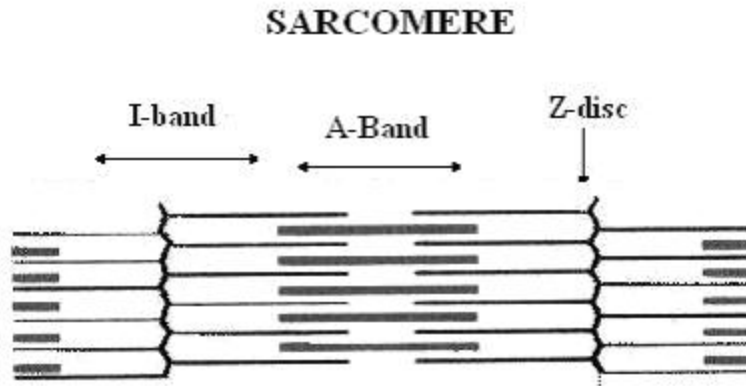


**Figure 3:** Illustration of the arrangement of skeletal muscle fibers—repeating units of the sarcomere.

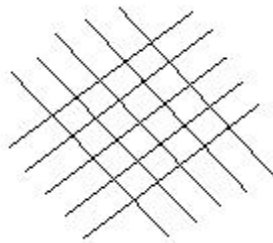


**Figure 4:** Arrangement of smooth muscle fibers in ordered arrays of crossed filaments.

### ***Mechanism of Contraction***

The mechanism by which increasing  $[Ca^{2+}]$  induces contraction in skeletal and smooth muscle differs, as well. In skeletal muscle,  $Ca^{2+}$  binds to troponin C (TnC)—a regulatory protein associated with actin through tropomyosin (Tm)—that causes a conformational change which moves tropomyosin from blocking the actomyosin interaction (Ebashi 1991).

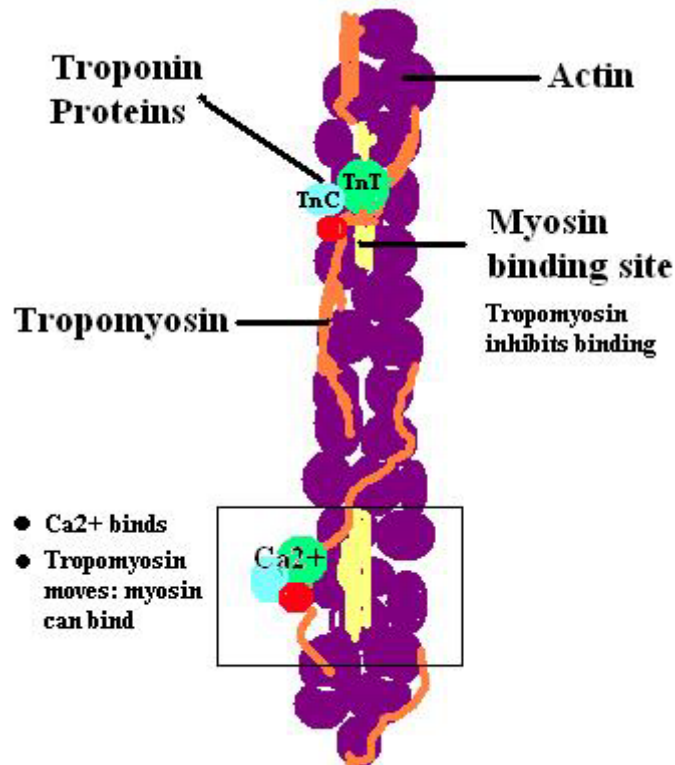


**Figure 5:** Illustration of the mechanism by which induces contraction in skeletal muscle. Troponin C binds Ca<sup>2+</sup> and causes a conformational change in Tropomyosin, which moves from inhibiting myosin from the actomyosin binding site.

SM does not have troponin proteins. It has calponin and caldesmon associated with its thin filaments. In SM, Ca<sup>2+</sup> binds to Calmodulin (CaM), and this complex then binds myosin light chain kinase (MLCK). The Ca-CaM-MLCK complex then phosphorylates MLC-20 at serine 19, allowing contraction (Hartshorne 1987; Sweeney 1994). However, it has been proposed that thin-filament-associated proteins in SM aid in regulation of contraction when phosphorylated by a kinase (Adam 1992; Sobue 1991; Marsten 1991; Winder 1993).

### ***Regulation of Contraction***

The two types of muscle also differ in the stimulus and regulation of contraction/relaxation. Skeletal muscle cell depolarization of the membrane is activated by nerve impulses that release acetylcholine and induce subsequent depolarization. Smooth muscle contraction is controlled not only by depolarization, but also by many signaling molecules and cross-talking pathways, called pharmacological coupling. Table 1 lists some common agonists

of contraction and relaxation. Contraction may be regulated by calcium-independent mechanisms, where constant  $[Ca^{2+}]$  levels are associated with changes in the level of MLC-20 phosphorylation and/or tension. This phenomenon is called calcium sensitization/desensitization, depending on whether the contractile response becomes more or less sensitive to  $[Ca^{2+}]$ .

<b>Agonists of Contraction</b>	<b>Stimulants of Relaxation</b>
High Cytosolic $Ca^{2+}$	Low cytosolic $Ca^{2+}$
High Extracellular $K^+$ (KCl)	Hyperpolarization of membrane
Depolarization of membrane	STICs
STOCs	Dantrolene
Angiotension	Kaurenoic acid
Norepinephrine	Adrenomedullin
Catecholamines	Prostaglandin $E_2$ ( $EP_2$ )
Histamine	Calcitonin gene-related peptide
Triethanolamine (TEA)	$\beta$ -Adrenergic receptor agonist
Polycations -spermin, neomycin, polylysine	Inhibitors of CaM -trifluoroperazine, mastoparan, W13
Endothelin (ET)	Elevators of cAMP/cGMP
Bradykinin	Forskolin
Phorbol esters	Isoproterenol
Prostaglandin $F_2$ ( $PGF_2$ )	Prazosin
Muscarine	Rnd1
Oxotremorin	Y-27632 (ROK inhibitor)
Serotonin	ERK inhibitors
5-hydroxytryptamine	Vasonatin peptide
Interleukin-1	Some tyrosine kinase inhibitors
Vasopressin	IBMX
Thrombin	NO
carbachol	Atrial natriuretic peptide
Methylene blue	ERF
Superoxide	EDHF (hyperpolarizing factor)
Oxytocin	

**Table 1:** Common agonists and inhibitors of contraction and relaxation in smooth muscle tissue.

Regulatory proteins demonstrate changes in function independent of cytosolic  $[Ca^{2+}]$ . Such regulation often occurs when contraction is stimulated by agonist-induced receptor activated contraction in what is called pharmacomechanical coupling. Such sensitization/desensitization

is manifested primarily in the regulation of MLC-20 phosphorylation, activity of MLCK, and/or activity of myosin light chain phosphatase (MLCP), as will be discussed.

### ***Mechanical Properties***

The differences in structure are accompanied by unique mechanical properties of SM tissue. For example, smooth muscle demonstrates maximum force generation at a specific given length. Yet, it operates at a length far below this optimum. When SM is stretched beyond this length, an increasing interference of passive force—that not generated by the active muscle—causes stress relaxation and hysteresis, which poses as a problem for those trying to measure its mechanical features, and is probably why SM does not operate in this range. Smooth muscle also demonstrates much greater series elasticity, which is the length to which the tissue can be stretched while maintaining its mechanical properties (Van Magstrigt 2002).

Smooth muscle tissue can demonstrate a sustained state of contraction, called tonic contraction, as well as phasic contraction. Skeletal muscles operate only as rapid phasic contractions (brief, intense contractions). However, skeletal muscle has a faster maximum shortening velocity and MgATPase activity (Somlyo 1988; Horiutu 1989).

The work of Wright et al. at the Marshall University School of Medicine (MUSOM) has demonstrated the ability of SM to generate more force per unit of cross-sectional area than skeletal muscle (Wright, 2003). Smooth muscle also demonstrates an increased number of cross-bridge attachments and is slow to redevelop force after quick release of tension (Somlyo 1967). Yet, SM shows improved energy metabolism, with the ability to use less ATP to maintain force (Hartshorne 1987; Siegman 1980; Rembold 1993).

Unique to SM is a phenomenon known as latch. There is no direct correlation between the level of MLC-20 phosphorylation and force (Pfitzer 2001), and this is probably due to maintenance of cross-bridge association without phosphorylation. This characteristic is known as latch (Huxley 1957). Such differences in mechanical properties are undoubtedly accompanied by differences in the biochemistry of involved proteins which perform and regulate contractility functions.

### ***SM Heterogeneity***



A striking lone aspect of SM tissue lies in its inherent heterogeneity. The same agonist can elicit different responses in different types of SM tissue, or even in different segments of the same vessel. The same pharamacochemical agent can cause contraction in one tissue, and relaxation in another (Bulbring 1993). Agonists can be coupled to  $\text{Ca}^{2+}$ -dependent or  $\text{Ca}^{2+}$ -independent contraction, and many agonists/relaxing agents are coupled to G-protein receptors. The efficiency with which an agonist induces a response can also differ greatly (Somlyo 1994).

### **Smooth Muscle Mechanics**

The mechanical properties of SM are characterized by force/tension development of tissue as a function of tissue length and time. Such properties are referred by measuring the velocity of change in tension when tissue is shortened or stretched. Properties are investigated from two perspectives 1) analysis of physiological muscle properties to generate normal force-velocity curves, and 2) analysis of properties outside the physiological range, which demonstrate series elasticity (Van Magstrigt 2002).

Two methods exist for producing force-velocity curves. One can either add load (weights) to active muscle and record length changes, or apply shortening velocities to the muscle to reach a given length, followed by recording of changes in force. However, activities should be repeated to eliminate measurements of passive force (Van Mastrigt 1985). Factors that affect mechanical properties include muscle size, number of cross-bridges, orientation of cross-bridges to each other (series, parallel), and duration of exposure to stimuli (Van Mastrigt 2002).

The force-velocity relationship in SM fits the parabolic curve generated by the Hill equation (Hill 1985), except when stretched, where the curve becomes more linear. Passive force becomes a large influence on measurements starting from the point of optimal force development and probably causes a large amount of this linearity (Uvelius 1977, 1979, 1980; Moriya 1985; Stephens 1985; Van Koeveringe 1997). No apparent explanation exists for the effects of stretching on shortening velocities, and conflicting supporting data is reflected in the literature (Uvelius 1977; Malmqvist 1991; Minekus 2001; Van Mastrigt 1999).

## Signal Transduction Pathways

The SM cell is a complex structure with many points of regulation. Several signaling pathways within the SM cell have been elucidated in the past 30 years. The following subsections include diagrams of the complex pathways, which will be discussed briefly within the text. Figure 6, below, defines the symbols used in the diagrams of signal transduction pathways.

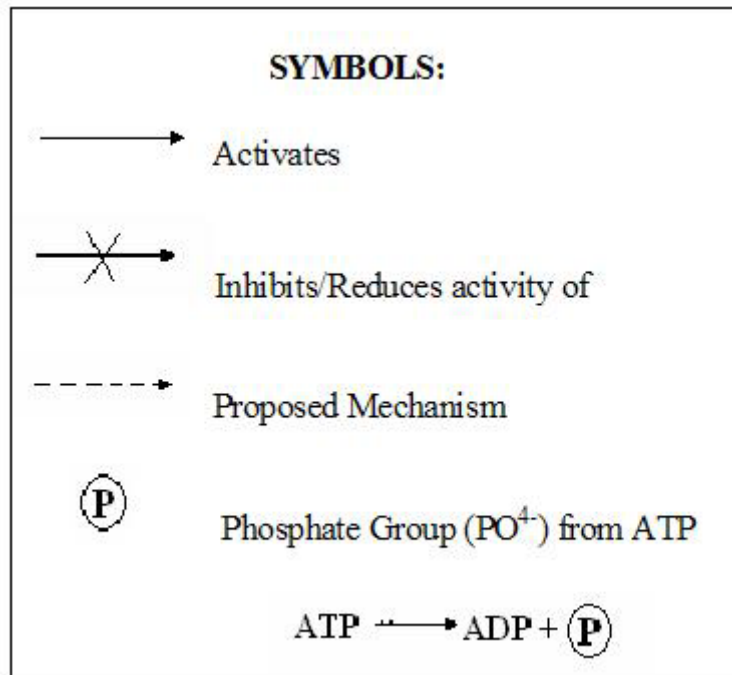


**Figure 6:** Legend defining the symbols used in the diagrams of signal transduction pathways in SM cells.

### *Ca<sup>2+</sup> Influx*

Calcium ( $\text{Ca}^{2+}$ ) influx occurs through  $\text{Ca}^{2+}$  channels in the plasma membrane (PM) and the sarcoplasmic reticulum (SR). The rate of influx depends on the kinetic properties of the ion channels (Kotlikoff 1999). Depolarization of the PM from resting potential to a more positive potential—from -70 to -40 mV, depending on cell type—causes opening of voltage-gated ion channels, and subsequent contraction. Repolarization of the cell membrane to a more negative potential results in relaxation (Somlyo 1989; Johansson 1980).

## Ca<sup>2+</sup> Flux in SM

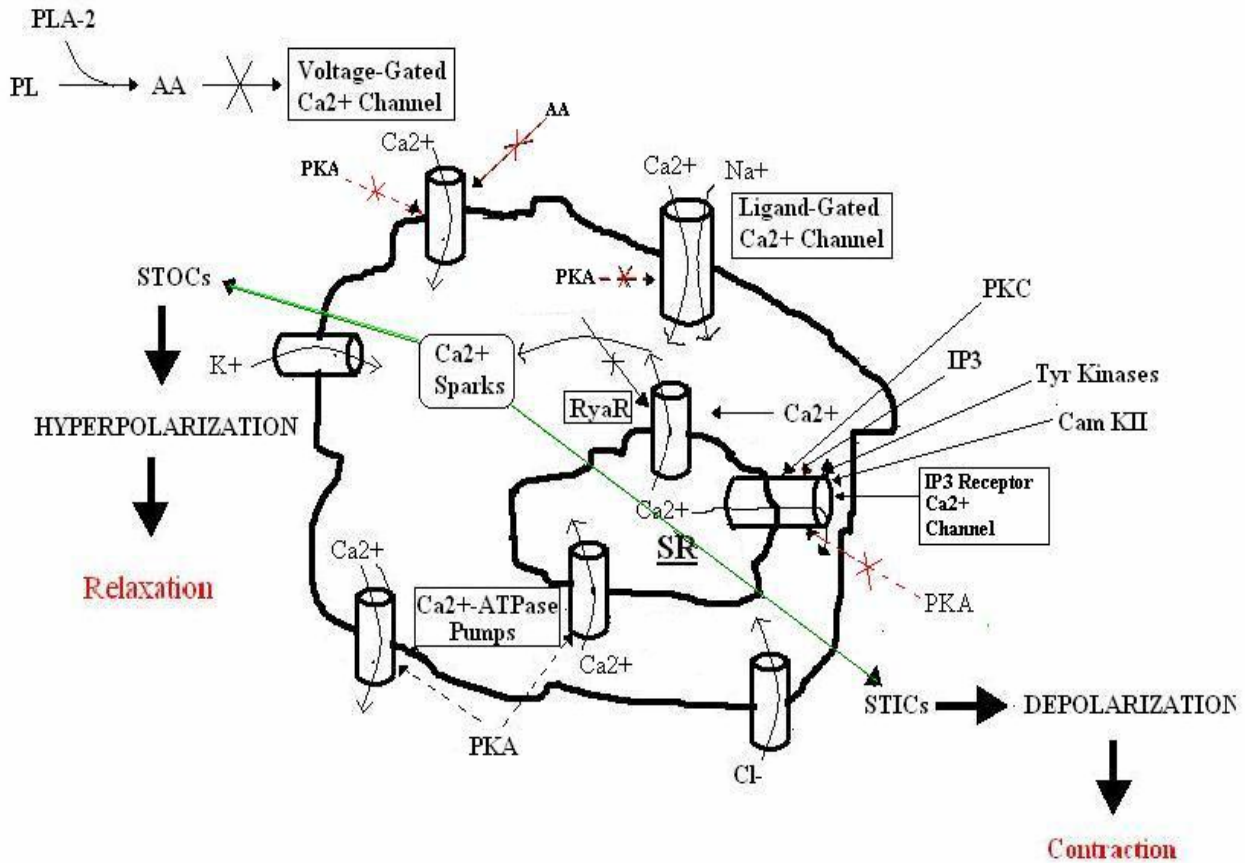


**Figure 7:** Diagram illustrating the flux of calcium ions within the SM cell.

In the cytoplasm, calcium-binding buffer proteins bind the influx of excess Ca<sup>2+</sup> (Kargacin 1994). It has now been proposed that the local distribution of buffers and contractile-regulating proteins near the site of influx governs the nature and the extent of the response (Iino 1989). An action potential in phasic SM exceeds the buffering capacity of the cell and the signal to contract is initiated (Bond 1984). The level of excess [Ca<sup>2+</sup>] depends on the extent of depolarization and the concentration of surrounding buffers.

Voltage-gated ion channels are activated by depolarization, and are specific for calcium. Ligand-gated ion channels are non selective and may function to activate voltage-dependent channels (Somlyo 1991; Somlyo 1994). The properties of ion channels vary between smooth muscle cell type, as well (Kuriyama 1992; McDonald 1994). To facilitate relaxation, most of the

$\text{Ca}^{2+}$  is removed from the cytosol by the  $\text{Ca}^{2+}$ -pump of the SR, though some is removed by the  $\text{Ca}^{2+}$ -ATPase pump and a  $\text{Na}^+/\text{Ca}^{2+}$  exchanger pump in the PM (Bond 1984; Carafoli 1993; Juhaszova 1993; Aaronson 1981).

Recently, the potent effects of  $\text{Ca}^{2+}$  sparks on membrane potential have been studied (Nelson 1995). These sparks are local, short-lived releases of  $\text{Ca}^{2+}$  through Ryanodine receptors (RyaR)—at least ten (ZhuGe 2000)—in the SR, causing a high local  $[\text{Ca}^{2+}]$ . The effect depends on the local environment of the spark. The excess local  $\text{Ca}^{2+}$  can 1) activate  $\text{IP}_3$  receptors to generate a larger “wave” of  $\text{Ca}^{2+}$  due to faster diffusion of  $\text{IP}_3$  (Jaggar 2000; Ganitkevich 2002), or 2) activate  $\text{Ca}^{2+}$ -activated potassium ( $\text{K}^+$ ) channels (BK channels), causing hyperpolarization and relaxation—STOCs (spontaneous transient outward currents) (Bolton 1996), or 3) may induce  $\text{Ca}^{2+}$ -activated chloride ( $\text{Cl}^-$ ) ion channels and cause depolarization and contraction—STICs (spontaneous transient inward currents) (ZhuGe 1998). Several messengers, in known signaling pathways, cause increases or decreases in  $\text{Ca}^{2+}$  spark frequency (Porter 1998; Wellman 2001; Bonev 1997; Jaggar 2000).

### ***Calcium Sensitization/Desensitization***

As referred to before, calcium sensitization/desensitization is mediated mostly through changes in the function of MLC-20, MLCK, MLCP, or even the actomyosin MgATPase itself. The extent of MLC-20 phosphorylation depends on the relative activation/deactivation of MLCK/MLCP, which are the main targets of regulatory proteins. However, changes in contraction can occur without changes in MLC-20 phosphorylation. It has been suggested that thin-filament-associated proteins—caldesmon, calponin—mediate cross-bridge attachments in smooth muscle as they do in skeletal muscle, possibly when phosphorylated by mitogen-activated protein kinase (MAPK) (Arner 1999; Adam 1992; Sobue 1991; Marston 1991; Winder 1993). It has also been found that small heat shock proteins may directly inhibit the MgATPase, when they are phosphorylated by PKA or PKG (Barany 1996; Beal 1997; Rembold 2000; Brophy 1999).

Phosphorylation has also been shown to decline without loss of tension (Kamm 1985; Fischer 1989; Sward 2000), and it has been suggested that MLC-20 is actually dephosphorylated while cross-bridges are still intact or are slowly detached (Murphy 1994). This is an example of

the latch state, where a low level of MLC-20 phosphorylation is associated with a high maintenance of force and low corresponding expenditure of ATP (Huxley 1957). Another suggestion allows that non-phosphorylated cross-bridges are attached with the assistance of calponin and caldesmon (CaD) (Arner 1987; Khromov 1995; Somlyo 1988; Vyas 1992; Albrecht 1997; Matsui 1996) or that of already attached cross-bridges (Somlyo 1988; Somlyo 1990). In addition, relaxation has been shown to occur while increased numbers of MLC-20 are still phosphorylated (Barany 1993; Katoch 1997; McDaniel 1992; Tansey 1990). The relation between the level of force and degree of phosphorylation may also depend on the type of agonist used (Suematsu 1991).

Many kinases other than MLCK have been discovered to phosphorylate MLC-20, including Rho-associated kinase, which phosphorylates MLC-20 in the peripheral region of the cell (ROK) (Amano 1996; Miyazaki 2002), Integrin-linked kinase (Deng 2001), ZIP kinase (Niuro 2001), MAPK (Takahashi 1998; Dessy 1998; Ohmichi 1997; Velarde 1999; Yousufzai 2000), Ca<sup>2+</sup>-Calmodulin Kinase II (CaM KII) (Pfitzer 1989), Protein Kinase C (PKC) (Lee 1999, Katoch 1999), some unidentified staurosporine-sensitive kinases (Kureishi 1999; Iizuka 1999; Weber 1999), and possibly some other unidentified kinases (Trinkle-Mulcahy 1995; Ichikawa 1996; Hartshorne 1998). The potency or relative importance of these kinases is not yet fully understood, and can vary with the type of agonist used (Ganitkevich 2002).

### **Contraction Pathways in SM**

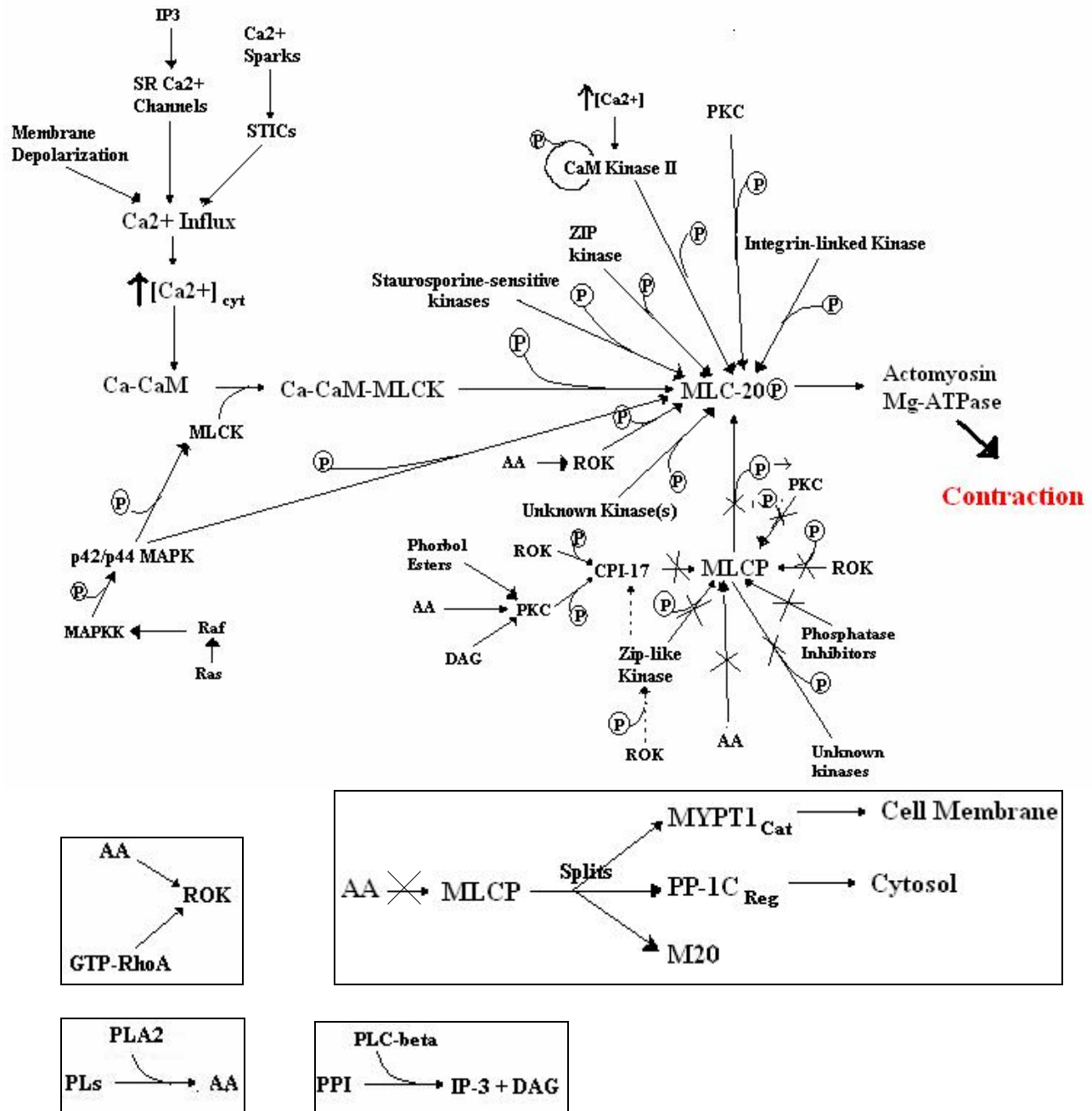


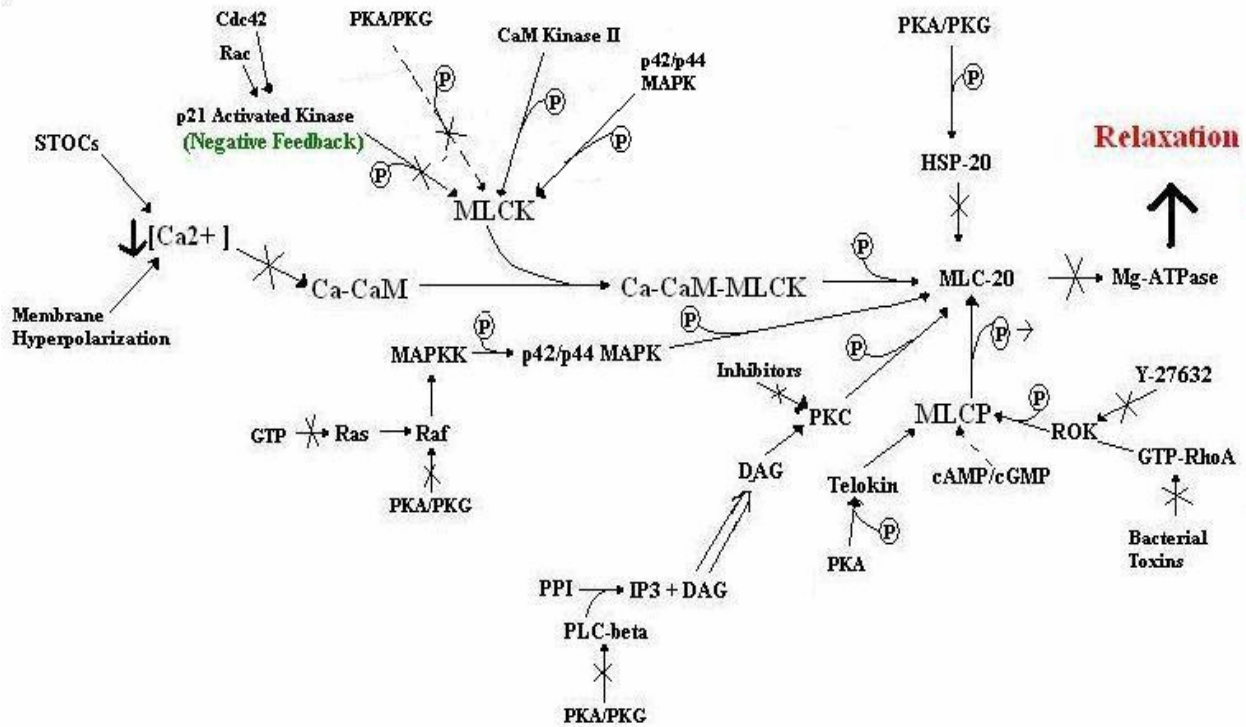
**Figure 8:** Diagram illustrating the signal transduction pathways involved in contraction of the SM cell.

Activation of MLCK by complexation with Ca-CaM causes it to phosphorylate MLC-20 and induce contraction. The affinity of MLCK for Ca-CaM can be decreased if it is

phosphorylated. It has been shown to be phosphorylated by p42/p44 MAPK (Klemke 1997), p21 activated protein kinase (PAK) (Sanders 1999), Cam KII (Tansey 1992), and cAMP-dependent protein kinase (PKA), which causes 10-fold decrease in  $\text{Ca}^{2+}$ -sensitivity (Conti 1981; De Lanerolle 1984; Adelstein 1982), . It has also been found that the myosin binding region of MLCK can bind to myosin heads and stimulate activation of the GTPase without phosphorylation of MLC-20 (Gao 2003).

Inhibition of MLCP prevents it from dephosphorylating MLC-20 and causes an increase in contraction. Activation of the phosphatase will, of course, lead to relaxation. Many G-proteins activate phospholipase  $\text{A}_2$  ( $\text{PLA}_2$ ), which cleaves arachidonic acid (AA)—a fatty acid (FA)—from phospholipids (PLs). Arachidonic acid causes dissociation of the MLCP holoenzyme into its constituent subunits: the regulatory subunit (MYPT-1), the catalytic subunit (PP-1), and a 20 kDa subunit of unknown function (Gong 1992; Alessi 1992; Shirazi 1994; Shimizu 1994; Haystead 1995; Gailley 1996; Harthorne 1998 [review]). The regulatory subunit, which targets MLCP to MLC-20 remains in the cytosol, while the catalytic subunit translocates to the cell membrane, where it experiences a reduced catalytic activity.

## **Relaxation Pathways in SM**



**\*Phosphorylation of MLCK at alternative sites causes:  
-Decreased affinity for Ca-CaM**

**Figure 9:** Diagram illustrating the signal transduction pathways of relaxation in SM cells.

MLCP is also inhibited by the phosphopeptide CPI-17, when it is activated by phosphorylation (Harshorne 1998). It has been hypothesized that many kinases—ROK, PKC, and ZIP-like kinase—phosphorylate and activate the peptide as a means of inhibiting MLCP (Kanecko 2001; Eto 1995; Kitazawa 1999; Gailly 1997; (Macdonald 2001a; Ichikawa 1996a; Pfitzer 2001; Trinkle-Mulcahy 1995).

Phosphorylation of the catalytic subunit (MYPT-1) of MLCP inhibits its function. This task is performed by many kinases, including ROK (Feng 1999; Kimura 1996), ZIP-like kinase (Ichikawa 1996; MacDonald 2001b), unidentified kinases sensitive to staurosporine-induced contraction (Kureishi 1999, Weber 1999), and other unidentified kinases (Feng 2000; Somlyo 1999).

In terms of activation, it has been proposed that either cGMP directly activates MLCP (Surks 1999) or does so through phosphorylation of telokin, which activates MLCP (Wu 1998).



## *IP<sub>3</sub>/DAG Signaling*

Inositol-triphosphate (IP<sub>3</sub>), a negligible signal in skeletal muscle (Pape 1988), has been confirmed as a secondary messenger in the contraction of smooth muscle by many sources (Kobayashi 1989; Hashimoto 1986; Miller-Hance 1988; Somlyo 1992, 1988).

### IP<sub>3</sub>/DAG Signaling in SM

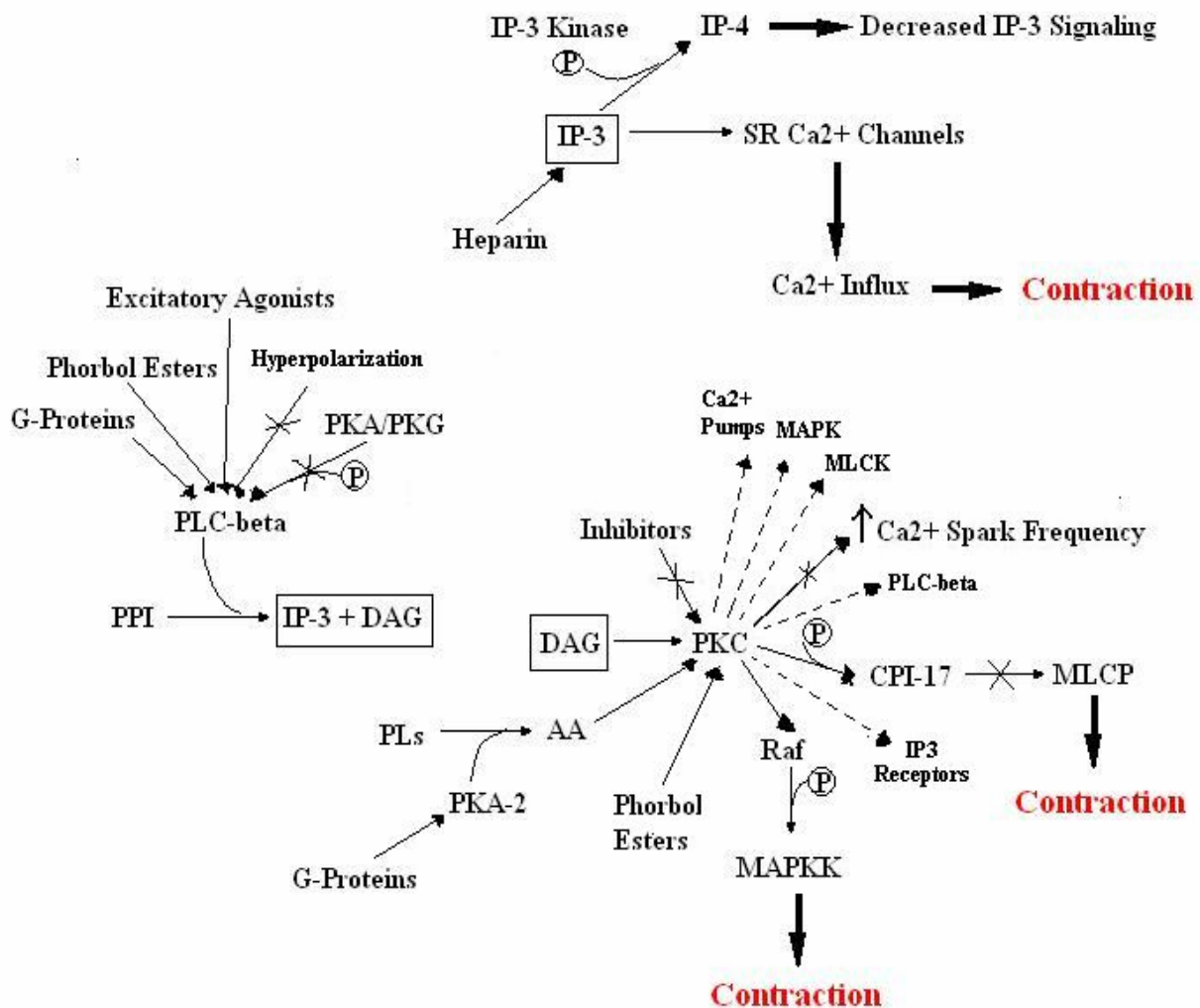


**Figure 10:** Diagram illustrating the signaling pathways of IP<sub>3</sub>/DAG in SM cells.

Most excitatory agonists are coupled by G-proteins that activate phospholipase-beta isoform (PLC-β), which cleaves phosphoinositol (PPI)—a phospholipid—into IP<sub>3</sub> and

diacylglycerol (DAG) (Figure 6). Generally, the G-proteins that activate the PLC- $\beta$  pathway also inhibit nucleotide cyclases, which will be discussed later (Somlyo 1994). Activators of PLC- $\beta$  include AA (Husain 1998, 1999), some tyrosine kinases (Zhou 1993), and phorbol esters (Jensen 1996; Walker 1998).

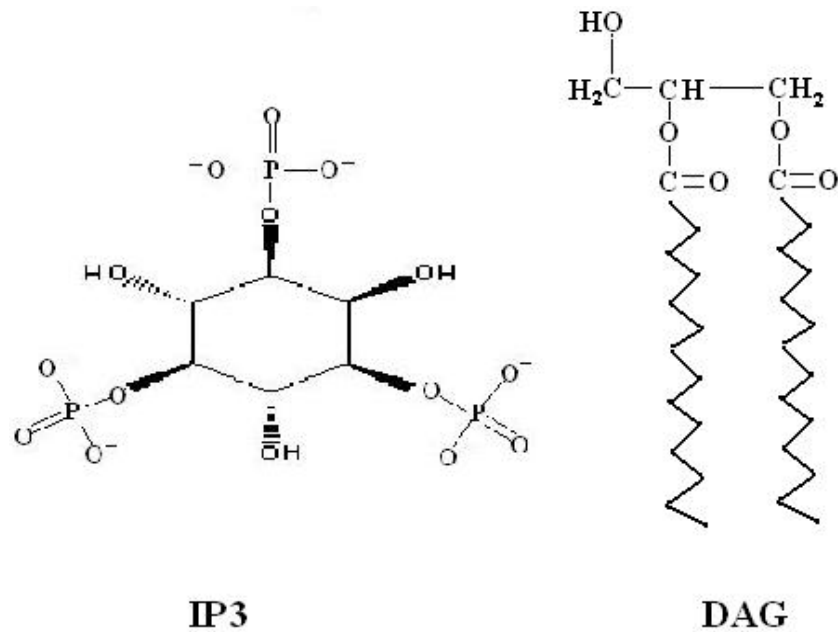


**Figure 11:** Structures of inositol-triphosphate (IP<sub>3</sub>) and diacylglycerol (DAG).

IP<sub>3</sub> activates IP<sub>3</sub>-receptor Ca<sup>2+</sup>-channels in the SR (Somlyo 1994). DAG activates PKC, which induces contraction by phosphorylating CPI-17, the MLCP inhibitor (Eto 1995; Kitazawa 1999; Gailly 1997). It can also phosphorylate the G-protein Raf, which activates MAPKK (Neary 1997). Arachidonic acid can also activate PKC (Gong 1992, 1995).

IP<sub>3</sub> can be phosphorylated by IP<sub>3</sub> kinase to produce the inactive IP<sub>4</sub>. The IP<sub>3</sub> receptor is phosphorylated by cAMP-dependent protein kinase (PKA), cGMP-dependent protein kinase (PKG), or CaM KII (Patel 1999). The pathway is also inhibited by heparin (Kobayashi 1989).

On a side note, time delays between agonist-induced receptor activation and tension development ranges from 200-500 ms. This delay is probably due to diffusion and reaction of signaling molecules (IP<sub>3</sub> production, diffusion of Ca-CaM). It is not limited by the act of MLC-20 phosphorylation (Somlyo 1990).

### *cAMP/cGMP Signaling*

The main secondary messengers for inducing relaxation are elevated levels of cAMP (cyclic adenosine monophosphate) and/or cGMP (cyclic guanosine monophosphate) (Karaki 1988; Kerrick 1981; Morgan 1984; Pfitzer 1986; Seguchi 1996; van Riper 1995). Receptors are activated and stimulate adenylyl/guanylyl cyclases, which catalyze the formation of cAMP/cGMP from ATP (adenosine triphosphate) or GTP (guanosine triphosphate) precursors (Pfitzer 1984) (Figures 7 and 8, below). Adenylyl cyclase is activated by many G<sub>βγ</sub>-protein receptors, and inhibited by many G<sub>α</sub>-protein receptors. Some stimulants of relaxation through the cAMP pathway include forskolin (Abdel-Latif 1996), Nitric oxide (NO), atrial natriuretic peptide, and (ERF) (Lincoln 1996).

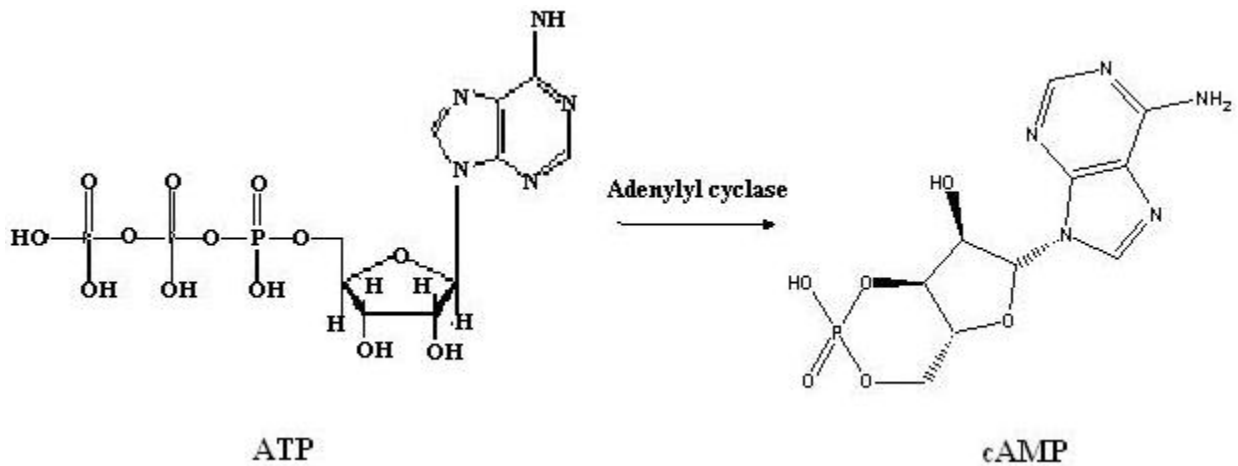
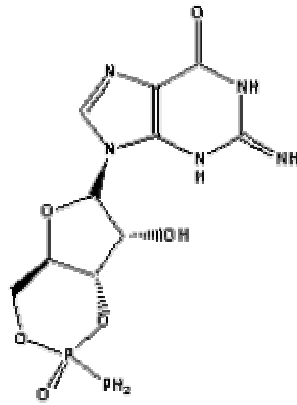


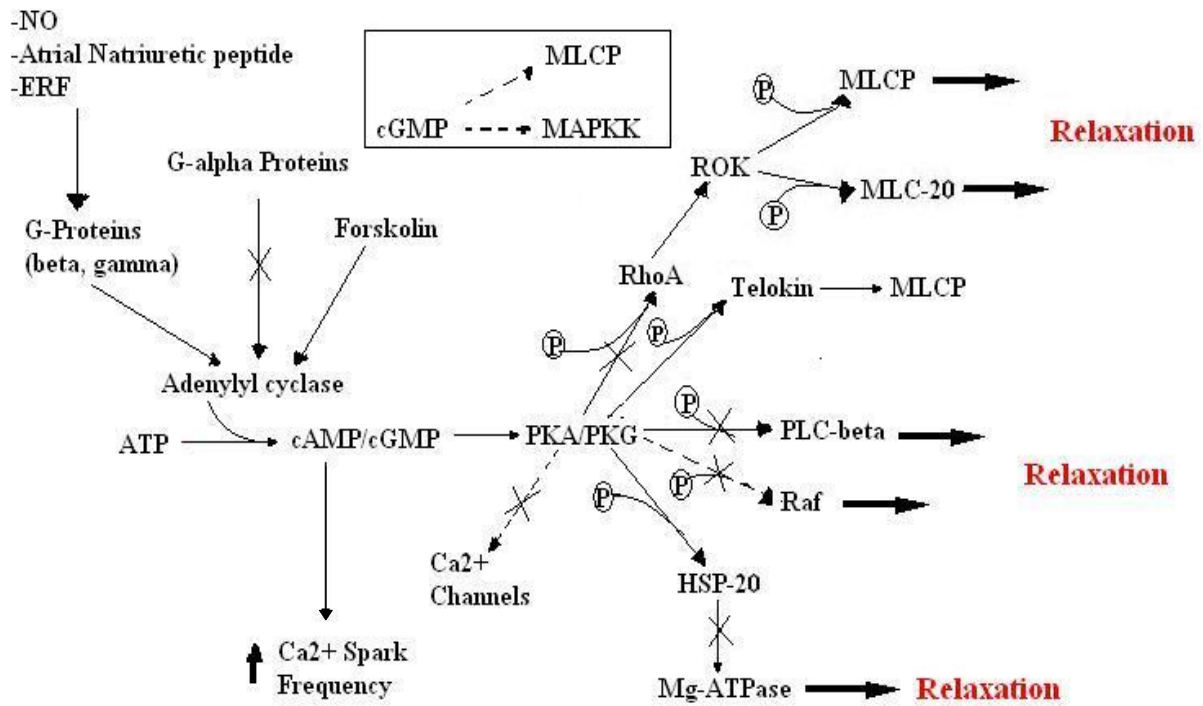
**Figure 12:** Conversion of Adenosine-triphosphate (ATP) into cyclic Adenosine-monophosphate (cAMP), catalyzed by adenylyl cyclase.



**cGMP**

**Figure 13:** Structure of cyclic guanosine-monophosphate (cGMP).

### Cyclic Nucleotide (cAMP/cGMP) Signaling in SM



**The effect of  $4 \times [cAMP] = [cGMP]$ .**

**Figure 14:** Diagram illustrating the signal transduction pathways of cAMP and cGMP in SM cells.

cAMP activates cAMP-dependent protein kinase (PKA) and cGMP activate cGMP-dependent protein kinase (PKG). There is evidence that cAMP may also activate PKG (Kotikoff 1996). Studies have also shown that four times the concentration of cAMP is required to cause 50% relaxation of vascular smooth muscle than cGMP (Dhanukoti 2000).

Increased levels of these cyclic nucleotides may cause reduction in cytosolic  $[Ca^{2+}]$ , via 1) Inhibition of PLC- $\beta$ , and thus  $IP_3$  production, 2) Inhibition of  $Ca^{2+}$  channels, 3) Activation of  $Ca^{2+}$  pumps in the PM and SR to remove  $Ca^{2+}$  from the cytosol (Abdel-Latif 2001). The secondary messengers have also been shown to increase the frequency of  $Ca^{2+}$ -sparks (Porter 1998).

PKA/PKG can phosphorylate and inhibit PLC- $\beta$  (Abdel-Latif 1996; Liu 1996) if it is anchored to the membrane by putative A kinase anchoring protein (AKAP86) (Dodge 1999). PKA/PKG can phosphorylate the G-protein Raf which stimulates mitogen-activated protein kinase kinase (MAPKK), but it is not clear whether this causes an inhibitory effect (Bornfeldt 1999; Cspedel 1999; Abdel-Latif 2001). Curiously, it has been found that cGMP may actually activate MAPKK, but the implications of this are not known (Komalavilas 1999; Kim 2000; Ho 1999).

PKA/PKG is capable of phosphorylating the GTPase protein RhoA to inhibit the Rho Kinase pathway, to be discussed later (Sauzeau 2000). PKA/PKG may also phosphorylate heat shock protein 20 (HSP-20), which directly inhibits the MgATPase, causing relaxation (Rembold 2000).

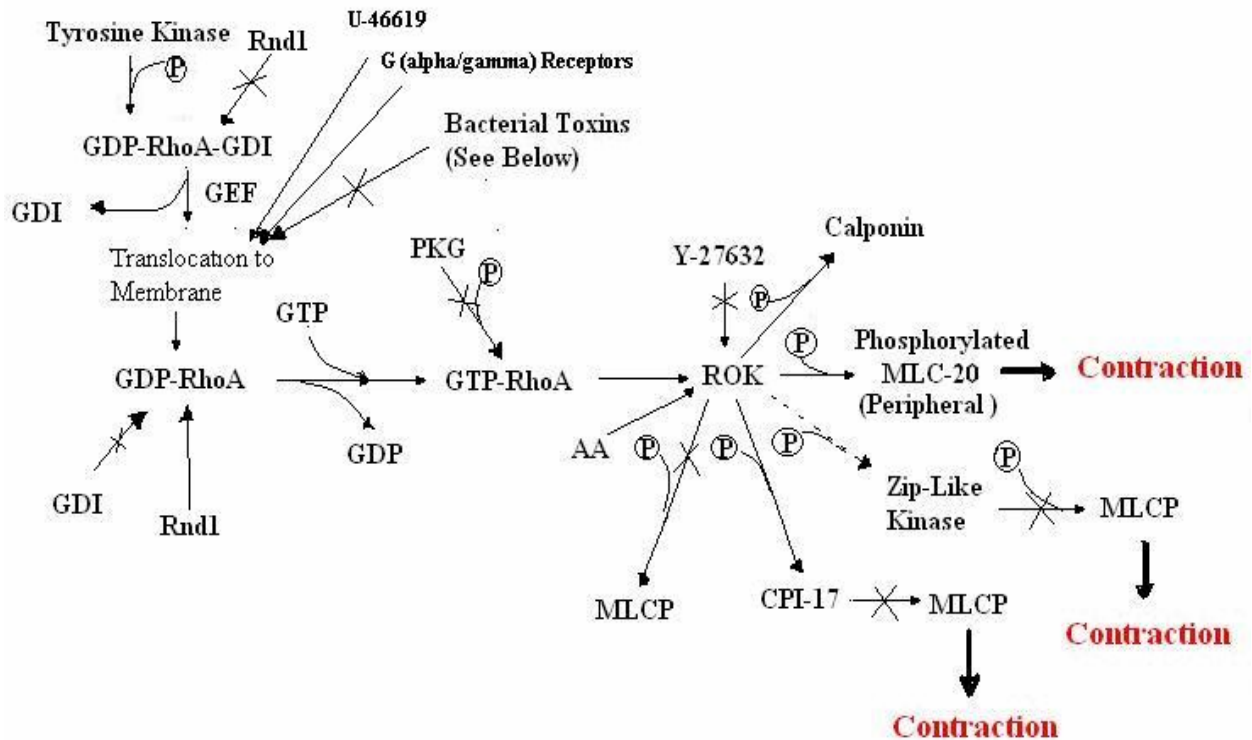
The pathway may also inhibit contraction by activating MLCP through phosphorylation of telokin, which activates the phosphatase (Wu 1998), and cGMP may activate MLCP directly (Lee 1997).

### ***RhoA/Rho Kinase Signaling***

Another important regulatory and recently studied pathway that is independent of  $[Ca^{2+}]$  is the RhoA/Rho kinase (ROK) pathway. RhoA is a small GTPase that is inactive when bound to GDP, and active when bound to GTP. Guanidine nucleotide dissociation inhibitors (GDIs) bind to RhoA-GDP in the cytosol (Gosser 1997; Longenecker 1999). The exchange of GDP for GTP is catalyzed by guanidine exchange factors (GEFs), which causes the GDI to dissociate (Kozasa

1998; Hart 1998). This facilitates the translocation of RhoA-GTP to the PM (Gong 1997; Fujihara 1997; Read 2000; Cherfils 1999).

### Rho Signaling in SM



Contraction = Tonic Phase Contraction

#### Bacterial Toxins (Reviewed-Sehr, 1998)

- Clostridium Botulinum*: ADP-ribosylation of RhoA at Asn-41
- Clostridium Difficile*: Monoglucosylates Thr-37 of RhoA

#### \*Calcium-Independent Regulation of Contraction (Calcium Desensitization)

**Figure 15:** Diagram illustrating the signaling pathways associated with RhoA/ROK in SM cells.

Many trimeric G-proteins activate the RhoA pathway by stimulation of GEFs (Kato 1998; Croxton 1998; Klages 1999; Hirshman 1999). It has also been found that tyrosine kinase inhibitors inhibit RhoA translocation to the PM, indicating that the pathway can be activated by tyrosine kinase receptors, as well (Sakurada 2001). U-46619 has also been shown to activate the pathway (Bradley 1987; Himpens 1988; Himpens 1990).

The active RhoA-GTP activates Rho kinase (ROK). However, activation requires that both units be translocated to the plasma membrane (Leung 1995; Gong 1997; Fujihara 1997; Taggart 1999). ROK can also be activated by AA (Fu 1998; Feng 1999). ROK induces contraction by phosphorylating and inhibiting MLCP (Kimura 1996; Feng 1999). ROK can also phosphorylate calponin (Katoch 1997) and CPI-17, which inhibits MLCP, as well (Koyama 2000; Kanecko 2000).

Ca<sup>2+</sup> sensitization facilitated by RhoA/ROK signaling only affects tonic SM contraction (Somlyo 2000). Inhibition of the pathway results in relaxation. Several points of inhibition have been observed. Some bacterial toxins can inhibit the translocation of RhoA-GTP to the PM. The toxin from *Clostridium botulinum* causes ADP-ribosylation at asparagine 41 (Asn-41) of the protein and that from *Clostridium difficile* causes monoglucosylation at threonine 37 (Thr-37) of RhoA (Fujihara 1997; Gong 1997). Y-27632 is a specific inhibitor of ROK (Uehata 1997; Somlyo 1997; Yoshi 1999; Fu 1998; Nakahara 2000). Rnd1 has properties that are antagonistic to RhoA, and inhibits the pathway (Loirand 1999). Also, hydrolysis of GTP complexed with RhoA to GDP, or re-complexation with GDI inhibits the pathway (Longenecker 1999).

It is interesting to note that the very specific Y-27632 ROK inhibitor has been shown to reduce blood pressure in hypertensive rats, but has no effect on normal rats (Uehata 1997), implicating that an overactive Rho pathway may cause some cases of high blood pressure. Use of the inhibitor as a drug is being investigated (Somlyo 1997).

It has been proposed that ZIP-like kinase—known to phosphorylate MLCP, and phosphorylate and activate CPI-17 (Macdonald 2001a; Ichikawa 1996a; Pfitzer 2001; Trinkle-Mulcahy 1995)—is a downstream link between PKC, ROK, and inhibition of MLCP. Two problems for direct phosphorylation of MLCP by ROK occur. First, the major phosphorylated site on MLCP is not inhibitory (Kitazawa 2002). Also, both RhoA-GTP and ROK are located at the PM, and MLCP is cytosolic (Pfitzer 2001). Thus, ZIP-like kinase has been found to co-purify with MLCP (Ichikawa 1996a), and is inhibited by ROK inhibitors and PKC inhibitors. So, it has been proposed as the missing link between converging pathways (MacDonald 2001a).

### ***MAPK Signaling***

Mitogen-activated protein kinase (MAPK) signaling has been more recently implicated in SM contraction. p42/p44 MAPK can directly phosphorylate MLC-20 (Takahashi 1998; Dessy 1998; Ohmichi 1997; Velarde 1999; Yousufzai 2000; Dechert 2001). It was found that potent inhibitors of the kinase inhibited PF<sub>2</sub>-induced contraction, but not IP<sub>3</sub> production (Yousufzai 1998), leading to the postulation that direct phosphorylation of MLC-20 is most important (Abdel-Latif 2001).

### MAPK Signaling in SM

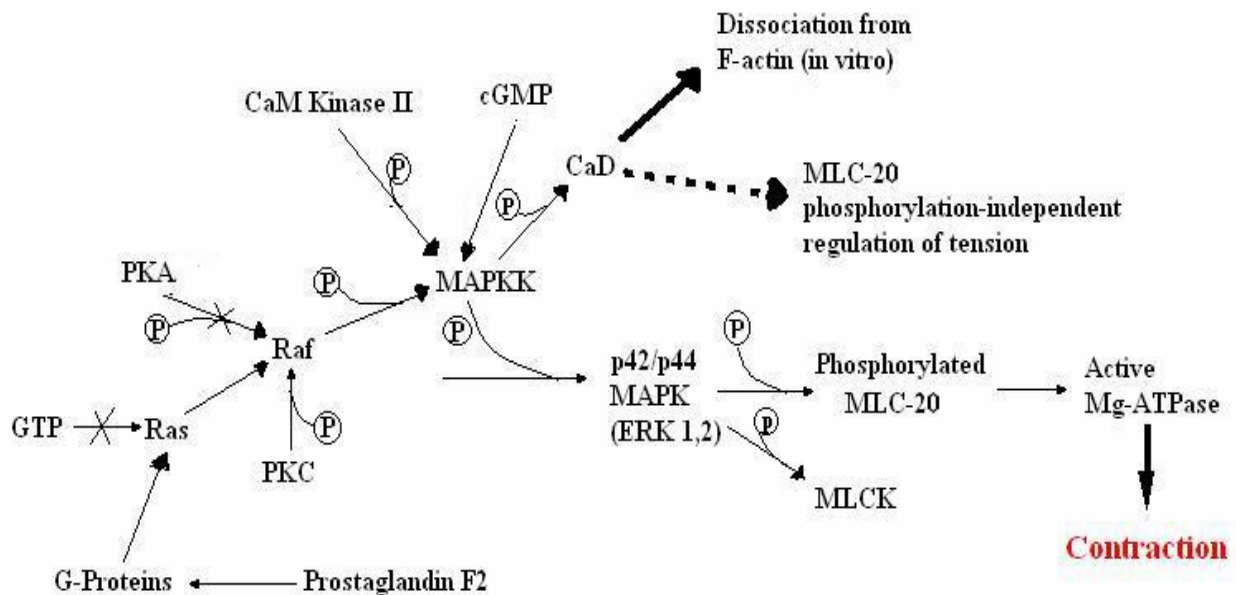


**Figure 16:** Diagram illustrating the signal transduction pathways associated with MAPK in SM cells.

MAPK signaling is induced by some G-protein receptors (Sah 2000). The complete mechanism leading to the MAPK cascade is still unclear (Abdel-Latif 2001). However, they may be facilitated by activation of the G-protein Ras, which activates Raf. Raf phosphorylates MAPKK, which phosphorylates MAPK (Neary 1997).

p42/p44 MAPK can also phosphorylate MLCK (Klemke 1997) to increase its activity. It has also been found to phosphorylate caldesmon (CaD) to cause its dissociation from F-actin. The effect of this dissociation is not, however, believed to have a large influence on contraction, as of now (Pearce 2003).



### ***Other Regulatory Proteins***

Calmodulin Kinase II (Cam KII) is activated when complexed with  $\text{Ca}^{2+}$  at a higher concentration than needed to activate MLCK (Tansey 1994). It can phosphorylate and inhibit MLCK to serve as a source of negative feedback for levels of  $\text{Ca}^{2+}$  that are too high, thus avoiding overconstriction (Word 1994). Autophosphorylation of Cam KII causes the effect to continue after  $[\text{Ca}^{2+}]$  levels have fallen (Somlyo 1994). Cam KII also activates MAPKK (Katoch 1999).

Phorbol esters stimulate contraction when added to SM tissue, and were the agonist used for studies conducted in this research, to be discussed later. They induce a modest increase in the level of MLC-20 phosphorylation (Itoh 1993), through activation of PKC, possibly phosphorylation of CaD (Adam 1992), or through activation of  $\text{PLA}_2$ , and subsequent release of AA. Slow phosphorylation of MLC-20, and slow development of tension at lower levels of MLC-20 phosphorylation are associated with contraction induced by phorbol esters (Itoh 1993), which has been proposed as an extreme case of latch (Somlyo 1994).

### **Caveolae**

An interesting recent discovery is that of caveolae—specialized gathering platforms of various shape. These platforms are composed of phospholipids and have been found in SM cells. It has been suggested that these platforms serve as meeting centers for interacting regulatory proteins involved in SM contraction, and are required for proper function of contraction, at least (Taggart 2001). Severe contraction disorders were observed in mice with a deficiency in caveolae (Drab 2001). Such caveolae may be important in other cell types and functions as well. More research needs to be done.

### **Study of SM**

As noted, SM demonstrates slightly different mechanistic properties. These properties are a function of its ultrastructural design and the biochemistry of its proteins. This project was begun in conjunction with colleagues Wright et al. from the Department of Physiology, Joan C.

Edwards School of Medicine (MUSOM), for the purpose of providing a comprehensive, global study of SM tissue. Wright et al. have investigated the mechanistic properties and dynamics of SM activity (including cytoskeletal rearrangement/remodeling of actin/myosin filaments, translocation of PKC within the cell, etc.) using confocal microscopy and methods similar to those mentioned previously (see smooth muscle mechanics), (Recent publications: Dykes 2003; Fultz 2003; Wright 2002; Li 2002, 2001a, 2001b; Geng 2001a/2001b; Fultz 2000; Fung 2000; Battistella-Patterson 2000; Wang 2000).

This composition focuses on the biochemistry of SM tissue at the level of the proteome. Operational behavior and regulation of the motor cross-bridges that facilitate motility and contractile properties occurs at the molecular level.

The complexity of the multiple pathways explains why such slow progress has been made on the understanding of signaling cascades in SM contraction. Different inhibitors and agonists of contraction converge at different points in the pathways. Much research has been done and is still being done on the effects of different agonists and receptor activation on contraction/relaxation (for example: Lincoln 1996; Luo 1997; Yang 1998; Yang 1999; de Alencar 2003. Reviews: Abdel-Latif 2001; Fernandes 2003; Koshimizu 2003).

Many traditional techniques have been utilized in the study of SM, such as cell culture and transgenic animal models coupled with gene transfections, and site-directed mutagenesis (for example: Yanboliev 2001; Cherie 2002; Hedges 2000, 1998; Dechert 2001). The physical dynamics of depolarization,  $Ca^{2+}$  levels in the cell, and protein translocation have also been probed, using such techniques as electrical field stimulation (EFS), patch clamps, and fluorescence confocal microscopy (for example: ZhuGe 2000; Huang 2003; Wang 2003; Dykes 2003; Fultz 2003; Li 2002). However, a major problem with this microscopy is that fluorescent indicator dyes must bind the cytosolic calcium in the cell. This binding removes  $Ca^{2+}$  from the cytosol and may greatly perturb the homeostasis of the system, affecting the accuracy of measured properties. Electron probe X-ray microanalysis allows the intracellular localization and transport of cellular components to be monitored (Review: Somlyo 2000). Extensive research is still conducted on the level of myosin phosphorylation, as well (for example: Facemire 2000; Sobieszek 2001).

## **Proteomics**

Although progress has been made using such techniques, it has been slow progress. Investigating each step individually takes more time. That is why it becomes necessary to develop a means of investigation that utilizes a broader perspective of the biological system.

This investigation focuses on the analysis of signal transduction at the proteome level through differential phosphorylation—the primary means of communication and activity modification of proteins. Protein phosphorylation serves as the on/off signal for many, if not most, of a cell's activities. The proteomic approach coupled with mass spectrometry (MS) analysis allows for high-throughput investigation of multiple proteins within a pathway, offering a glimpse of the entire picture of cellular activities under a given set of conditions. It must be emphasized that cellular communication does not occur linearly along a single pathway, but branches into multiple associations of messenger molecules and proteins. The pathways are interconnected.

This approach opposes the standard reductionist perspective of analysis in which isolated steps or individual proteins/enzymes are investigated. Such considerations explain why it has become necessary to incorporate the big picture into analysis. The proteome may be described as the sum of proteins expressed by a specific cell or tissue type under given physiological conditions. Proteins are the machinery which perform the vital functions that make life possible. Dysfunctional proteins are frequently the pathogen behind many human disorders.

The human genome project (HGP) has provided a comprehensive starting point for investigation. However, the genome provides only the blueprints for the cell's activities, furnishing a two-dimensional model that is often not straightforward. Not everything encoded in the blueprint goes into the finished product, and modifications are made along the way. After mRNA processing and post-translational modifications, the protein product is no longer equivalent to its gene complement. Proteins are often manufactured as nonfunctional pre-proteins, often with signaling peptides that instruct where it should be shipped to in or outside the cell. A peptide is clipped off the before the protein can fold correctly into the functional product.

With the capabilities of modern proteomic techniques the entire proteome of a cell can be viewed and investigated at once. Structural information and physical characteristics of proteins can be obtained using proteomic/MS analysis (see Appendix II). In general, proteomics

involves: 1) separation/isolation of proteins, 2) purification of analyte, and 3) analysis (see Appendix III).

The proteomic techniques used in this study were based on methodology developed by the research of Neal (2001) at Marshall University, with alteration of protocols, as necessary.

## Phosphoproteomics

Phosphoproteins were specifically targeted for the purpose of this investigation. As has been demonstrated and discussed in the preceding pathways, differential phosphorylation/dephosphorylation is a very important means of signal transduction and regulation in SM tissue. However, because of the standard analytical methods used thus far, few of the actual phosphorylation sites within these proteins are known (Appendix VI).

Phosphorylation of a protein or peptide occurs at serine, threonine, and/or tyrosine residues (Appendix V), and is mediated through a kinase. Dephosphorylation is catalyzed by a phosphatase, (Figure 17).

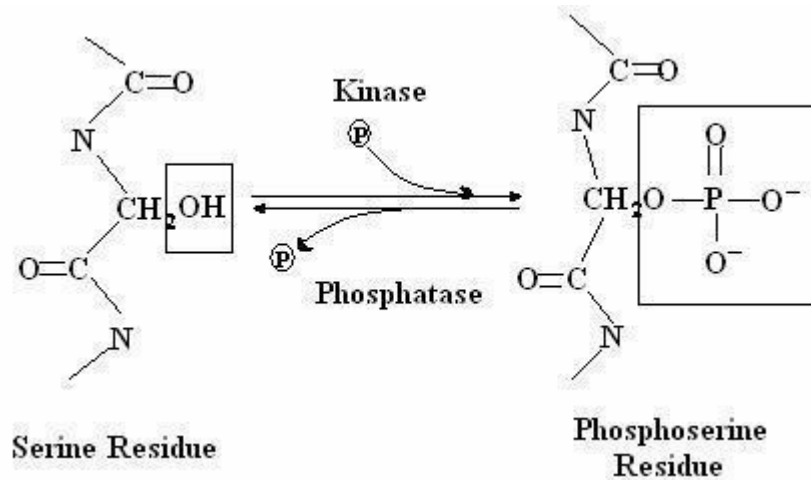


**Figure 17:** Illustration of the phosphorylation/dephosphorylation of serine.

Specific methodology exists for the analysis of phosphopeptides/proteins, including 1) means of detection and identification of phosphomoiety, 2) allocation of phosphorylation sites, 3) selective isolation of phosphopeptides, and 4) derivitization of phosphopeptides/proteins. Detection of phosphoproteins can be done on a 1D or 2D SDS-PAGE gel, either by specific

phosphoprotein stains, such as the ProQ Diamond Phosphoprotein Stain by Molecular Probes (Martin 2003), or via detection of autoradiography from cell lysates treated with radioactive isotopes of phosphorous ( $P^{33}$ ,  $P^{32}$ ). The latter method was based on a SM phosphorylation study done by Takuwa et al., in which several differentially phosphorylated proteins were noted, but not identified (Takuwa 1988). This was the initial driving force for the approach. However, the technique poses much more of a hassle due to the hazards and safety precautions associated with working with radioactive materials. It is also more expensive due to the high cost of radioactive  $P^{33}$ . Both methods have been explored in this research.

After phosphoproteins are subjected to proteolytic digest by an endoprotease, phosphopeptides can be selectively isolated through the use of  $Fe^{3+}$ -IMAC (Immobilized metal affinity chromatography) at relatively low expense. Phosphopeptides are negatively-charged species that demonstrate a high affinity for  $Fe^{3+}$  (Posewitz 1999). Other negatively-charged peptides—such as highly acidic peptides—are also bound by the IMAC. However, this problem can be circumvented if carboxylic acid groups are esterified prior to IMAC separation (Ficarro 2002).

Low stoichiometric abundance of phosphopeptides makes them more difficult to detect. Pre-isolation of such peptides increases their relative abundance in mass spectra, as interference of the more abundant non-phosphorylated peptides is removed. This methodology is known as enrichment, and has been used in many applications (Cao 2000; Stensballe 2001; Ficarro 2002; Raska 2002; Rocher 2003).

A condition for the analysis of phosphopeptides in positive ion mode is a low pH solution (see Appendix II). An acidified solution will facilitate protonation of phosphate groups, and allow molecular ions to obtain a net positive charge. Phosphoproteins normally carry a negative charge, which makes them hydrophilic, as well. This makes reverse-phase HPLC less efficient, which is set up to purify hydrophobic peptides. Therefore, it is best to purify phosphopeptides on a special column, such as the POROS OligoR3 (Wilm 1996; Neubauer 1999).

Many other methods for characterization of phosphoproteins/peptides exist, but were not investigated in this research. Direct dephosphorylation of peptides in triple quad mass spectrometers is an excellent example of the capabilities of more advanced instrumentation. Only a MALDI-TOF instrument was used in this work.

Phosphopeptides can also be reacted with various agents to create an analyzable derivative. Oxidation of the carbon-carbon (C-C) bond coupled with loss of the phosphate group next to it is termed  $\beta$ -elimination. This reaction is usually facilitated by the alkaline metal barium hydroxide ( $\text{Ba}(\text{OH})_2$ ), because of its greater efficiency at lower concentration than would be required of sodium hydroxide ( $\text{NaOH}$ ) (Figure 18). Serine, threonine, and carbamidocysteine residues are also safe against hydrolysis by  $\text{Ba}(\text{OH})_2$ , though free cysteines ( $\text{CH}_3\text{SH}$ ) and cystines ( $\text{CH}_3\text{S-SCH}_3$ ) are not (Bydford 1991).

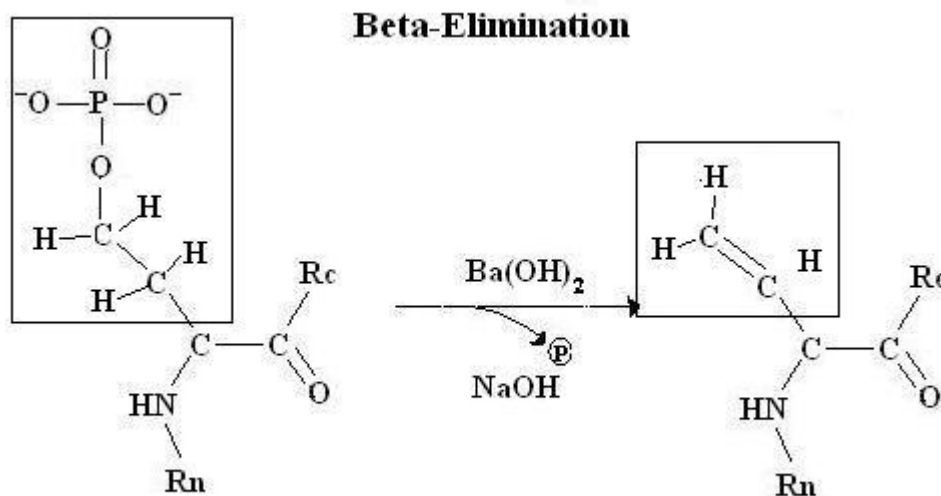


**Figure 18:**  $\beta$ -elimination of phosphate groups from a peptide using a barium hydroxide ( $\text{Ba}(\text{OH})_2$ ) catalyst, where  $\text{R}_c$  = C-terminal portion of peptide, and  $\text{R}_n$  = N-terminal portion of peptide.

Groups can then be added across the double bond via Michael addition to create useful derivatives, such as 2-aminoethanethiol or ethanedithiol (Figure 19). Derivatized peptides can be identified with MS and post source decay (PSD) (see Appendix II). The group can also be

oxidized off, leaving a neutral peptide to help confirm identification (Cole 1967; Mega 1996, 1990; Adamczyk 2001; Goshe 2001; Rusnak 2002; Steen 2002, 2003) (Figure 20).

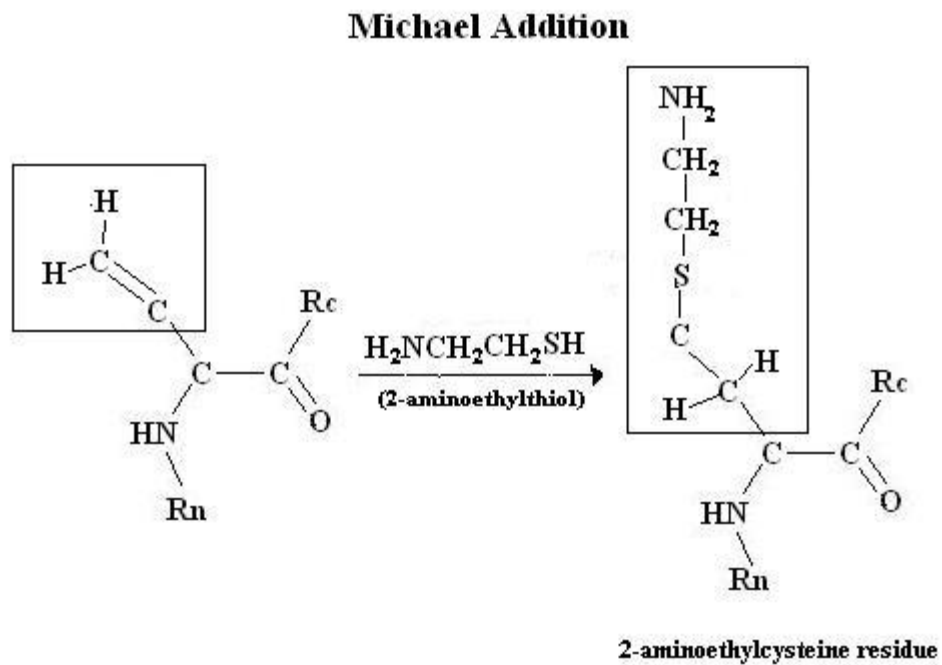


**Figure 19:** Michael addition of the nucleophilic 2-aminoethylthiol across the double bond of the peptide, creating a lysine-like residue, where Rc = C-terminus of peptide, and Rn = N-terminus of peptide.

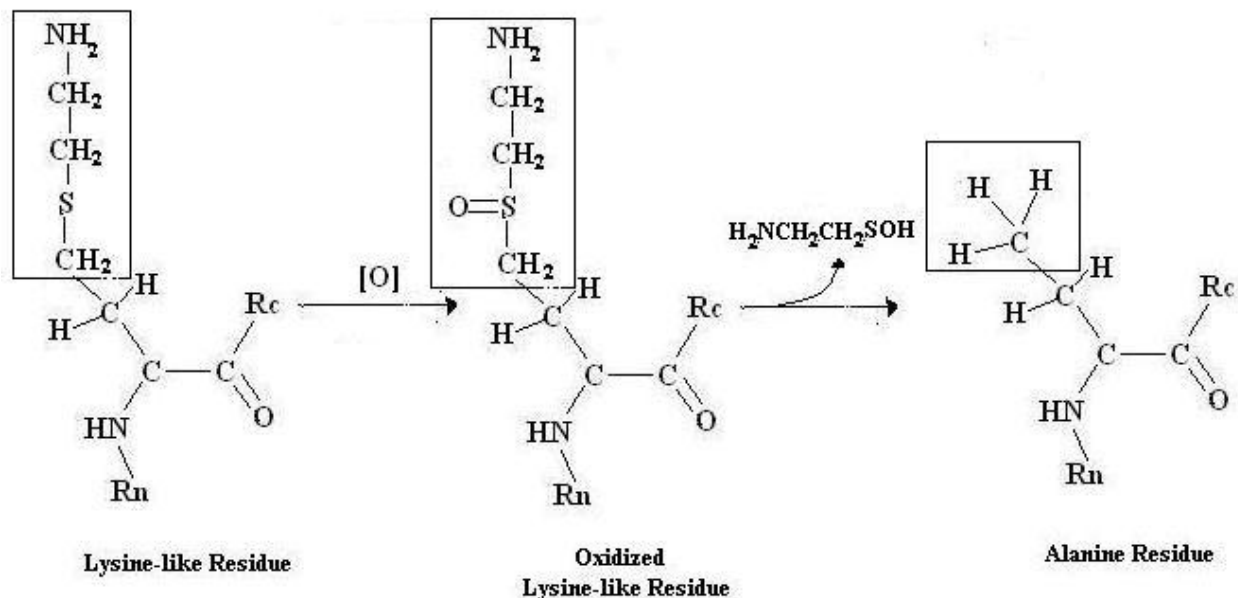


**Figure 20:** Oxidation of the lysine-like residue produces a sulfur-oxygen double bond which then dissociates from the peptide, finally leaving an alanine residue.

Another exciting and innovative capability of this method lies in the capacity of the 2-aminoethylcysteine derivatives (Figure 19) to be proteolytically cleaved by endoproteases specific for lysine—trypsin. Subsequent analysis of the fragments with MS will allow determination of phosphorylation sites within peptides with more than one serine/threonine residue, because only a phosphorylated Ser/Thr residue will be derivitized and cleaved. However, the technique is not useful for analyzing tyrosine phosphorylations.

In this research, the tonic phase of contraction, facilitated by prolonged exposure to an agonist, was investigated using aortic SM tissue from *Sprague Dawley* rats. It should be noted that due to prolonged exposure, functional remodeling of actin filaments and delayed relaxation post-contraction can occur, as was investigated by our colleagues at MUSOM.

Differential phosphorylation in resting and phorbol-contracted (Figure 21) tissue was probed using a phosphoproteomic approach coupled with MALDI-TOF MS. The goal was to look at the whole proteome and the signal transduction pathways there involved.



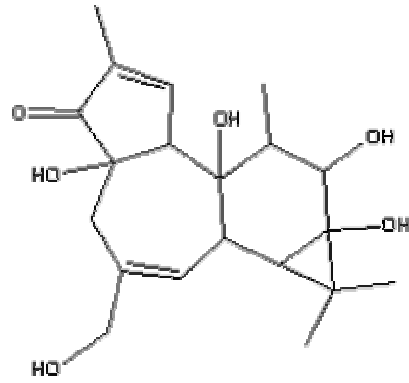


**Figure 21:** Structure of phorbol—the agonist used to contract the aortic SM tissue in this research.

## MATERIALS

### *Materials*

COMPANY	MATERIALS
American National Corp. (Chicago, IL)	-Parafilm
Becton-Dickinson (Franklin Lakes, NJ)	-Polystyrene conical tubes (15/50 mL)
BioRad (Hercules, CA)	-Eppendorf pipets -Ready gels
Fisher (Pittsburgh, PA)	-Redi-tips (1-10 $\mu$ L, 1-200 $\mu$ L, 1000 $\mu$ L) - Alkacid pH test paper - Microcentrifuge tubes (0.5 mL, 1.5 mL)
Genomic Solutions (Ann Arbor, MI)	-microtiter plates
Harvard Biosciences (Holliston, MA)	-DisposoBioDialyzers
Kimberly-Clark Corporation (Irving, TX)	-Kimwipes Ex-1
Millipore (Billerica, MA)	-ZipTips
Scientific Product (Cambridge, MA)	-Eppendorf pipets

### *Reagents*

COMPANY	REAGENTS
Acros Organics (Pittsburgh, PA)	-Acetone -Acetonitrile -Acetic acid (HPLC grade) -Glacial Acetic acid -EDTA

	<ul style="list-style-type: none"> <li>-Formic acid</li> <li>-H<sub>2</sub>O<sub>2</sub></li> <li>-Isopropanol</li> <li>-Iodoacetamide</li> <li>-Methanol (HPLC grade)</li> <li>-Sodium carbonate</li> </ul>
BioRad Lab. (Hercules, CA)	<ul style="list-style-type: none"> <li>-Silver stain plus kit</li> <li>-SYPRO ruby protein gel stain</li> <li>-Dithiothreitol</li> <li>-Prestained Precision protein stds.</li> <li>-Tris/Glycine/SDS buffer</li> <li>-Laemmli Sample Buffer</li> </ul>
Bruker-Daltonics (Billerica, MA)	<ul style="list-style-type: none"> <li>-HCCA</li> <li>-Sinapinic acid</li> <li>-peptide calibration stds.</li> </ul>
Fisher-Scientific (Pittsburgh, PA)	<ul style="list-style-type: none"> <li>-Ammonium acetate</li> <li>-Ammonium bicarbonate</li> <li>-Ammonium hydroxide</li> <li>-Dibasic sodium phosphate (Na<sub>2</sub>PO<sub>4</sub>)</li> <li>-Monobasic potassium phosphate (KH<sub>2</sub>PO<sub>4</sub>)</li> <li>-Dibasic potassium phosphate (K<sub>2</sub>H PO<sub>4</sub>)</li> <li>- ethylenediaminetetraacetic acid (EDTA)</li> <li>-Glycerol</li> <li>-Magnesium chloride (MgCl<sub>2</sub>)</li> <li>-Calcium chloride (CaCl<sub>2</sub>)</li> <li>-Sodium bicarbonate (NaHCO<sub>3</sub>)</li> <li>-Sodium chloride (NaCl)</li> <li>-SDS</li> <li>-Sodium thiosulfate</li> <li>-Triethanolamine</li> </ul>

	<ul style="list-style-type: none"> <li>- Tris</li> <li>-Potassium chloride (KCl)</li> <li>-Potassium ferricyanide</li> <li>-Urea</li> <li>-pH buffer std solutions (pH 4.00, 7.00, 10.00)</li> </ul>
Genomic Solutions (Ann Arbor, MI)	<ul style="list-style-type: none"> <li>-Pre-cast duracryl slab gels</li> <li>-Pre-cast carrier ampholyte pH 3-10 tube gels</li> <li>-Pre-cast immobilized pH gradient pH 3-10 tube gels</li> <li>-IEF Anode Concentrate (85% phosphoric acid)</li> <li>-IEF Cathode Concentrate (10.0 N sodium hydroxide)</li> <li>- IPG Urea/Thiourea Solubilization/Rehydration Buffer</li> <li>-Sample Buffer I</li> <li>-Sample Buffer II</li> <li>-Sample Buffer III</li> <li>-Tris-acetate buffer—25x concentration</li> <li>-Tris-acetate equilibration buffer</li> <li>-Tris/Tricine/SDS running buffers</li> </ul>
ICN Pharmaceuticals (Costa Mesa, CA)	<ul style="list-style-type: none"> <li>-Actin (rabbit muscle)</li> <li>-Ketamine</li> <li>-Xylazine-20</li> </ul>
Kodak	<ul style="list-style-type: none"> <li>- XOMAT-AR film (8" × 10") for autoradiography</li> </ul>
Molecular Probes (Eugene, OR)	<ul style="list-style-type: none"> <li>-ProQ Emerald 300 Glycoprotein stain Kit</li> <li>-ProQ Diamond Phosphoprotein stain</li> <li>-SYPRO Ruby Protein Stain</li> </ul>
Pierce (Rockford, IL)	<ul style="list-style-type: none"> <li>-GelCode Blue Protein Stain reagent</li> </ul>
Sigma-Aldrich (St. Louis, MO)	<ul style="list-style-type: none"> <li>-Brilliant Blue G (Coomassie Protein Stain)</li> <li>-Trifluoroacetic acid</li> <li>-Myoglobin</li> </ul>

<ul style="list-style-type: none"> <li>-β-Mercaptoethanol</li> <li>-Proteoprep Universal Extraction Kit</li> <li>-Sodium Phosphate</li> <li>-Trypsin—Proteomics grade</li> </ul>
--

### *Instrumentation*

COMPANY	INSTRUMENT
Applied Biosystems (Foster City, CA)	-130A Separation System HPLC
Barnstead (Boston, MA)	-Nanopure Infinity—Ultrapure water system
BioRad Lab (St. Louis, MO)	-Ready Gel Cell (1D SDS-PAGE) -GelDoc w/ Quantity One software
Bruker-Daltonics (Billerica, MA)	-Biflex III (MALDI-TOF MS)
Denver Instruments (Denver, CO)	-M-220D Electronic Balance
Fisher-Scientific (Pittsburgh, PA)	-Dry Bath Incubator -FS30 Sonicator -Micro-7 Microcentrifuge -Vortex Genie
Forma-Scientific (Marietta, OH)	-Lab/Pharmacy Freezer
Genomic Solutions (Ann Arbor, MI)	-ProGest Investigator (version 2.01.15) -ProPic Investigator Imager/Robot picking w/ Investigator HT Analyzer software -Investigator 2D Electrophoresis system w/ Investigator 5000 Programmable Power Supply
Lab-Line Instruments (Boston, MA)	-Shaking bath
Savant Instruments (Holbrook, NY)	-SpeedVac SC110 vacuum microcentrifuge w/

	refridgerated vaportrap RVT 4104 -μSpeed Fuge SFR13K refridgerated microcentrifuge
Thermo-Finnigan (San Jose, CA)	-LCQ

<i>BUFFERS AND SOLUTIONS</i>	
Krebbs Buffer (Incubation medium)	0.184 g CaCl <sub>2</sub> x H <sub>2</sub> O 0.29 g MgCl <sub>2</sub> 6.90 g NaCl 0.35 g KCl 0.16 g KH <sub>2</sub> PO <sub>4</sub> 2.1 g NaHCO <sub>3</sub> 0.9 g glucose -1 Liter H <sub>2</sub> O (37°C)
Lysis Buffer	500 μL Tris (0.1 M) 500 μL Glycerol (1mg/mL) 10 μL EDTA (0.5M) 5 μL Lupeptin (1 mg/mL in PBS) 5 μL Pepstatin (17.4 mg/mL in EtOH) 5 μL Aprotinin (1 mg/mL in EtOH) 25 μL PMSF -5 mL PBS
RIPA Buffer	50 mM Tris-HCl, pH 7.4 1% NP-40 0.25% Sodium Deoxycholate 150 mM NaCl 1 mM EDTA 1 mM PMSF 1 μg/mL aprotinin 1 μg/mL leupeptin 1 μg/mL pepstatin 1 mM Na <sub>3</sub> VO <sub>4</sub> 1 mM NaF
Phosphate Buffered Saline (PBS)	8.0 g NaCl

	0.2 g KCl 0.115 g Na <sub>2</sub> PO <sub>4</sub> 0.2 g K <sub>2</sub> HPO <sub>4</sub> 0.1 g CaCl <sub>2</sub> (Anhydrous) 0.1 g MgCl <sub>2</sub> -1 L H <sub>2</sub> O
Ketamine	100 mg/mL
Xylazine-20	20 mg/mL
Radioactive Phosphorous Solution	10 mCi P <sup>33</sup> / 0.5 μL H <sub>3</sub> PO <sub>4</sub>
Phorbol Solution	10 nm Phorbol in DMSO 10 μm Phorbol in DMSO (Excess)
Proteoprep Universal Extraction Kit (Sigma-Aldrich)	-Soluble Cytoplasmic Extraction Reagent -Cellular and Organelle Membrane Solubilizing Reagent -Soluble Protein Resuspension Reagent
Dialysis Buffer I	1.84 g Tris 5.8 g NaCl -1 L H <sub>2</sub> O
Dialysis Buffer II	Nanopure H <sub>2</sub> O
Laemmli Sample Buffer	62.5 mM Tris-HCl 2% SDS 25% Glycerol 0.01% Bromophenol blue
Tris/Glycine/SDS Buffer (1D SDS-PAGE)	25 mM Tris-HCl 192 mM Glycine 0.1% SDS
Sample Overlay Buffer	0.5 M Urea 0.2% Triton X-100



	0.1% Ampholytes 50 mM DTT (1/20 Sample Buffer Mix)
Sample Buffer I	0.3% SDS 200mM DTT 28 mM Tris HCl 22 mM Tris Base (Store -70° C)
Sample Buffer II	24 mM Tris Base 476 mM Tris HCl 50 mM MgCl <sub>2</sub> 1 mg/mL DNase I (Store -70° C)
Sample Buffer III	9.9 mM Urea 4% Triton X-100 2.2% Ampholytes 100 mM DTT (Store -70° C)
Sample Buffer Mix	80 mL Sample Buffer III <u>+ 20 mL Sample Buffer I</u> 7.92 M Urea 0.06% SDS 1.76% Ampholytes 120 mM DTT 3.2% Triton X-100 22.4 mM Tris HCl 17.6 mM Tris base (Store -70° C)
Modified Sample Buffer Mix	Sample Buffer Mix 1.5% SDS 150 mM DTT
IEF Cathode Buffer (1 <sup>st</sup> Dimension of 2D)	100 mM NaOH
IEF Anode Buffer	10 mM H <sub>3</sub> PO <sub>4</sub>
IPG Urea/Thiourea Solubilization/Rehydration	7 M Urea

Buffer	2 M Thiourea 2% CHAPS 65 mM DTT 1% Zwittergent 0.01% Bromphenol Blue 0.80% Ampholytes (pH 3-10)
IPG Equilibration Buffer I	6 M Urea 130 mM DTT 30% Glycerol 45 mM Tris Base 1.6% SDS 0.002% Bromphenol Blue --pH 7
IPG Equilibration Buffer II	6 M Urea 135 mM Iodoacetamide 30% Glycerol 45 mM Tris Base 1.6% SDS 0.002% Bromphenol Blue --pH 7
Tris/Acetate Equilibration Buffer	0.112 M Tris 5 % SDS 0.1 % Bromophenol blue 50 mM DTT (Refridgerated)
2D SDS-PAGE Cathode (2 <sup>nd</sup> Dimension of 2D)	0.2 M Tris 0.3 M Tricine 0.4 % SDS (Refridgerated)
2D SDS-PAGE Anode	25 mM Tris/Acetate (Refridgerated)
Coomassie Brilliant Blue Stain	0.25 g Brilliant Blue R250 40 mL MeOH

	50 mL H <sub>2</sub> O 10 mL Glacial AcOH (Filtered)
Coomassie Fixing/Destain	40% MeOH 50% H <sub>2</sub> O 10% Glacial AcOH
Silver Stain Fixing Solution	50% MeOH 10% AcOH 10% BioRad Fixative Enhancer Concentrate (Silver Stain Plus Kit) 30% H <sub>2</sub> O
Silver Stain (BioRad Silver Stain Plus Kit)	15.0 mL Silver Complex Solution 15.0 mL Reduction Moderator Solution 15.0 mL Image Development Reagent 105 mL H <sub>2</sub> O 150 mL Development Accelerator Solution
Silver Destain	30 mM K <sub>2</sub> Fe(CH <sub>3</sub> ) <sub>6</sub> in 100 mM Na <sub>2</sub> SO <sub>3</sub>
Silver Stain Stop Solution	5% AcOH
SYPRO Ruby Fixing/Destain Solution	10% MeOH 7% AcOH
SYPRO Ruby Protein Gel Stain	Use as is.
GelCode Blue Protein Stain	Use as is.
GelCode Blue Destain	H <sub>2</sub> O
ProQ Diamond Phosphoprotein Gel Stain	Use as is. (Keep from light)
Phosphoprotein Fixing Solution	10% TCA 50% MeOH
Phosphoprotein Destain Solution	50 mM Sodium Acetate 4% AcCN
Tryptic Digest Solutions—Manual	Washing/swelling—100 mM NH <sub>4</sub> HCO <sub>3</sub> Drying/shrinking—AcCN

	<p>Reduction—10 mM DTT in 100 mM NH<sub>4</sub>HCO<sub>3</sub></p> <p>Modification—55 mM Iodoacetamide in 100 mM NH<sub>4</sub>HCO<sub>3</sub> (Light protected)</p> <p>Digestion—2 µg/mL trypsin in 40 mM NH<sub>4</sub>HCO<sub>3</sub></p>
Tryptic Digest Solutions—ProGest	<p>Washing/swelling—40mM mM NH<sub>4</sub>HCO<sub>3</sub></p> <p>Drying/shrinking—AcCN</p> <p>Reduction—10 mM DTT in 40 mM NH<sub>4</sub>HCO<sub>3</sub></p> <p>Modification—100 mM Iodoacetamide in 40 mM NH<sub>4</sub>HCO<sub>3</sub> (Light protected)</p> <p>Digestion—20 µg/mL trypsin in 40 mM NH<sub>4</sub>HCO<sub>3</sub></p>
HPLC Base Solvent	<p>70% AcCN</p> <p>0.85% Glacial AcOH</p> <p>~30% H<sub>2</sub>O</p>
HPLC Water Solvent	<p>0.1% AcOH</p> <p>~100% H<sub>2</sub>O</p>
ZipTip (C-18) Solutions	<p>Wetting—50% AcCN</p> <p>Equilibration—0.1% TFA</p> <p>Wash—0.1% TFA</p> <p>Elution—70% AcCN in 0.1% TFA</p>
MALDI-TOF Matrix Solutions (Two Layer Spottin)	<p>1<sup>st</sup> Layer solution—5 mg/mL HCCA in 50% acetone</p> <p>2<sup>nd</sup> Layer solution—Saturated HCCA in 50% AcCN</p>

\*Solutions were prepared with >17 MΩ nanopure water.

## METHODS

**\*Procedures were performed at room temperature, unless specified otherwise in the protocol.**

## **I. Sample Preparation**

### ***Dissection/Tissue Extraction***

Male *Sprague dawley* rats of approximately the same size and weight were anesthetized with ~0.75 mL 2:1 Ketamine:Xylazine (100 mg/mL:20 mg/mL). Rats were obtained from MUSOM, care of Dr. Gary Wright and/or Dr. William McCumbee. Filled the tip of a syringe with ~20 mL heparin sodium, and drew blood from the heart, ~12 mL. Living aortic tissue was then surgically removed, and thoroughly cleaned of any adherent material. Tissues were temporarily stored/incubated in Krebbs buffer, 37°C.

### ***Radioactive Phosphorous Labeling***

Excised aortas were incubated in phosphate-free Krebbs buffer after extraction from the chest cavity at 37C. One hundred microliters of H<sub>3</sub>PO<sub>4</sub> was added to dilute a 1 μL aliquot of \_\_\_ mCi H<sub>3</sub><sup>33</sup>P<sub>04</sub>. All of the diluted radioactive phosphorous solution was added to the Krebbs buffer surrounding the aortas. The mixture was allowed to incubate for ~3.5 hours, to allow for cell uptake and chemical exchange of <sup>31</sup>P for the radioactive <sup>33</sup>P. All procedures were performed in designated radioactive work areas.

### ***Phorbol Incubation***

Aortic tissue was incubated in 37°C Krebbs buffer. Excess phorbol agonist was added to stimulate contraction—25 μL of 10<sup>-5</sup> M phorbol in DMSO per ~2.5 mL Krebbs buffer. Tissue was incubated ~0.5 hrs to facilitate a prolonged exposure to the contractile agonist.

### ***Cell Lysis***

#### **PROCEDURE 1**

Cells were lysed in 0.5-1.0 mL, depending on amount of tissue, chilled lysis buffer with grinding to homogenize tissue. Homogenate was then centrifuged at 12,000 RPM, ~12 min. The supernatant was collected as the aqueous protein extract.

#### PROCEDURE 2

Cells were lysed in 0.5 mL chilled RIPA lysis buffer, containing phosphatase inhibitors, with grinding to homogenize tissue. Homogenate was centrifuged at 12,000 RPM, ~12 min. The supernatant was collected as the aqueous protein extract, with lyophilization to concentrate, as necessary. The pellet was saved for extraction of membrane proteins.

### ***Solubilization of Membrane Proteins***

#### PROCEDURE 1

The pellet was boiled in 10% SDS to solubilize membrane proteins, ~10 min. The supernatant was collected as the membrane protein extract.

#### PROCEDURE 2

The pellet was boiled in sample buffer I, 100°C for ~5 min. The mixture was vortexed, and boiled again ~5 min. The mixture was centrifuged 12,000 RPM, ~10 min. The supernatant was collected as the membrane protein extract.

#### PROCEDURE 3

Genomic Solutions Protocol—The pellet was boiled in sample buffer I, 100°C for ~7 min. The mixture was then chilled on ice. Forty-five microliters of sample buffer II, containing RNase and DNase, were added. The mixture was chilled on ice ~8 min with sonication. Nine hundred microliters of acetone were added to produce an 80% v/v solution. The mixture was chilled on ice ~20 min. Then, the mixture was centrifuged at 10,000 RPM, ~15 min. The supernatant was removed, and the pellet was allowed to dry. The pellet was then redissolved in sample buffer mix.

#### PROCEDURE 4

Sigma ProteoPrep Universal Extraction Reagent—One milliliter of soluble cytoplasmic protein reagent was added to the pellet. The mixture was sonicated on ice, ~5 min, and then centrifuged at 4°C, 13,000 RPM for 45 min. The supernatant was collected as the aqueous membrane protein extract, which was then lyophilized to dryness, and redissolved in the soluble protein resuspension reagent. The pellet was redissolved in 1 mL of the cellular and organelle

membrane solubilizing reagent, and warmed to room temperature. The mixture was vortexed and sonicated, ~10 min, and then centrifuged at 13,000 RPM, ~45 min at 4°C. The supernatant was collected as membrane protein extract.<sup>178</sup>

## **II. Sample Purification**

### ***Acetone Precipitation***

Ice cold acetone was added to the supernatant and to the pellet to solubilize and wash away unwanted contaminants, leaving a more pure protein precipitate. The pellet was then redissolved in sample buffer mix, ready for gel electrophoresis.

### ***Dialysis***

One hundred  $\mu\text{L}$  of sample mixture were loaded into a DispoBioDialyzer unit from Harvard Biosciences. Air bubbles were removed from the surface of the dialysis membrane as the unit was placed into the dialysis buffer. Samples were dialyzed overnight in either dialysis buffer I or dialysis buffer II, with at least one change of buffer.

## **III. Separation/Isolation of Proteins**

### ***1D SDS-PAGE***

A 1D gel apparatus from BioRad was used to facilitate 1D SDS-PAGE. All parts of the apparatus should be sufficiently cleaned and rinsed with nanopure water. Samples were mixed in a 1:1 ratio with Laemmli Sample Buffer to reduce the sample. Samples were then heated to 95° for approximately 3 minutes. Tris/Glycine/SDS running buffer was added to the tank of the apparatus to serve as both the anode and cathode buffer. Fifteen to twenty  $\mu\text{L}$  of the sample mixture was loaded into the well of the gel. Every other well was used to avoid cross-contamination of proteins during propagation through the gel. Prestained MW standards from BioRad were loaded into the wells at each end of the gel. Gels were subjected to 100 V for ~45-90 minutes, or until the blue dye front reached the bottom of the gel.

## ***2D SDS-PAGE***

A 2D gel apparatus from Genomic Solutions was used to facilitate 2D SDS-PAGE. All parts of the apparatus should be sufficiently cleaned and rinsed with nanopure water. Eleven liters of freshly prepared SDS-PAGE anode buffer was poured into the lower tank of the slab gel apparatus. The cooling plate was turned on to allow the buffer to cool overnight. Three liters of freshly prepared SDS-PAGE cathode solution was refrigerated overnight, as well.

### ***1<sup>st</sup> Dimension Separation***

#### **Tube Gel Procedure**

IEF anode buffer was poured into the tank of the IEF apparatus. The tube gel apparatus was lowered into the tank. One tube gel per sample was installed into the apparatus, with removal of air bubbles from both sides of the tube with a syringe filled with the appropriate anode or cathode solution. Approximately 50  $\mu\text{L}$  of sample overlay buffer was then loaded into each tube gel. Samples were mixed 1:1 with sample buffer mix, if not already solubilized in this buffer. Fifty  $\mu\text{L}$  of the sample mixture was loaded into the tube gel. Eight hundred milliliters of IEF cathode buffer was poured into the upper chamber of the apparatus. Gels were focused for 17.5 hours at a maximum voltage of 2000 V and a maximum current of 110  $\mu\text{A}$  per gel.

Tube gels were placed on ice for ~10 minutes. Tube gels were then extruded into ~2 mL of IEF equilibration buffer, and allowed to incubate for no more than 2 minutes. Tube gels were loaded onto slab gels for second dimension separation.

#### **IPG Strip Procedure**

Four hundred microliters of IPG urea/thiourea solubilization/rehydration buffer was added to the protein precipitate obtained from the acetone precipitation. This mixture was distributed evenly between the electrodes of the pHaser tray. IPG strips were placed gel-side down over top of the mixture, removing air bubbles from underneath the strip. Tray was placed in a plastic bag with a piece of moistened filter to keep gels from drying out. Samples were allowed to rehydrate for ~16 hours.

The pHaser tray was placed into the voltage housing unit. The unit was set on top of a chiller. A moistened wick was placed between the electrodes and the ends of the gel strips. Approximately two milliliters of mineral oil was spread over the top of the strip. Strips were



focused for 24.5 hours with a maximum voltage of 5000 V and a maximum current of 80  $\mu$ A per gel. The temperature was maintained between 15-20 °C during focusing. Wicks were replaced every hour for three hours to aid in the removal of salts.

IPG strips were placed in ~10 mL IPG equilibration buffer I and agitated for ~10 minutes. The buffer was discarded and this step was repeated. The buffer was discarded and ~10 mL of IPG equilibration buffer II was added to the tray. The strips were agitated for ~10 minutes. Strips were removed from buffer and loaded onto slab gels for second dimension separation.

### ***2<sup>nd</sup> Dimension Separation***

The 2D SDS PAGE anode and cathode buffers were previously chilled overnight. The tank of the slab gel was filled with 11 L of 2D SDS PAGE anode buffer. Grooves of slab gels (housing the tube gels or IPG strips) were filled with 2 $\times$  2D SDS PAGE cathode buffer. Slab gels were loaded into the slab gel apparatus, securing grommets around slab gel to prevent leakage of solutions. The slab gel apparatus was lowered into the tank. The upper chamber of the apparatus was filled with three liters of 2D SDS PAGE cathode buffer. A maximum of 500 Volts was applied across the gel for approximately 4.5-5 hours, or until the blue dye front reached the bottom of the gel. Gels were removed from cassettes and washed in nanopure water for 10 minutes with one change of water.

## **IV. Analysis**

### **Visualization of Protein Bands**

## ***Autoradiography***

2D gel with proteins was wrapped in plastic wrap and placed into an autoradiography cassette. In the dark, a piece of XOMAT-AR film paper was placed on top of the gel. The cassette was closed and sealed that no light could get into the cassette. Gels were exposed for 12 hours for the first trial, and then 36 hours for the second trial.

## ***Gel Staining***

### GelCode Blue Protein Stain

One dimension protein gels were agitated in GelCode Blue protein stain for three hours. The solution was removed. Gels were then agitated in nanopure water to reduced background staining. Gels were imaged with a visible light source.

### Phosphoprotein Stain

Gels were agitated in ~500 mL of phosphoprotein fixing solution for one hour with one change of fixing solution. The solution was removed. Gels were then washed with ~500 mL of nanopure water for ~15 minutes to remove the methanol and acetic acid from the gel. This step was repeated three times. Gels were agitated in 500 mL of ProQ Diamond Phosphoprotein Gel Stain in the dark for four hours. The solution was removed, and gels were agitated in phosphoprotein destain solution in the dark for a total of four hours with three changes of destain solution. Gels were imaged with a visual source.

### Coomassie Brilliant Blue Protein Stain

Gels were agitated in ~500 mL of Coomassie fixing/destain solution for one hour to fix proteins to gel and remove any remaining SDS from the gel. The solution was discarded. Gels were then agitated in ~500 mL of Coomassie Brilliant Blue stain overnight. The solution was removed, and ~500 mL of Coomassie fixing/destain was added. Gels were agitated in destain for one hour. The destaining step was repeated up to four times to remove enough background stain for protein bands to be effectively visualized. Gels were imaged with a visual light source.

### SYPRO Ruby Protein Gel Stain

Gels were agitated in ~500 mL of Ruby fixing/destain solution for 30 minutes. The solution was removed. Gels were then agitated in ~500 mL SYPRO Ruby protein gel stain overnight. The solution was discarded, and gels were agitated in ~500 mL of SYPRO Ruby fixing destain solution for 30 minutes. Gels were imaged with a UV light source.

## Silver Stain

Gels were agitated in ~800 mL of silver fixing solution for 30 minutes. The solution was removed. Gels were then washed with nanopure water for 20 minutes with agitation. This step was repeated. The silver stain was prepared fresh immediately prior to use, and gels were agitated in stain for ~20 minutes, or until protein bands were effectively visualized. The solution was removed, and the silver stop solution was added immediately. Gels were imaged with a visual light source.

## **Gel Imaging**

Gels were imaged and analyzed using either the BioRad GelDoc Imager or the Genomic Solutions ProPic Investigator Imager. Either a visible or UV light source was used to image the gels, according to that required by the excitation/emission wavelength of the method of staining.

## **Proteolytic Digest of Proteins—In Gels (Tryptic Digest)**

Protein bands were excised from the gel either by hand for manual excision or by the Genomic Solutions ProPic Investigator for automatic excision. For silver stained gels, excised bands were incubated in silver destain solution for 30 minutes. This solution was then removed and bands were washed three times with nanopure water for a total of 30 minutes, 10 minutes between changes of water.

Gel bands were incubated in AcCN for 10 minutes to destain and/or dehydrate gel pieces. Gel bands were then lyophilized in a SpeedVac to remove the AcCN. A reducing buffer of 10 mM DTT in 100 mM  $\text{NH}_4\text{HCO}_3$  was added to the gel pieces, which were then incubated for one hour at 56°C.

The solution was discarded and gel bands were allowed to cool to room temperature. A modification buffer of 55 mM iodoacetamide in 100  $\text{NH}_4\text{HCO}_3$  was added to the gel pieces, which were then incubated at room temperature in the dark for ~45 minutes.

The solution was discarded and gel pieces were washed with 100 mM  $\text{NH}_4\text{HCO}_3$  for 20 minutes. This solution was discarded and gel pieces were dehydrated with AcCN. The AcCN was removed. These steps were repeated. Gel pieces were then lyophilized to remove all AcCN.

Twenty microliters of a 2  $\mu\text{g/mL}$  (pH 8.5) solution of modified trypsin in 40 mM  $\text{NH}_4\text{HCO}_3$  was added to the gel pieces. The trypsin was allowed to digest the proteins overnight at 37°C to cleave the protein at arginine and lysine amino acid residues.

The supernatant was collected. Peptide fragments were extracted with one change of 20 mM  $\text{NH}_4\text{HCO}_3$  and three changes of 5% formic acid in 50% AcCN. All washes were collected, and the solution was lyophilized in a SpeedVac to necessary volumes.

## **Desalting**

### ***Reverse Phase HPLC***

Fifty microliters of the sample was loaded into the HPLC injection port. For protein samples, a C-4 column was used, and for peptide samples, a C-18 column was used. Samples were passed over the appropriate column. Salts and contaminants were washed through the column with 0.1% AcOH. Proteins/peptides were eluted off the column with a gradient increase of 70% AcCN in 0.085% AcOH. A UV/Visible wavelength spectroscopic detector set at 214 nm was used to detect the amine groups of the proteins/peptides. The eluant was lyophilized in a SpeedVac to approximately two microliters in preparation for MALDI-TOF MS. If samples were lyophilized to dryness, they were redissolved in 5% formic acid in 50% AcCN.

### ***Ziptip desalting***

Samples were previously concentrated to 10  $\mu\text{L}$  of volume, or were redissolved in 10  $\mu\text{L}$  of 0.1% TFA if dry. A ziptip was attached to an eppendorf pipette. For proteins, a C-4 packed tip was used, and for peptides, a C-18 packed tip was used. The ziptip was wetted by aspirating 10  $\mu\text{L}$  of wetting solution. The ziptip was then equilibrated by aspirating 10  $\mu\text{L}$  of equilibration/wash solution. Proteins/peptides were bound to the beads of the tip by aspirating the sample mixture for 10-15 cycles. The sample was washed by aspirating 10  $\mu\text{L}$  of equilibration/wash solution three times. Proteins/peptides were eluted with 20  $\mu\text{L}$  of elution solution, followed by a third extraction of 100% AcCN to remove all proteins/peptides from the tip. The eluant was lyophilized in a SpeedVac to approximately two microliters in preparation for MALDI-TOF MS. If samples were lyophilized to dryness, they were redissolved in 5% formic acid in 50% AcCN.

## MALDI-TOF Analysis

### *Spotting*

Samples were spotted using the two layer method of spotting to ensure homogenous spots of samples. A volume of 0.7  $\mu$ L of the first layer solution was spotted onto the MALDI probe to create a homogenous layer of matrix. The volatile solvent assures fast evaporation.

Concentrated and desalted samples were mixed 1:1 with the second layer solution, with aspiration to mix. A volume of 0.7  $\mu$ L of this mixture was spotted on top of the dried first layer. This layer was allowed to dry before the MALDI probe was inserted into the instrument.

### *Calibration*

#### External Calibration

A Bruker Biflex III MALDI-TOF MS was used for analysis in this investigation. The instrument was calibrated in the peptide fingerprint range using a sample of peptide standards of known m/z value. The standards were stored in a solution of 0.1% TFA, and spotted on the MALDI probe according to the procedure outlined above. A linear calibration was performed using the monoisotopic m/z values of the standards listed in table 2.

External calibration was performed immediately preceding acquisition of data for sample analysis. It is important that a calibration be performed if any of the parameters of the instrument are changed—voltage, laser power, etc.—prior to acquisition of data.

**Calibration Standards**

<b>Peptide Standard</b>	<b>M/Z Value</b>
Angiotensin II	1046.542
Angiotensin I	1296.685
Substance P	1347.736
Bombesin	1619.823

ACTH clip 1-17	2093.086
ACTH clip 18-39	2465.199
Somatostatin-28	3147.47

**Table 2:** List of the peptide standards and corresponding m/z peak values used for external and internal calibration of MALDI spectra.

### Internal Calibration

An aliquot of the sample mixture was spotted on the MALDI probe as outlined above. One microliter of a 1/20 dilution of the peptide standards from table 2 was added to the sample:matrix solution, with aspiration to mix. This mixture was then spotted as the second layer in the spotting method outlined above.

A suitable spectrum was collected for each spot. The spectrum containing the standards was calibrated using the correct m/z values for the standard peaks. Then, three to four sample peaks that spanned a range representative of the sample spectrum were selected to calibrate the spectrum from the sample. These peaks were matched to their corresponding peaks in the uncalibrated spectrum, and used to calibrate this spectrum.

### ***Data Acquisition***

Samples were analyzed on a Bruker Biflex III MALDI-TOF MS. Analysis was performed in reflectron mode (see Appendix II) in the range of 500 to 4000 Da. The delayed extraction time period was set to medium. Preliminary data from a sample spot was collected to fine tune the attenuation of the laser power and IST voltages of the instrument to a level which provided the best spectrum. The instrument was then calibrated externally under these parameters.

The sample spot was searched for an area which gave the highest S/N ratio peaks. Then an averaged spectrum of ~100 laser shots was collected. This was done for each sample to provide digest (peptide fingerprint) spectra for each.

### ***Post Source Decay (PSD)***

The instrument was externally calibrated according to the procedure outlined above. A standard sample spot of ACTH clip 18-39 was used to calibrate the instrument. The ion gate was

set to the m/z value for the standard to deflect unwanted particles (see Appendix II). A suitable spectrum was collected for each mass range afforded by the KE filter. Various parameters were manipulated—deflection time, IS/T voltages, laser power—to optimize the conditions of the instrument to provide the best spectra. The series of pre-pasted spectra were collected for the standard, and then compared by the instrument to the known m/z fragmentation values of the standard. The instrument was calibrated in this manner to produce the final calibrated fragmentation spectrum.

The m/z of the peptide to be analyzed was set in the ion gate. The sample spectra were collected in the same way as the standard. Data was acquired under the same parameters as the standard to maintain calibration.

### **Identification of Unknown Proteins/Protein Database Searching (MASCOT)**

Peptide fingerprints of proteins were matched to those found in online protein databases using the MASCOT search engine from Matrix Science of London<sup>237</sup>, using the specifications listed in table 3, below.

<b>Missed Cleavages</b>	<b>Cystine Modifications</b>	<b>Methionine Modifications</b>	<b>M/Z Mass Range</b>	<b>Taxonomy</b>
Up to 2	Carbamidomethyl (Acetamide)	Oxidized	2 Da	Rodentia

**Table 3:** List of the specifications entered into the search form of the MASCOT search engine protein database.

Contaminating trypsin peaks were first eliminated from the peak list. Trypsin peaks were determined from a peptide fingerprint map of a theoretically digested trypsin protein with dimethylated lysines and oxidized methionines and/or from a self-digested mixture of trypsin and a blank piece of gel, as performed in the laboratory at Marshall University.

Once the matching fingerprints were identified using MASCOT, likely protein candidates were produced by the database search engine. The peptide fingerprint of the smooth muscle isoform of the putative protein, if available, may have been compared manually to the sample's spectra to look for possible phosphorylation sites or other modifications, assuming the putative

protein produced was within the correct molecular weight range estimated from the position of the protein band on the 2D gel and the score of the putative match is significant.

The search engine matches peaks and uses a probability function to provide a score. The score is a representation of the probability that a correct match has been obtained, (equation \_\_\_).

$$\text{MASCOT score} = -10 \log P \quad (19)$$

where P = the probability that the match could occur randomly in nature. Only those candidates with significant scores (>56) were reported in the results section of this work.

The website search engine also provides a percentage of the protein's amino acid peptide fragment sequence covered by the m/z peak list entered into the database.

## **RESULTS AND DISCUSSION**

The primary objective of this work focused on the analysis of differential protein phosphorylation between resting and contracted aortic SM tissue using proteomic techniques and MALDI-TOF mass spectrometry. It was hoped that this versatile technique coupled with the application of protein database information would help clarify the signal transduction pathways at work in smooth muscle tissue. However, many challenges were encountered in pursuit of this goal, so that the body of this discussion focuses, instead, on the development of protocol for the



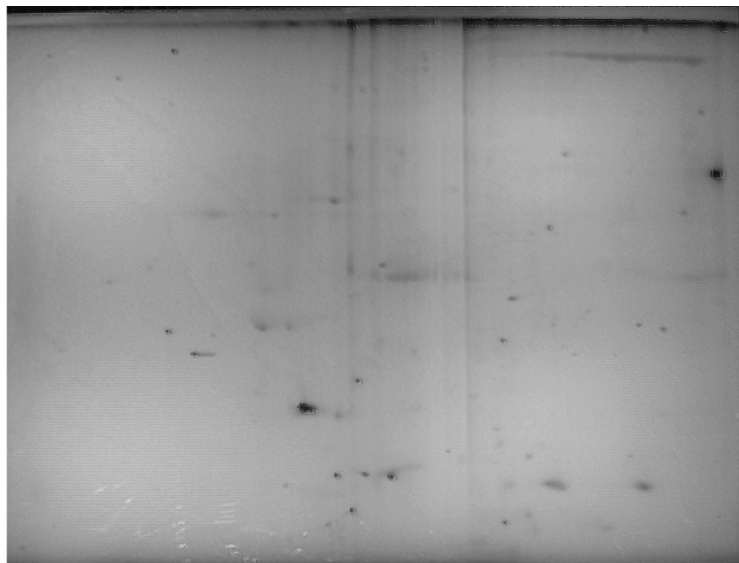
analysis of phosphoproteins. Many problems have been investigated and resolved, while some difficulties remain. These difficulties limit the scope of this research.

## **2D Gel Electrophoresis**

The quantity of proteins separated and visualized on a 2D gel using tube gel IEF focusing was found to be too low to allow adequate sample analysis. A tube gel apparatus was initially used to focus proteins based on their pI in the first dimension separation of the 2D electrophoresis. The maximum quantity of protein that may be loaded into the tube gel is 100  $\mu\text{g}$ , dissolved in 50  $\mu\text{L}$  of buffer. The 2D gels obtained by this method had to be stained with the more sensitive stains, such as silver stain or SYPRO ruby stain with a limit of detection near 1 ng, to allow any type of visualization. Staining with the colloidal Coomassie blue stain (limit of detection—1  $\mu\text{g}$ ) proved to be insufficient.

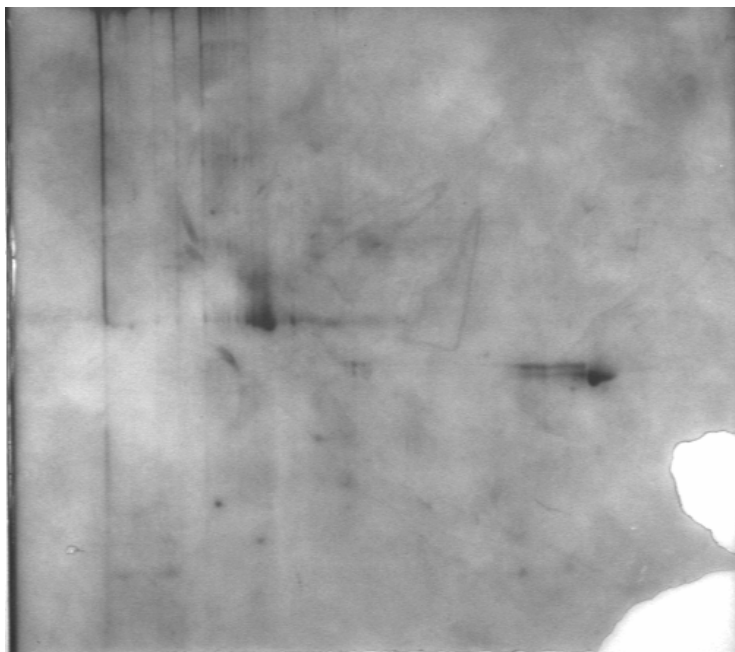
Some gels showed very little visualization of protein bands even with such sensitive stains. Figures 22-32 depict gels stained with the more sensitive silver stain and SYPRO ruby protein gel stain. A considerable amount of nonspecific or artifact staining (blots of stain that do not represent protein bands) can be seen on those gels stained with silver stain.

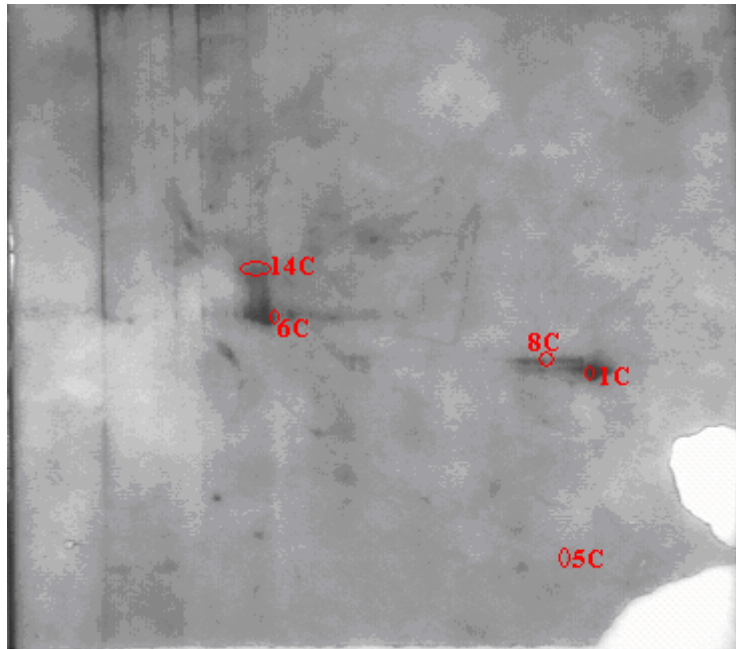
**2D\_7\_24\_01\_Phorbol\_sup**



**Figure 22:** Example of a 2D gel containing supernatant or aqueous proteins from phorbol-contracted aortic SM tissue stained with silver stain, revealing very little evidence of protein bands.

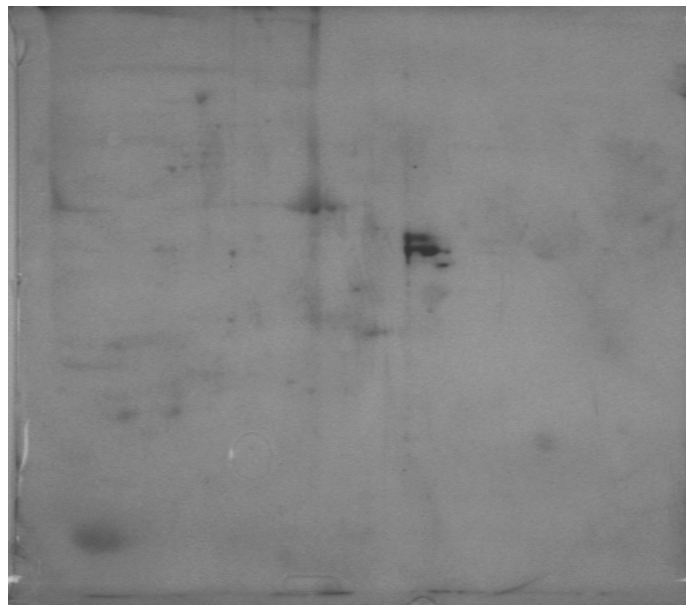
**2D\_7\_30\_02\_Control**

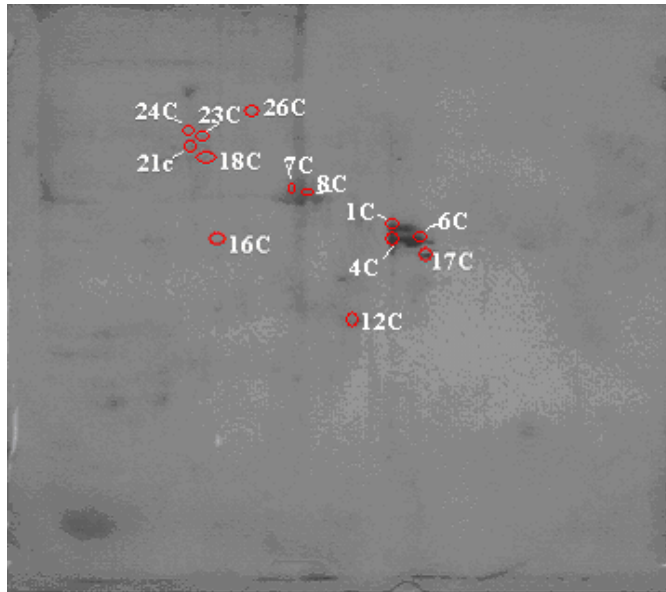




**Figure 23:** Example of a 2D gel containing supernatant or aqueous proteins from resting aortic SM tissue stained with silver stain, revealing very little evidence of protein bands.

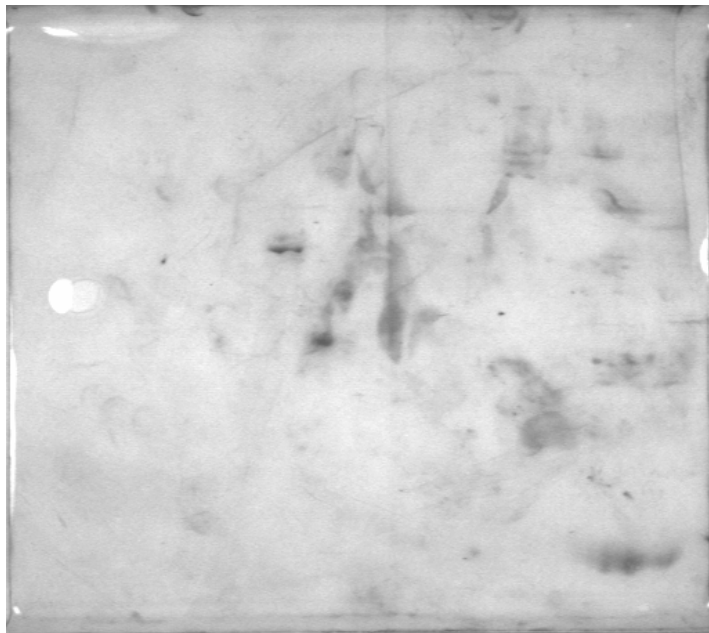
### **2D\_10\_09\_02\_Control**





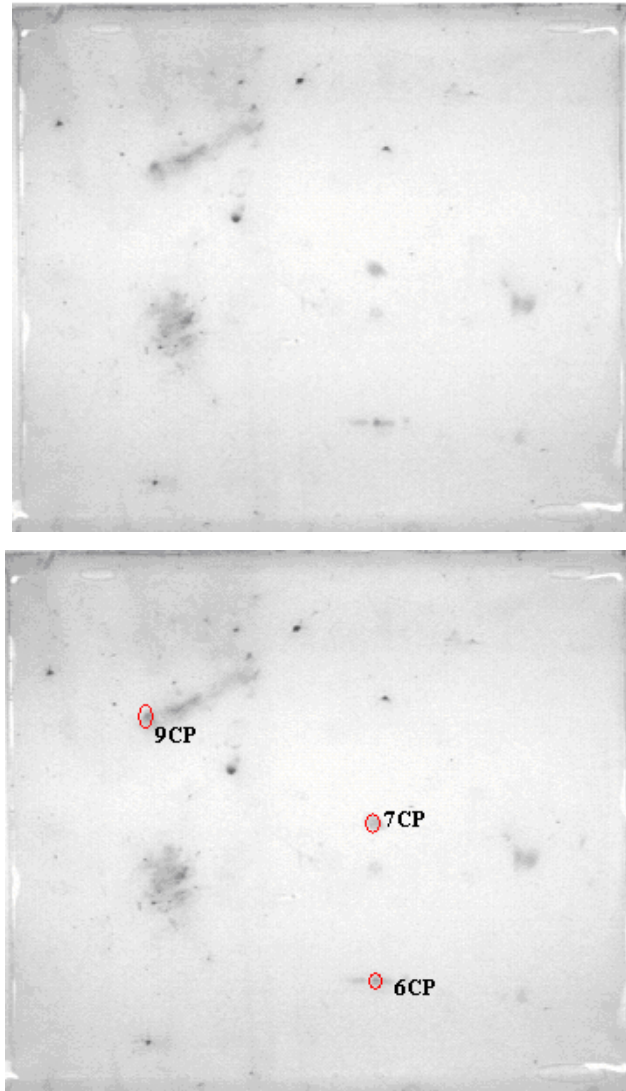
**Figure 24:** Example of a 2D gel containing supernatant or aqueous proteins from resting aortic SM tissue treated with RNase and DNase prior to electrophoresis. This gel was stained with silver stain, and reveals very little evidence of protein bands.

#### 2D\_10\_09\_02\_Phorbol



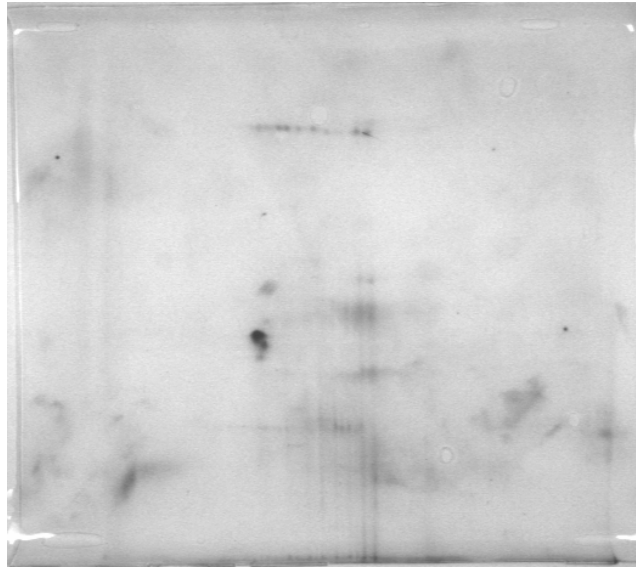
**Figure 25:** Example of a 2D gel containing supernatant or aqueous proteins from phorbol-contracted aortic SM tissue treated with RNase and DNase prior to electrophoresis. This gel was stained with silver stain, and reveals very little evidence of protein bands.

**2D\_10\_09\_02\_Control\_Pell**



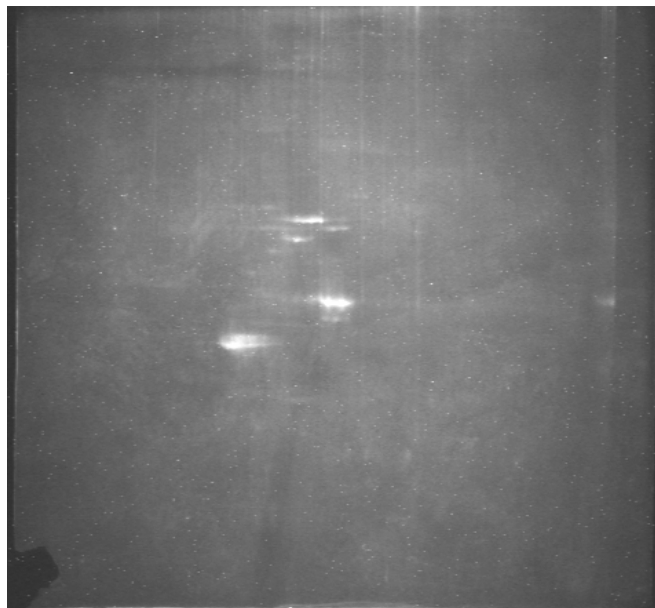
**Figure 26:** Example of a 2D gel containing membrane proteins from resting SM tissue, where proteins were solubilized in boiling 10% SDS and treated with RNase and DNase prior to electrophoresis. This gel was stained with silver stain, and reveals very little evidence of protein bands.

**2D\_10\_09\_02\_Phorbol\_Pell**



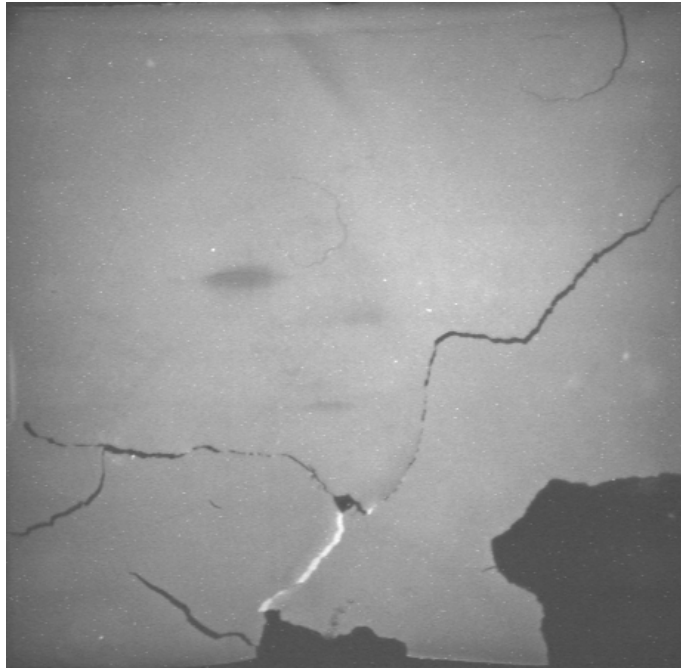
**Figure 27:** Example of a 2D gel containing membrane proteins from phorbol-contracted SM tissue, where proteins were solubilized in boiling 10% SDS and treated with RNase and DNase prior to electrophoresis. This gel was stained with silver stain, and reveals very little evidence of protein bands.

**2D\_6\_18\_02\_Control**



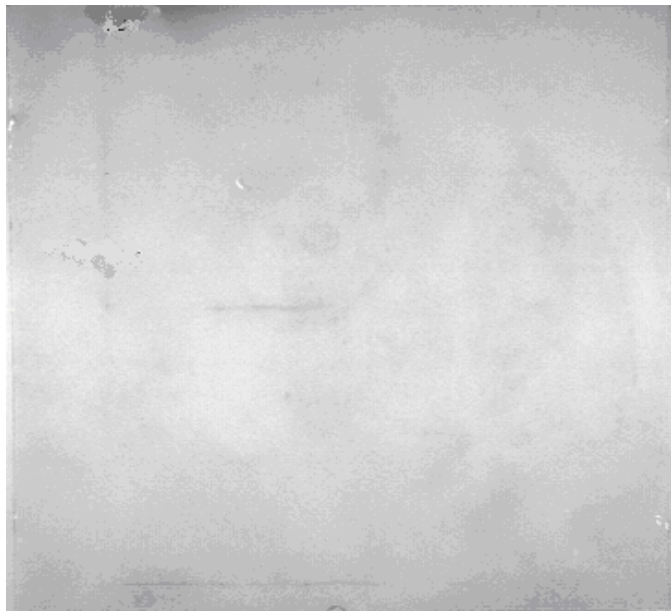
**Figure 28:** Example of a 2D gel containing supernatant or aqueous proteins from resting aortic SM tissue stained with SYPRO ruby protein gel stain, revealing very little evidence of protein bands.

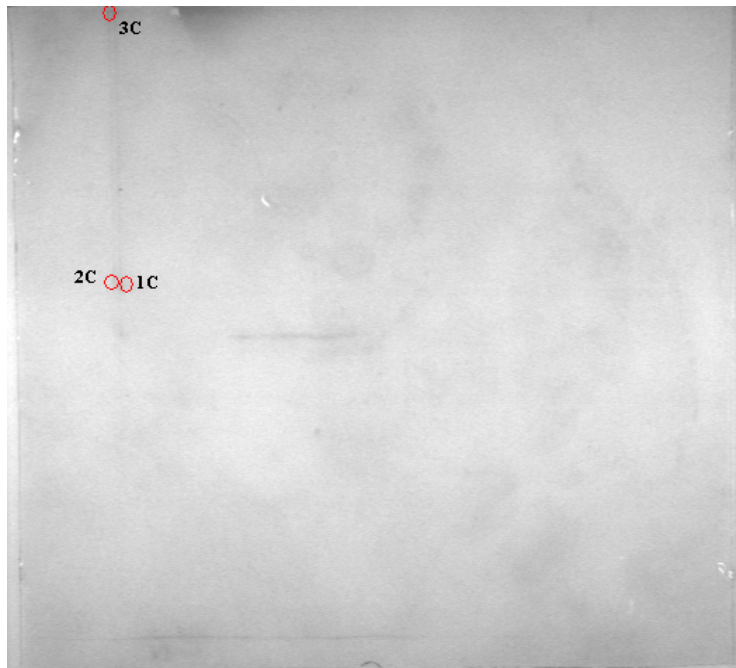
**2D\_6\_18\_02\_Phorbol**



**Figure 29:** Example of a 2D gel containing supernatant or aqueous proteins from phorbol-contracted aortic SM tissue stained with SYPRO ruby protein gel stain, revealing very little evidence of protein bands.

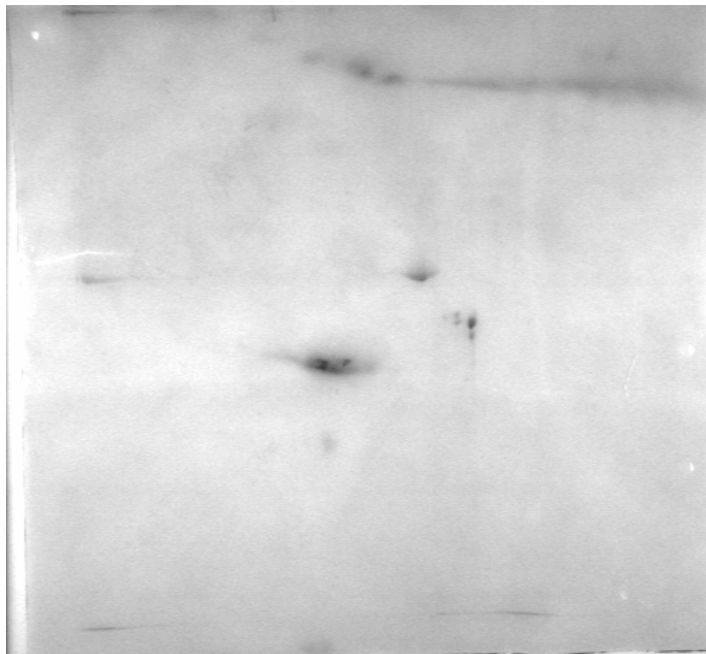
**2D\_7\_12\_02\_Control**



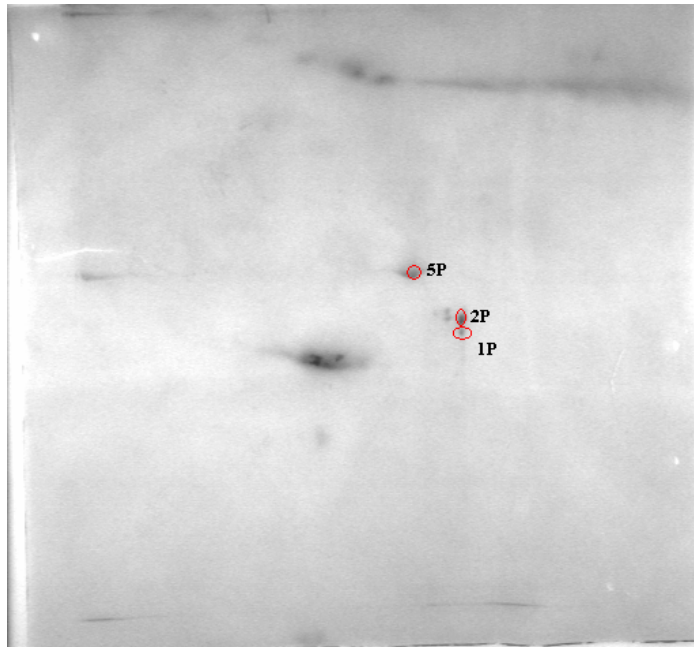


**Figure 30:** Example of a 2D gel containing supernatant or aqueous proteins from resting aortic SM tissue stained with SYPRO ruby protein gel stain, revealing very little evidence of protein bands.

### 2D\_7\_12\_02\_Phorbol

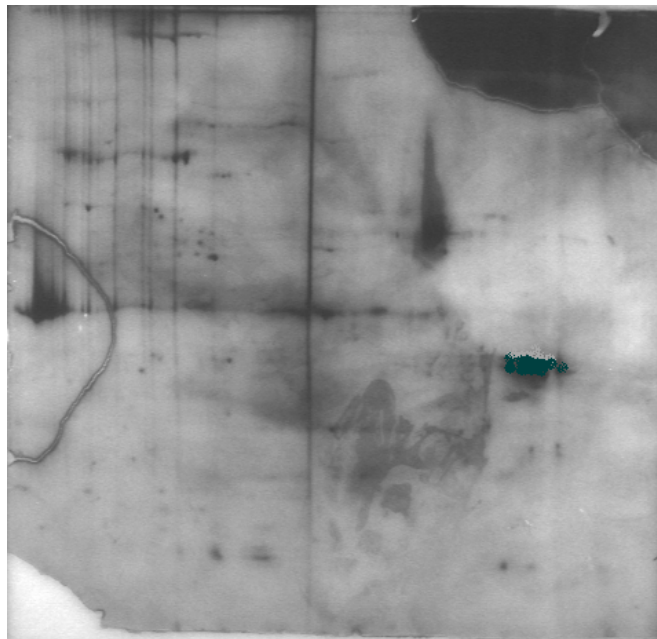






**Figure 31:** Example of a 2D gel containing supernatant or aqueous proteins from phorbol-contracted aortic SM tissue stained with SYPRO ruby protein gel stain, revealing very little evidence of protein bands.

### 2D\_7\_30\_02\_Phorbol



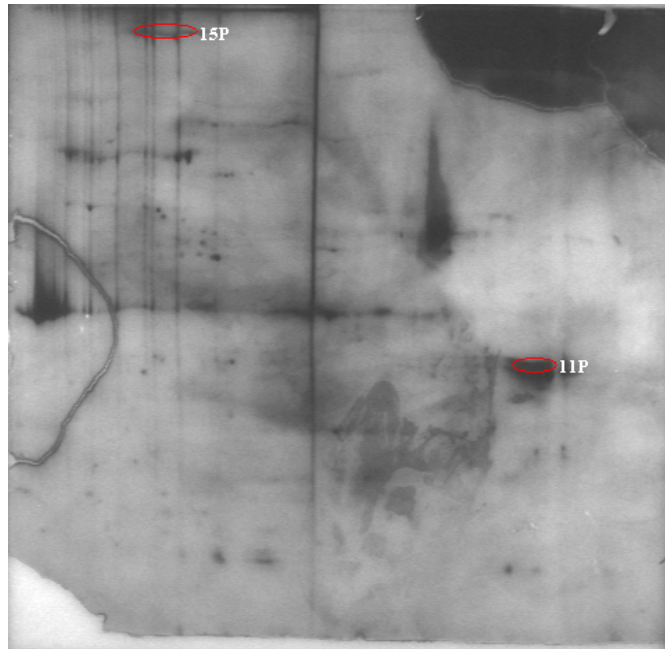


**Figure 32:** Example of a 2D gel containing supernatant or aqueous proteins from resting aortic SM tissue stained with silver stain.

Overall, silver staining provided the best visualization of protein bands. However, because of the low quantity of protein per band, limited success was achieved for analysis by tryptic digest and subsequent MS analysis. Many of the averaged digest spectra obtained from these gels were of poor signal to noise (S/N) ratio. Examples of these types of digest spectra can be seen in figures 33-45, below. The location of the digested bands on the corresponding 2D gel may be seen in the figures, above.

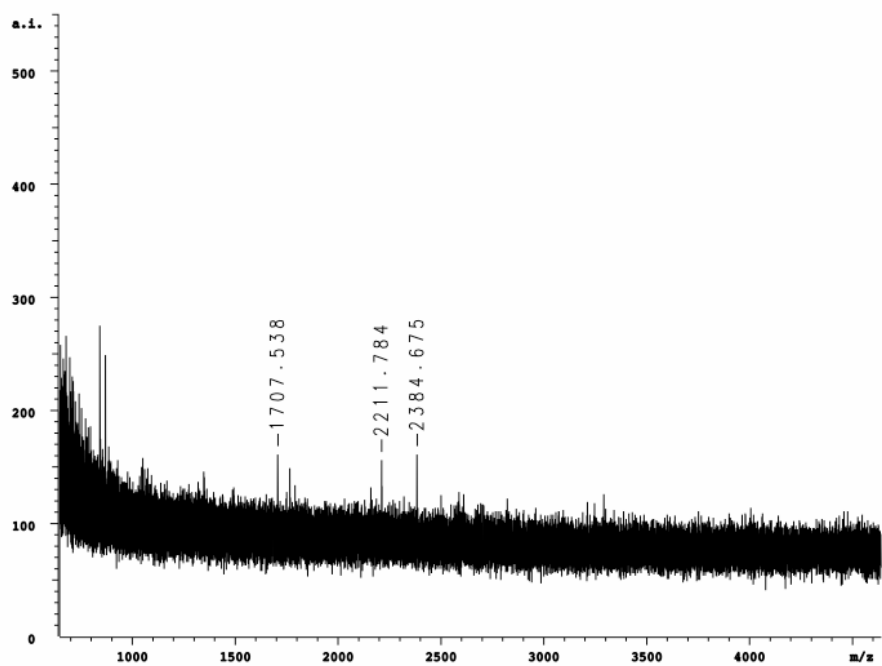


**Figure 33:** Example of an averaged tryptic digest spectrum obtained from protein band 8C the gel 2D\_7\_30\_02 Control, revealing low S/N ratios for peptide peaks.

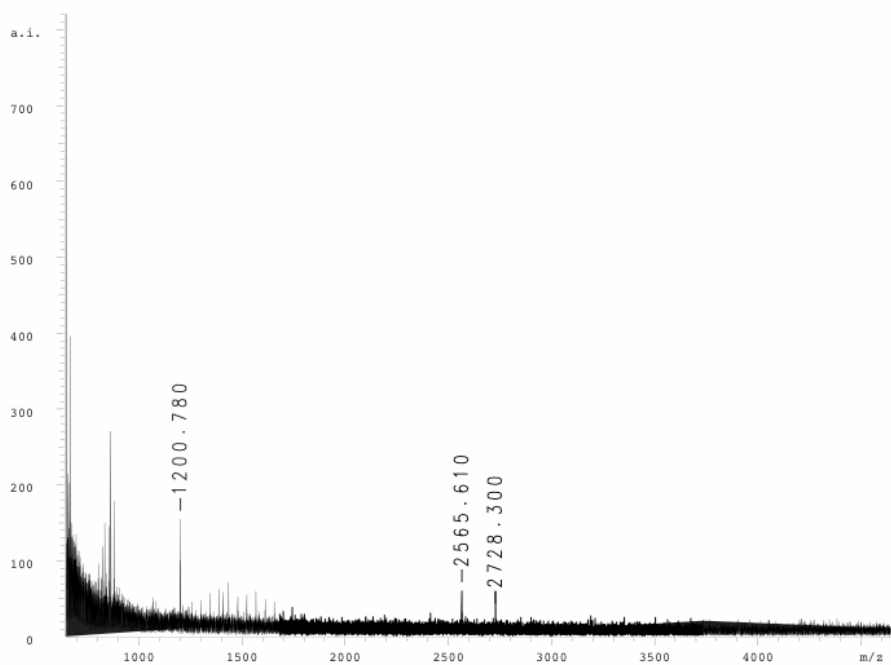


**Figure 34:** Example of an averaged tryptic digest spectrum obtained from protein band 4P the gel 2D\_7\_30\_02 Phorbol, revealing low S/N ratios for peptide peaks.

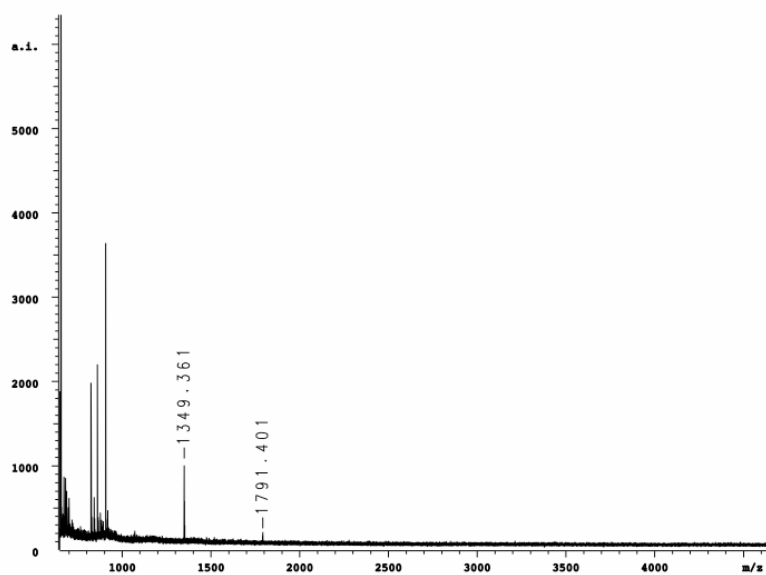


**Figure 35:** Example of an averaged tryptic digest spectrum obtained from protein band 5C the gel 2D\_7\_30\_02 Control, revealing low S/N ratios for peptide peaks.

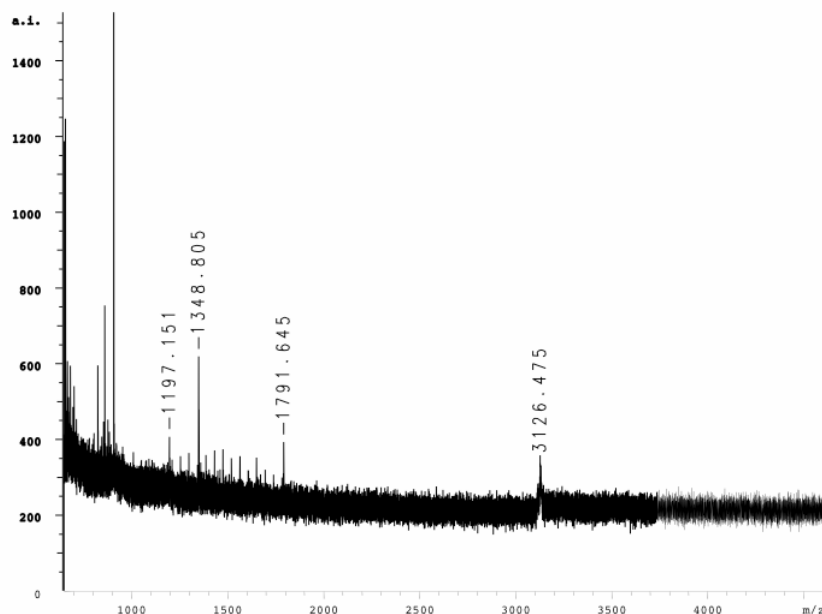


**Figure 36:** Example of an averaged tryptic digest spectrum obtained from protein band 2P the gel 2D\_7\_30\_02 Phorbol, revealing low S/N ratios for peptide peaks.

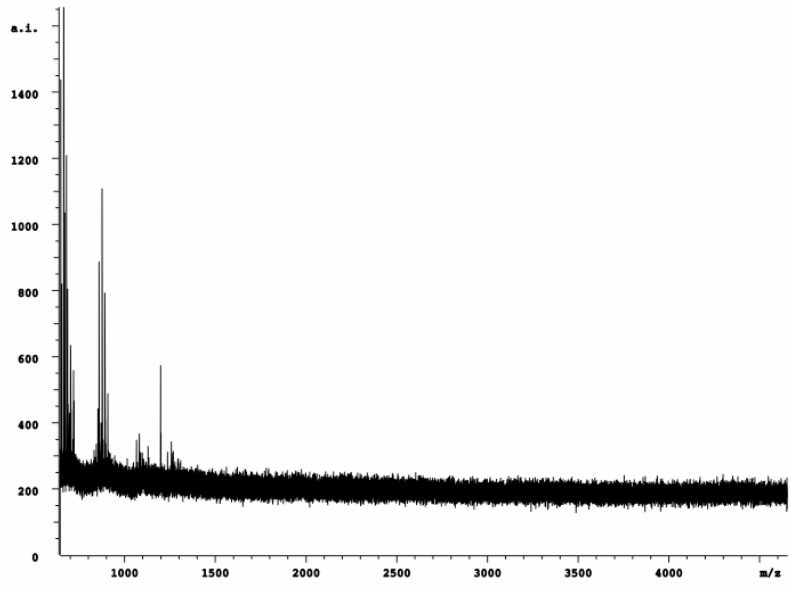


**Figure 37:** Example of an averaged tryptic digest spectrum obtained from protein band 2C on the gel 2D\_7\_12\_02 Control, revealing low S/N ratios for peptide peaks.

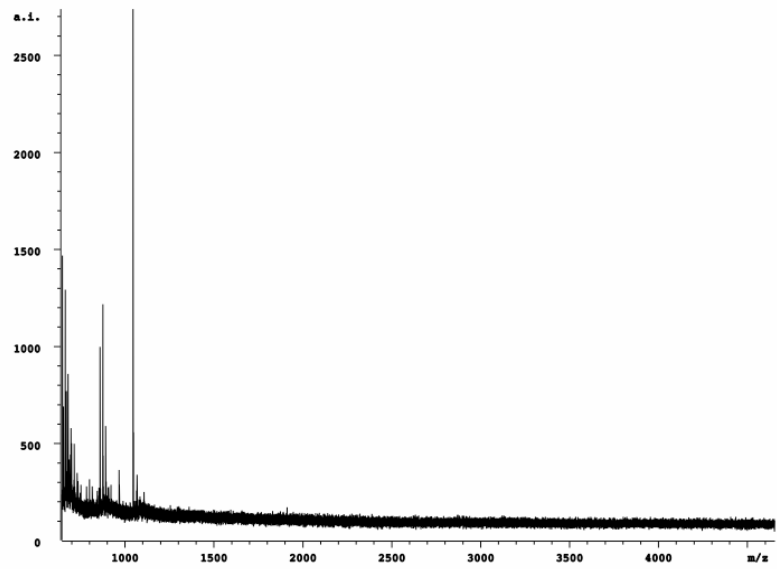


**Figure 38:** Example of an averaged tryptic digest spectrum obtained from protein band 3C on the gel 2D\_7\_12\_02 Control, revealing low S/N ratios for peptide peaks.

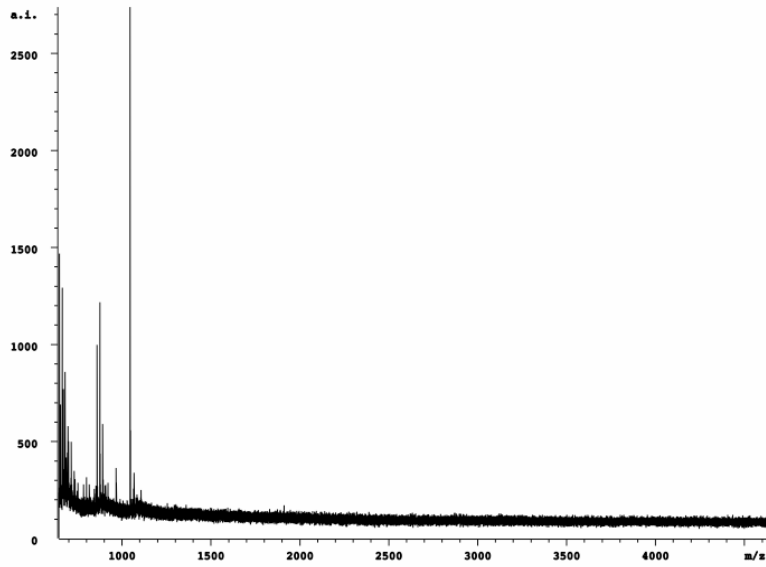


**Figure 39:** Example of an averaged tryptic digest spectrum obtained from protein band 1P on the gel 2D\_7\_12\_02 Phorbol, revealing low S/N ratios for peptide peaks.

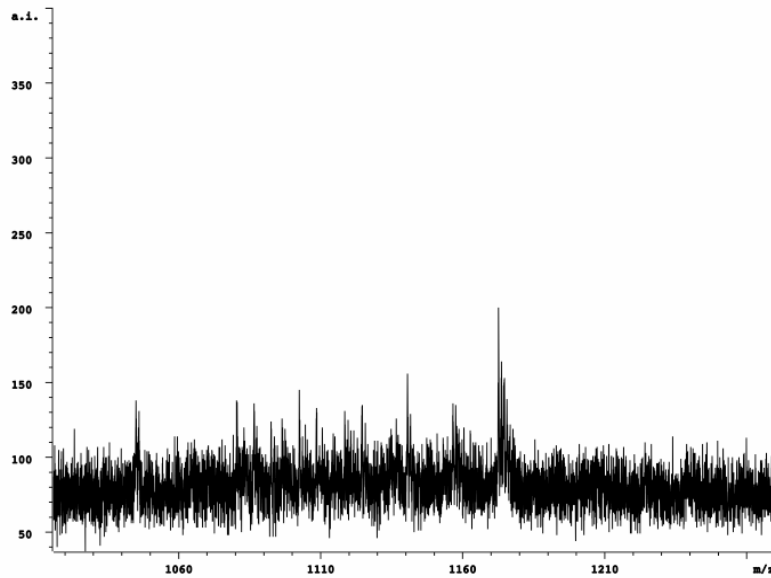


**Figure 40:** Example of an averaged tryptic digest spectrum obtained from protein band 2P on the gel 2D\_7\_12\_02 Phorbol, revealing low S/N ratios for peptide peaks.

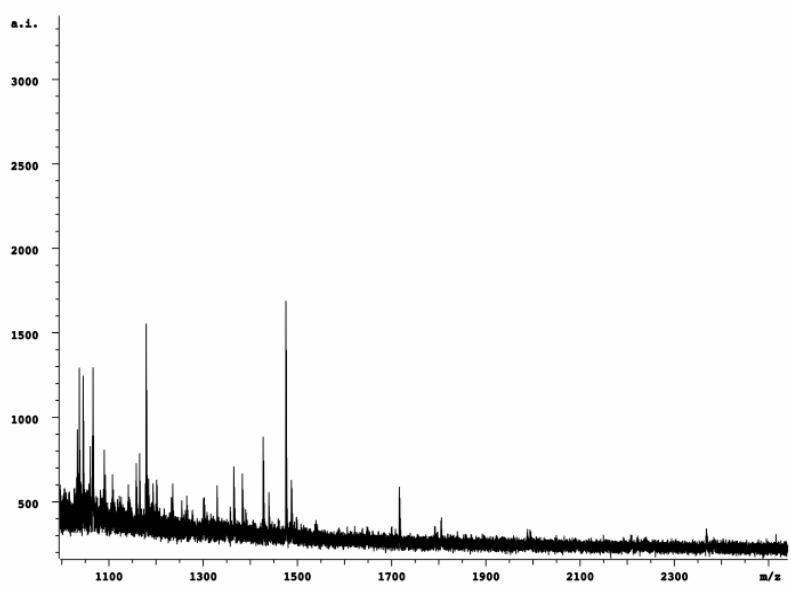


**Figure 41:** Example of an averaged tryptic digest spectrum obtained from protein band 18C on the gel 2D\_10\_09\_02\_Control, revealing low S/N ratios for peptide peaks.

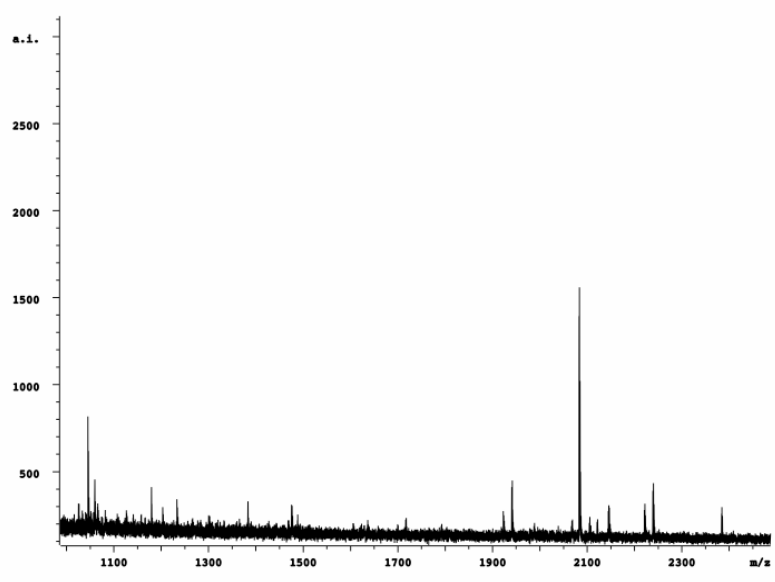


**Figure 42:** Example of an averaged tryptic digest spectrum obtained from protein band 24C on the gel 2D\_10\_09\_02\_Control, revealing low S/N ratios for peptide peaks.

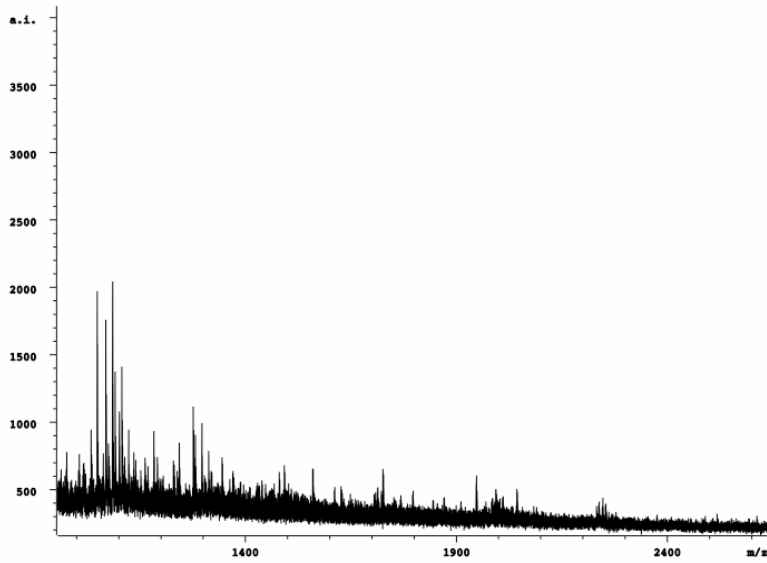


**Figure 43:** Example of an averaged tryptic digest spectrum obtained from protein band 15P on the gel 2D\_7\_30\_02\_Phorbol, revealing low S/N ratios for peptide peaks.

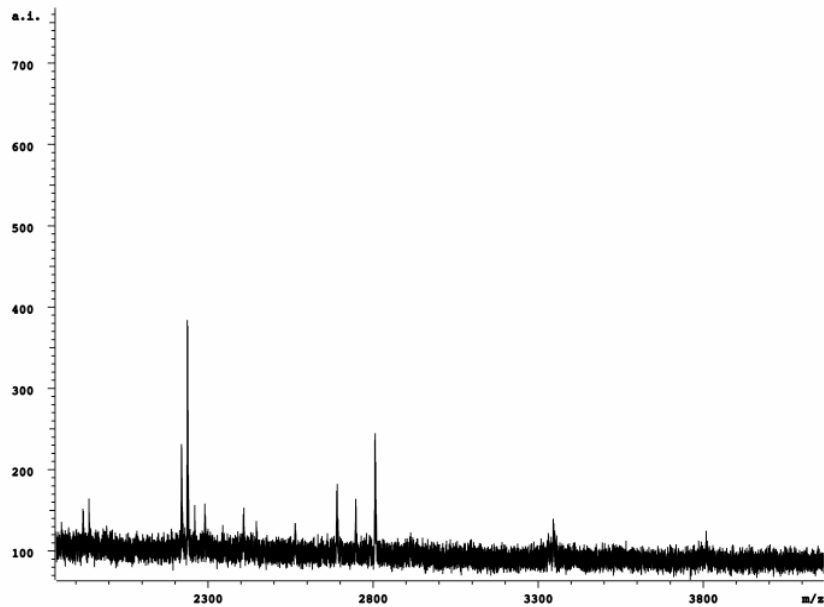


**Figure 44:** Example of an averaged tryptic digest spectrum obtained from protein band 7CP on the gel 2D\_10\_09\_02\_Control\_Pell, revealing low S/N ratios for peptide peaks.



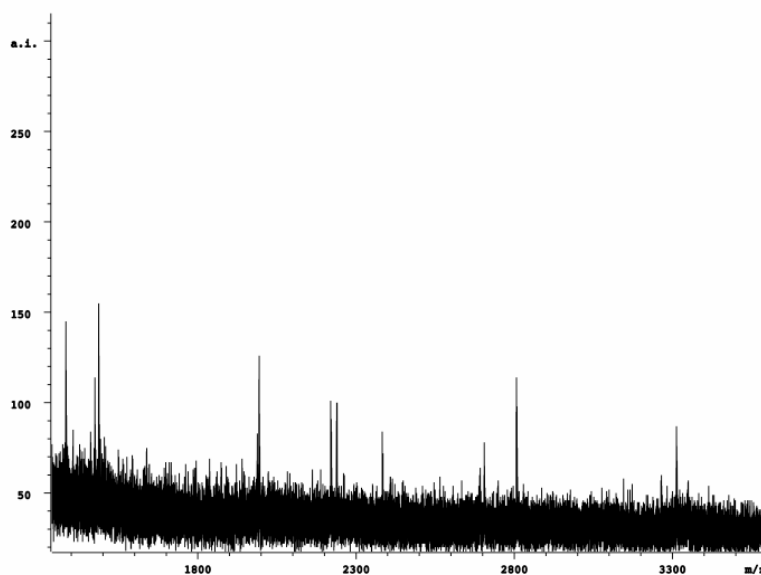


**Figure 45:** Example of an averaged tryptic digest spectrum obtained from protein band 6CP on the gel 2D\_10\_09\_02\_Control\_Pell, revealing low S/N ratios for peptide peaks.

Because of such difficulties, the focus of the research was simplified to mapping the proteome through identification of proteins on the gel in resting SM tissue in attempt to confirm the protocol.

Other explanations for the production of inadequate gels have been investigated. Poor solubilization of proteins was suggested as one possible explanation for this phenomenon. Many different methods of protein solubilization were attempted with little improvement of protein band intensity and subsequent data acquisition.

The cellular extract was first boiled in 10% SDS to help denature and solubilize all proteins. Protein concentration was not high enough for visualization with Coomassie, and had to be stained with silver stain (Figure 46). Though bands were visualized for this method, no identifications were made from the data collected for this gel.

## 2D\_7\_12\_01\_Phorbol\_pell

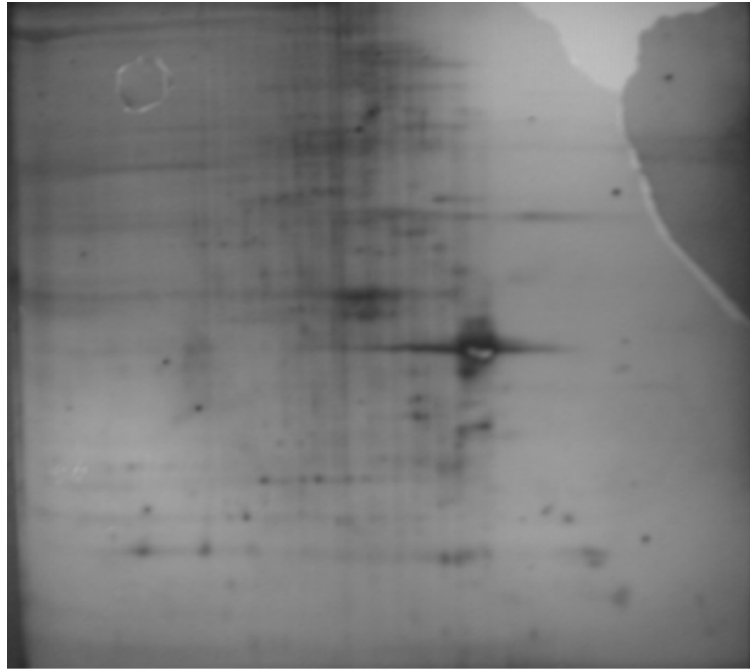


**Figure 46:** Example of a 2D gel containing membrane proteins solubilized with boiling in 10% SDS, from phorbol-contracted aortic SM tissue stained with silver stain.

At one point, it was believed that too much cellular debris (RNA, DNA, etc.) existed in the sample mixture to allow adequate migration within the tube gel, even though a chelating agent (EDTA) was added to the lysis buffer to chelate the negatively charged DNA/RNA in the sample. Samples were treated with RNase and DNase enzymes prior to separation, but this did not appear to improve sample migration (Figures 24-27).

It was also proposed that too much salt in the sample mixture prevented efficient IEF separation in the tube gels. Therefore, samples were thoroughly dialyzed prior to separation to remove salt contamination. Salts are naturally present in biological samples, and they may also have been introduced to the sample during cell lysis (RIPA buffer) or when tissue was incubated in salt-containing buffers (Krebs buffer, PBS). Samples were dialyzed for extended periods of time—overnight—with several changes of different dialysis buffers, both a low salt dialysis buffer (dialysis buffer I) and nanopure water. Dialyzed samples were always lyophilized prior to 1<sup>st</sup> dimension separation to concentrate the protein, as well. However, 2D gels with adequate protein concentration were never obtained (Figures 24-32). Finally, protein extracts were

submitted to acetone precipitation to remove salt/detergent contaminants and other cellular debris to purify the protein extract prior to electrophoresis (Figures 51 and 52).

It was concluded that tube gel separation did not allow an adequate amount of protein to pass into the tube gel, and thus inhibited proper 2D gel sample analysis. The tube gel holds only 50  $\mu$ L of solubilized protein. Despite several attempts to concentrate and remove salt interference, little improvement was ever observed.

To further support this conclusion, sample extracts of both the contracted and uncontracted tissue were run on a 1D gel to facilitate analysis (Figure 47). From this gel, the presence of actin and tropomyosin were detected. Band 1C was found to be tropomyosin with a MASCOT score of 63. The placement of the band on the gel agrees with the MW of tropomyosin (~33 kDa). Band 2C and 2P were identified as actin with MASCOT scores of 107 and 81, respectively. Their approximate MW on the gel also agrees with that of actin (~42 kDa). The digest spectra, peak lists, and MASCOT analysis data can be seen below (Figures 48-50, Table 4). No further identifications were made from this gel.

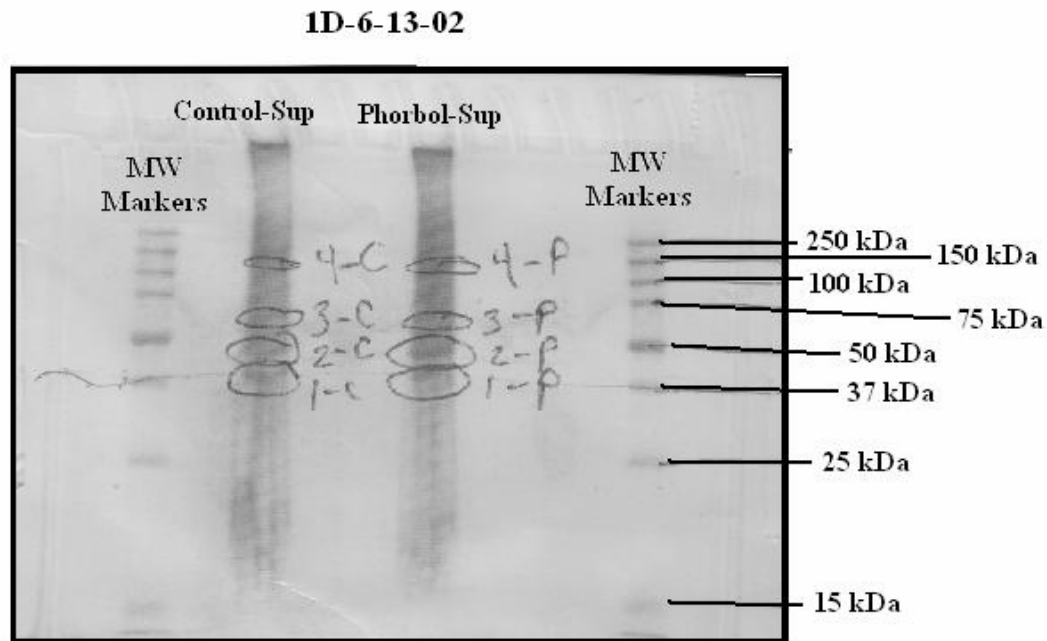


**Figure 47:** 1D gel stained with Coomassie Brilliant Blue protein stain, depicting the location of excised bands 1C, 2C, and 2P submitted to tryptic digest and MS analysis for successful identification. Control-SuP = resting aortic SM tissue. Phorbol-Sup = phorbol-contracted aortic SM tissue.

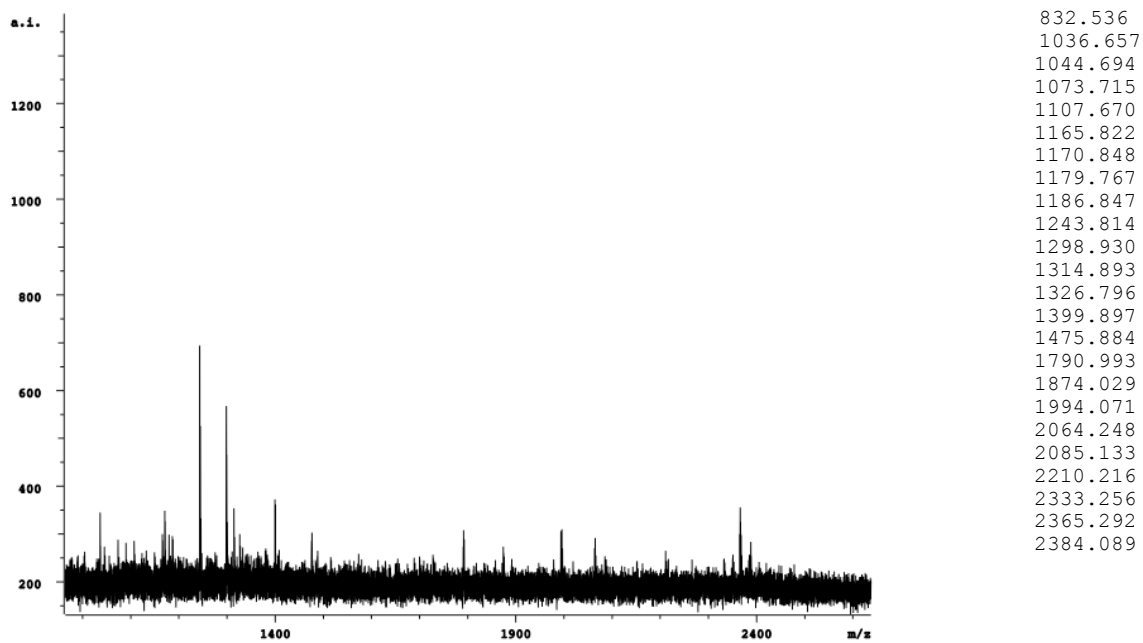


**Figure 48:** Tryptic digest spectra and generated peak list of excised protein band 1C from the gel 1D-6-13-02, above. This peak list was searched in MASCOT, which identified it as tropomyosin with a score of 63.

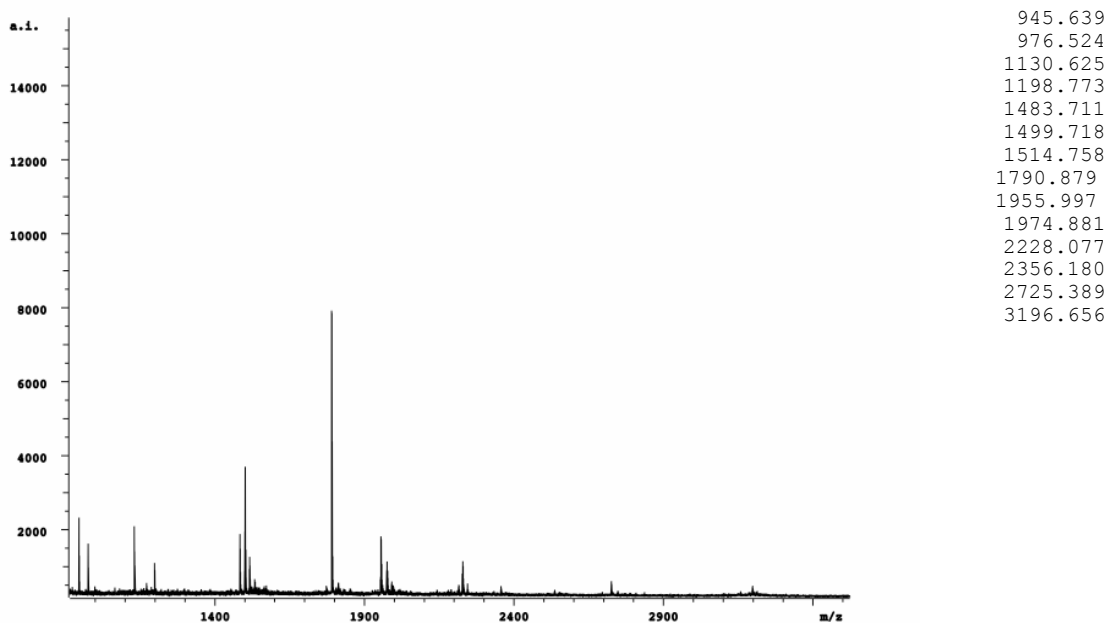


**Figure 49:** Tryptic digest spectra and generated peak list of excised protein band 2C from the gel 1D-6-13-02, above. This peak list was searched in MASCOT, which identified it as actin with a score of 107.

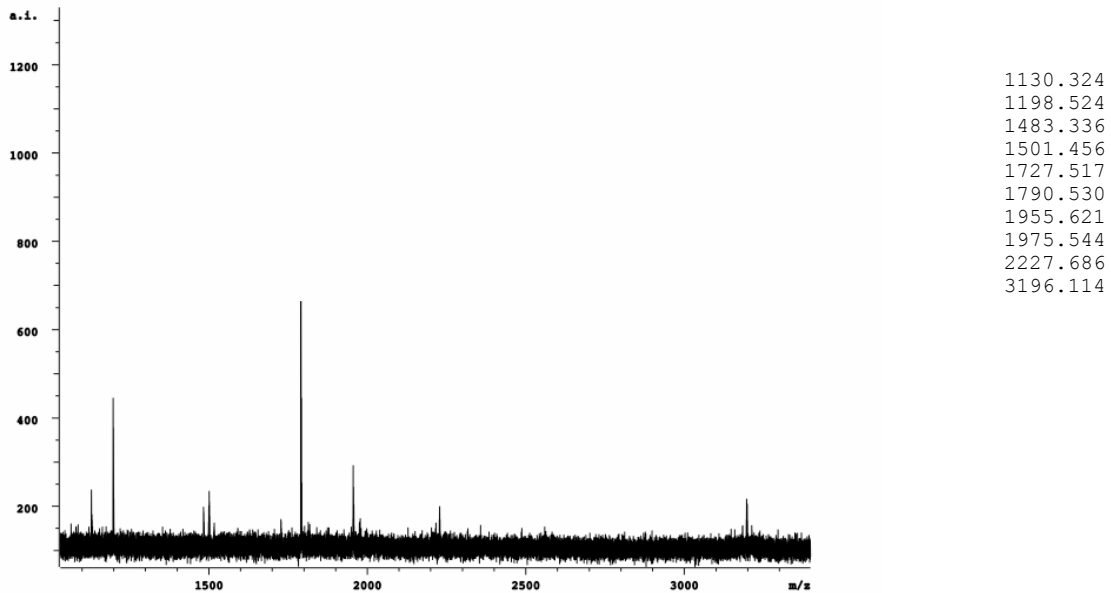


**Figure 50:** Tryptic digest spectra and generated peak list of excised protein band 2P from the gel 1D-6-13-02, above. This peak list was searched in MASCOT, which identified it as tropomyosin with a score of 81.

### MASCOT Search Results

Gel	Protein Band	Identification	MASCOT Score	Sequence coverage	Mass (kDa)	pI
1D-6-13-02	1C	Tropomyosin	63	52%	~33	4.6
1D-6-13-02	2C	Actin	107	73%	~42	5.2
1D-6-13-02	2P	Actin	81	59%	~42	5.2

**Table 4:** List of the MASCOT search results for protein bands digested with trypsin from the 1D gel 6\_18\_02. Digest mixtures were analyzed with MALDI-TOF MS and searched in a protein database using the MASCOT search engine.

IPG strips, which allow an upper limit of 1 mg of protein dissolved in 1 mL of buffer, were then used for IEF separation to improve protein band intensities. The 2D gels obtained

from this technique were considerably more concentrated, and could be stained with Coomassie Brilliant Blue stain (Figures 49-50).

### 2D\_9\_26\_03\_Control

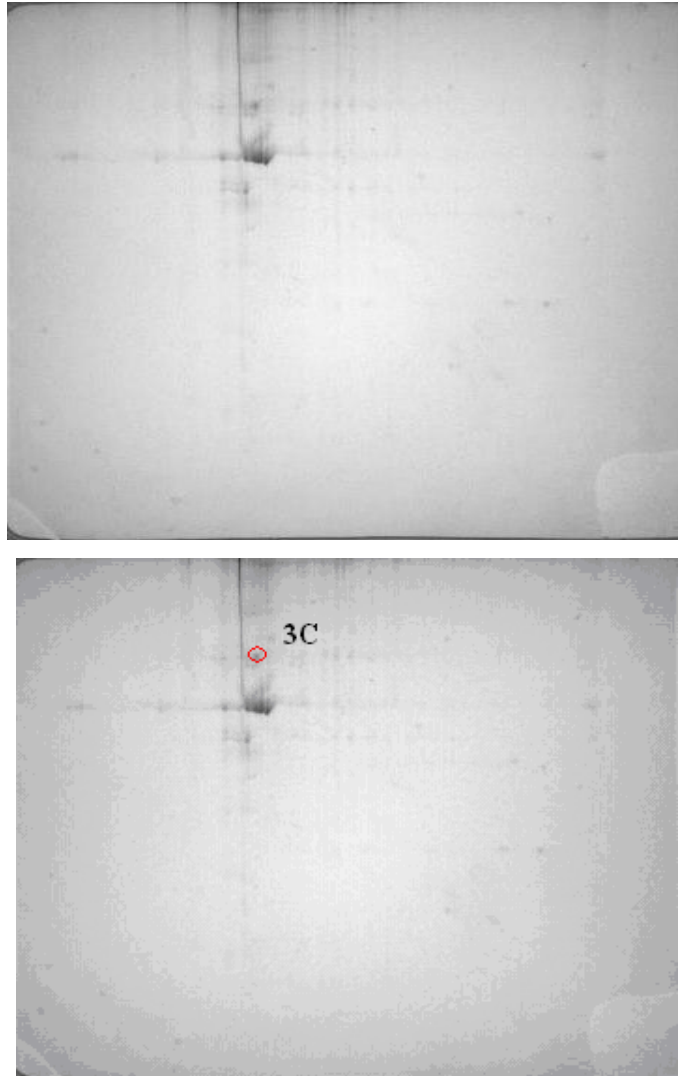


**Figure 51:** Example of a 2D gel containing membrane proteins from resting aortic SM tissue solubilized with boiling in 10% SDS, and later purified via acetone precipitation. The protein quantity in the bands of this gel was high enough to be visualized by Coomassie Brilliant Blue staining.

## 2D\_9\_26\_03\_Phorbol

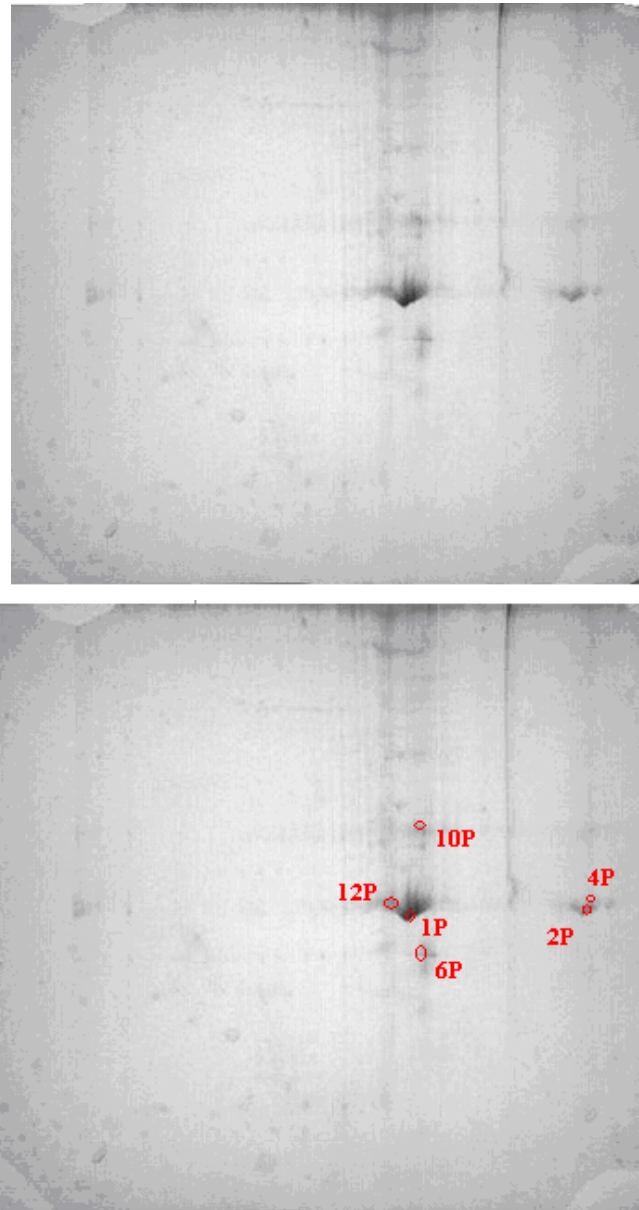


**Figure 52:** Example of a 2D gel containing membrane proteins from phorbol-contracted aortic SM tissue solubilized with boiling in 10% SDS, and later purified via acetone precipitation. The protein quantity in the bands of this gel was high enough to be visualized by Coomassie Brilliant Blue staining.

It has also been observed that few low molecular weight proteins exist on the 2D gels. This may be because low MW proteins either migrated off the 2<sup>nd</sup> dimension slab gel due to over-extended running times or because they migrated out of the tube gel during equilibration of the tube gels in methylene blue. The second explanation is more likely, because it is not

believed that the second dimension separation time was too long. Applied voltages were stopped before the line of methylene blue dye migrated off the gel, after approximately 4.5 to 5.0 hours. The MW of methylene blue is 319.85 Da, much smaller than the MW of proteins expected to be in biological samples.

Once a gel of adequate protein level—that able to be detected by Coomassie staining—was produced, then phosphoprotein detection and protein identification through MS analysis could be conducted. In the future, it is recommended that a Bradford Protein Assay—to determine the concentration of protein—be conducted prior to electrophoresis to assure that equal amounts of total protein from the contracted and uncontracted tissue are used.

### **MALDI-TOF MS Analysis**

Low S/N ratios of peaks made MS analysis difficult. Such poor quality spectra are partly explained by the low concentration of protein on the gels produced for tube gel IEF separation. Examples of such spectra may be seen in figures 32-46, above. Once the problem of low protein abundance in gel plugs was solved by using IPG strips in the 1<sup>st</sup> dimension separation of 2D SDS-PAGE, another problem was discovered in MS analysis. The instrument did not appear to hold calibration.  $M/z$  values shifted irregularly over time. MS spectra provided by the instrument used in this research proved to be ambiguous and not reproducible, which would largely explain the lack of sufficient results. Parameters for the LASER attenuation and extraction voltages were not changed, and are not the source of ambiguity.

Equilibration of the acceleration voltage, delayed extraction voltages, and/or reflectron voltages was targeted as an initial source of error. Deviation in these voltages from the set voltage will result in deviant computations of  $m/z$  (see Appendix I). The voltages were checked with a voltmeter and did not deviate from the set values. However, approximately 15 minutes was allowed for equilibration of the high voltages prior to acquisition of data. This did not solve the problem.

Improportional depth of the target probe has also been proposed as a source of error. Slight deviations in the depth of analyte within the ionization chamber can cause differences in the distance traveled by the ions, and subsequent deviations in computed  $m/z$  values. Methods to combat inhomogeneity on the surface of the probe, such as the two-layer method of spotting,



were always applied. In this method, a homogenous layer of matrix is spotted using a volatile solvent, and the matrix-embedded sample is spotted on top of this layer to create a homogenous surface layer of analyte. The purchase of a new probe may also aid in this problem. It is possible that the probe may have been damaged due to mishandling and may not be even. This has not yet been tried.

The application of an internal standard was then utilized to combat this problem, with limited success. For this application a diluted extract of peptide standards was added to a fraction of the sample mixture, which was then spotted on the MALDI probe. The acquired spectrum containing the internal standards was calibrated. Abundant sample peptide peaks were chosen as calibrants for the spectrum containing only peaks from the sample mixture—no internal standards. Using this methodology, the localization of some proteins on the 2D gel were discovered, including actin, tropomyosin, and MHC. The data supporting these conclusions may be seen in figures 53-63 and table 5, below.

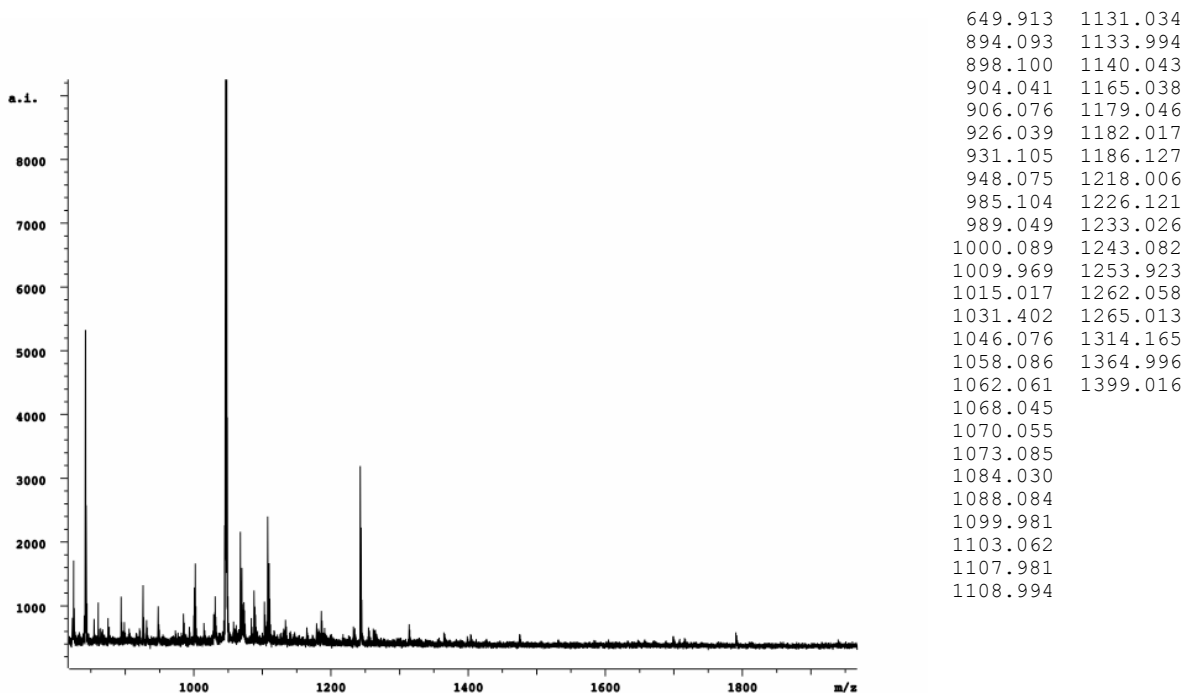


**Figure 53:** Tryptic digest spectra and generated peak list of excised protein band 1C from the gel 2D\_10\_9\_02\_Control. This peak list was searched in MASCOT, which identified it as tropomyosin with a score of 278.

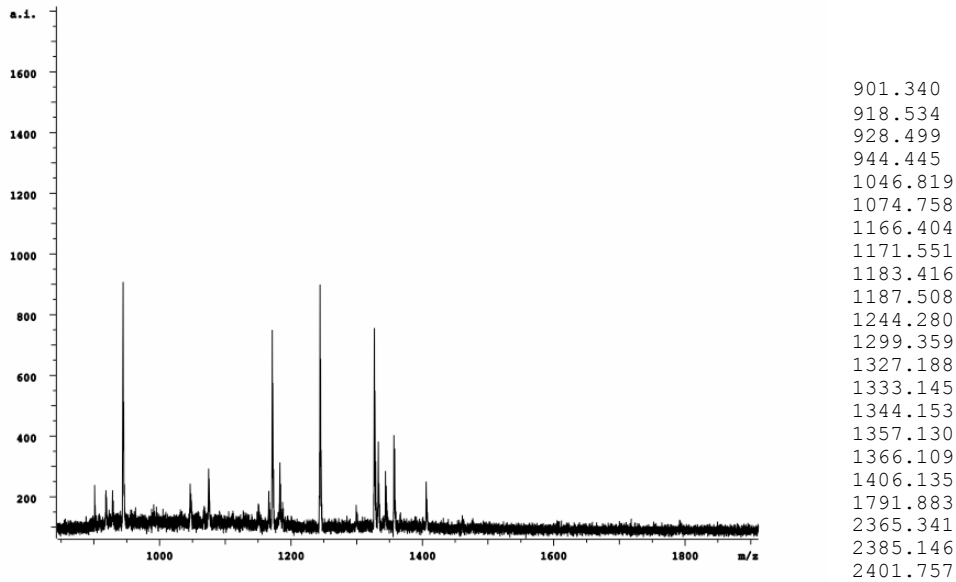


**Figure 54:** Tryptic digest spectra and generated peak list of excised protein band 4C from the gel 2D\_10\_9\_02\_Control. This peak list was searched in MASCOT, which identified it as tropomyosin with a score of 88.

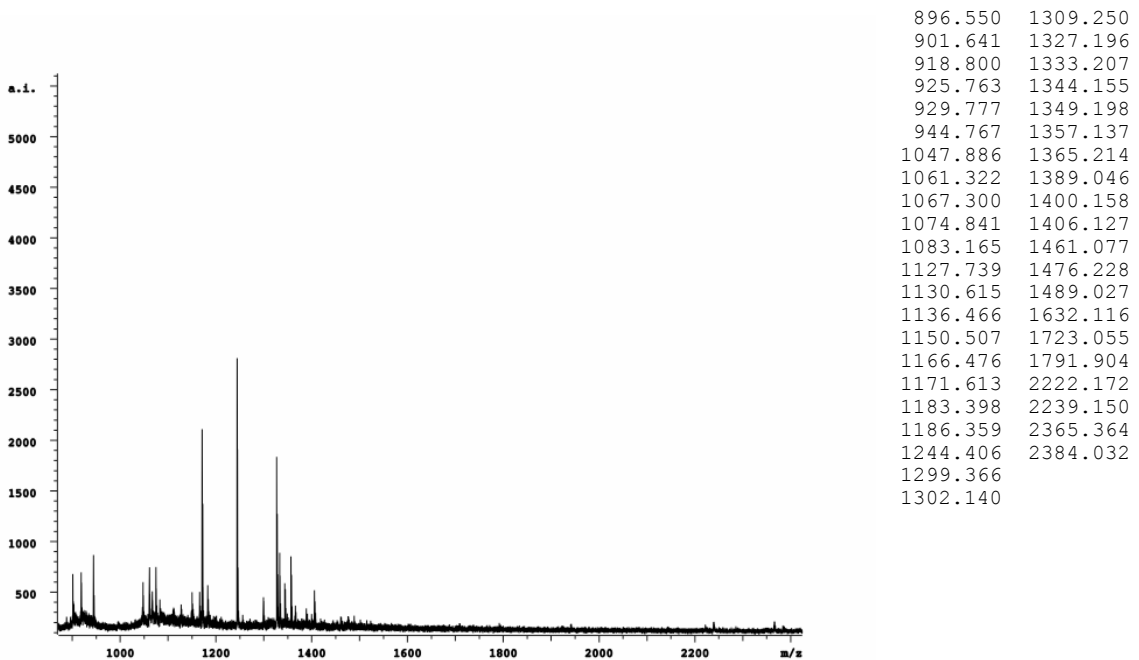


**Figure 55:** Tryptic digest spectra and generated peak list of excised protein band 6C from the gel 2D\_10\_09\_02\_Control. This peak list was searched in MASCOT, which identified it as tropomyosin with a score of 112.

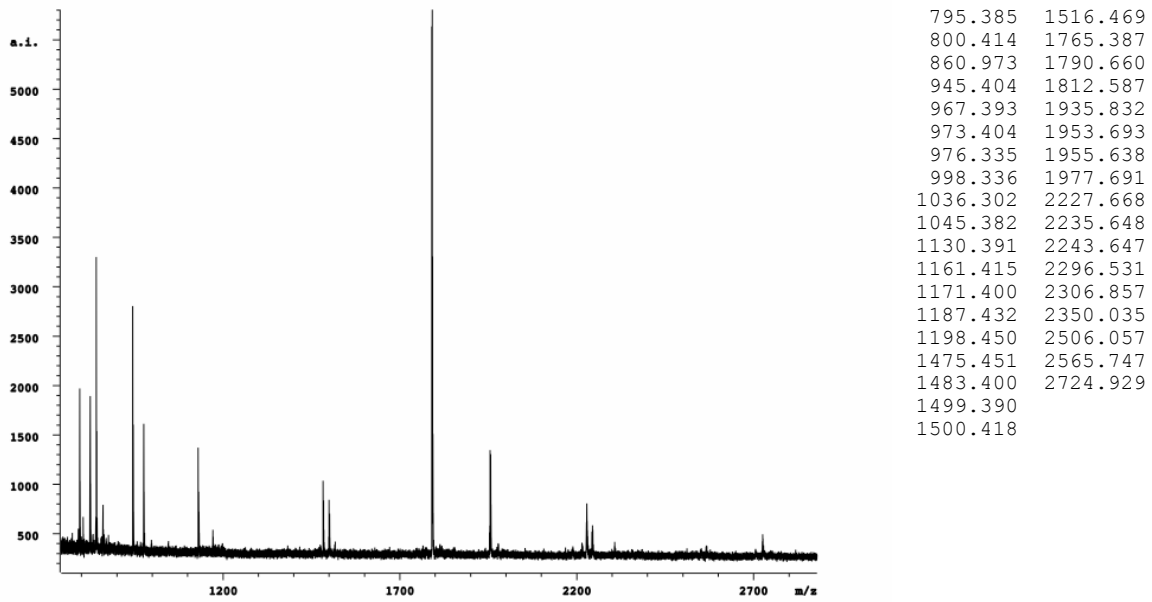


**Figure 57:** Tryptic digest spectra and generated peak list of excised protein band 8C from the gel 2D\_10\_09\_02\_Control. This peak list was searched in MASCOT, which identified it as actin with a score of 108.

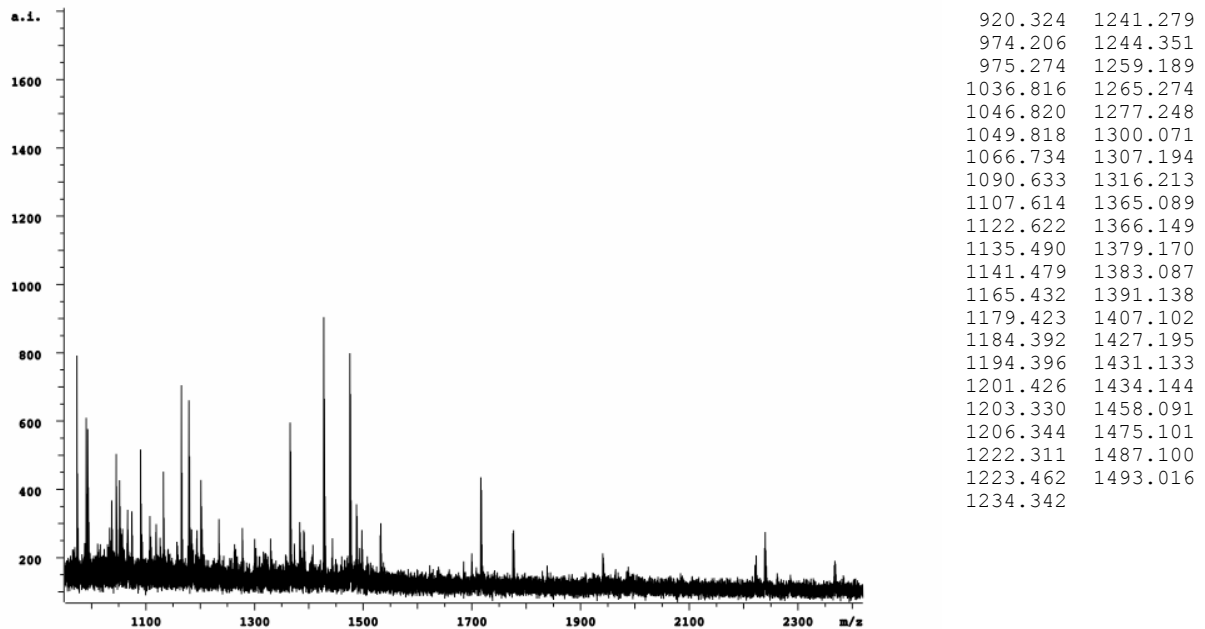
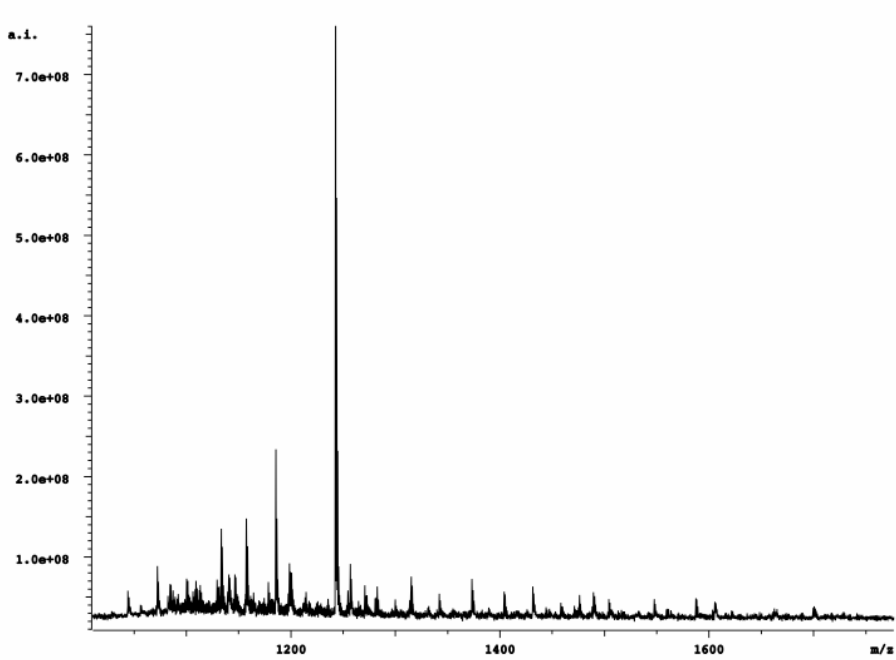
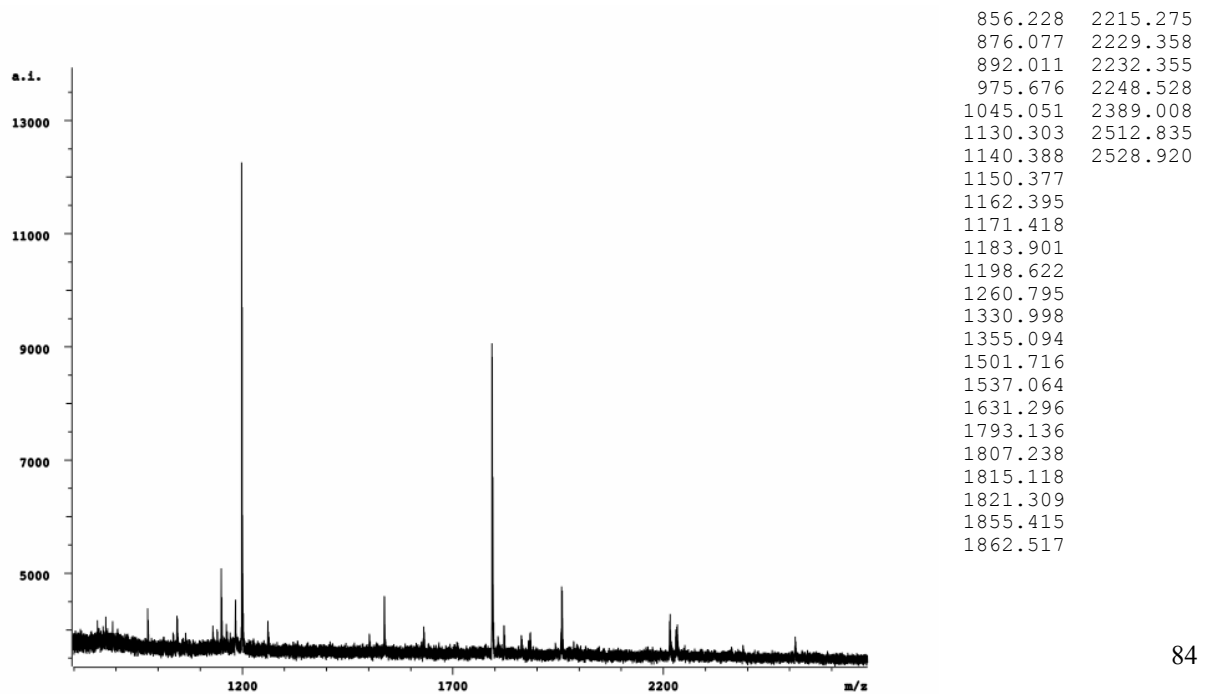


**Figure 58:** Tryptic digest spectra and generated peak list of excised protein band 12C from the gel 2D\_10\_09\_02\_Control. This peak list was searched in MASCOT, which identified it as MHC with a score of 86.



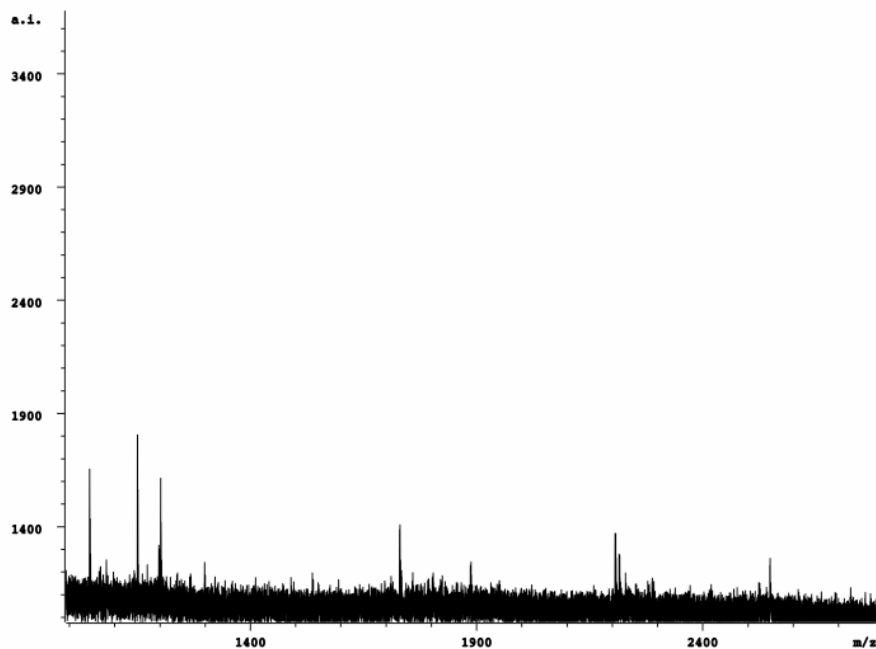
1471.326

**Figure 59:** Tryptic digest spectra and generated peak list of excised protein band 11P from the gel 2D\_7\_30\_02\_Phorbol. This peak list was searched in MASCOT, which identified it as tropomyosin with a score of 74.



1879.648  
 1883.679  
 1957.012  
 1959.006  
 1987.086

**Figure 60:** Tryptic digest spectra and generated peak list of excised protein band 1C from the gel 2D\_7\_12\_02\_Control. This peak list was searched in MASCOT, which identified it as tropomyosin with a score of 59.



This peak list was searched in MASCOT, which identified it as tropomyosin with a score of 59.

1045.136  
 1065.838  
 1081.691  
 1097.643  
 1150.498  
 1197.721  
 1201.743  
 1267.993  
 1299.093  
 1490.064  
 1537.327  
 1730.038  
 1758.119  
 1792.239  
 1802.430  
 1820.334  
 1886.805  
 1949.033  
 2206.461  
 2215.500  
 2229.623  
 2280.740  
 2287.946  
 2524.225  
 2548.429

**Figure 61:** Tryptic digest spectra and generated peak list of excised protein band 5P from the gel 2D\_7\_12\_02\_Phorbol. This peak list was searched in MASCOT, which identified it as MHC with a score of 61.

### MASCOT Search Results

Gel	Protein	Identification	MASCOT	Sequence	Mass	pI
-----	---------	----------------	--------	----------	------	----

	<b>Band</b>		<b>Score</b>	<b>coverage</b>	<b>(kDa)</b>	
10_09_02_Control	1C	Tropomyosin	278	73%	~33	4.6
10_09_02_Control	4C	Tropomyosin	88	47%	~33	4.6
10_09_02_Control	6C	Tropomyosin	112	43%	~33	4.6
10_09_02_Control	8C	Actin	108	45%	~42	5.2
10_09_02_Control	12C	MHC	86	44%	~150- 250	--
10_09_02_Phorbol	11P	Tropomyosin	74	40%	~33	4.6
7_12_02_Control	1C	Tropomyosin	59	34%	~33	4.6
7_12_02_Phorbol	5P	MHC	61	56%	~150- 250	--

**Table 5:** List of the MASCOT search results for protein bands digested with trypsin that were successfully identified with the aid of internal standards from various gels (as designated in the figures, above). Digest mixtures were analyzed with MALDI-TOF MS and searched in a protein database using the MASCOT search engine.

The acquisition of quality spectra for both the sample spot and the sample with standards spot was difficult, given the already low S/N ratios of peaks. The same problem of low protein quantity described before contributed to the lack of adequate spectra. This trend hindered the ability to calibrate the spectra using this method.

The application of an internal standard within sample mixtures helped to demonstrate the inconsistencies encountered during operation of the MALDI-TOF instrument. The following spectra were acquired chronologically as they are listed in the text. The correct m/z values for the internal standards used are listed in table 2. The shift in the reported m/z values corresponding to these standards can be seen in the spectra, below.

The first three spectra are from the same sample spot (Figures 62-64). The standard peaks first shift down in m/z and then shift back up without changing any parameters, though the position on the spot where the LASER was fired was changed.

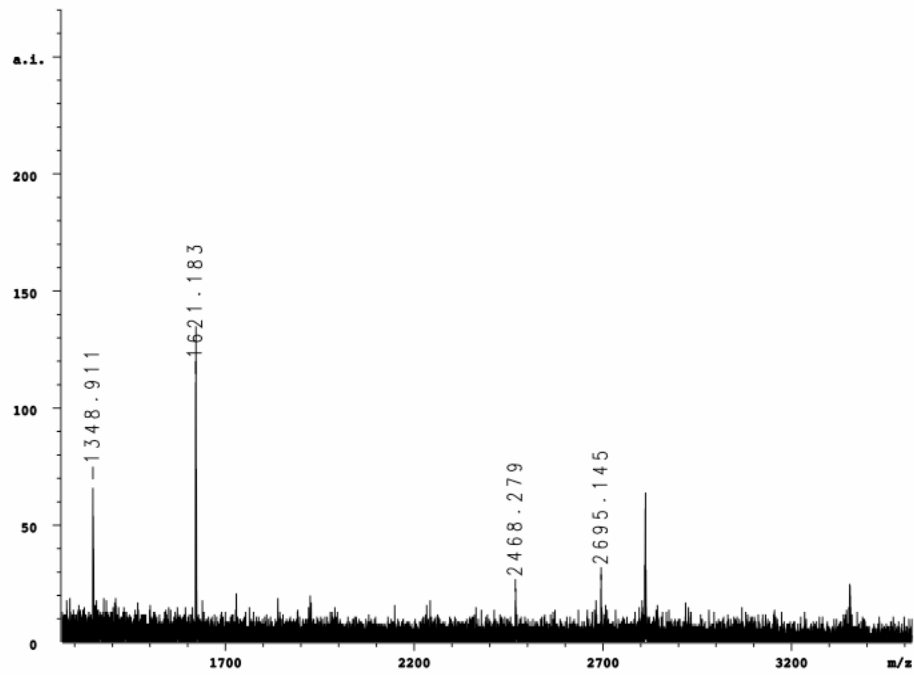


**Figure 62:** Tryptic digest from band 10P from the gel 2D\_9\_26\_03\_Phorbol. The uncalibrated m/z peaks for the standards substance P, bombesin, and ACTH clip 18-39 can be seen. When compared to the other spectra of this same spot (Figures 61 and 62), the shifts in the m/z values can be seen.

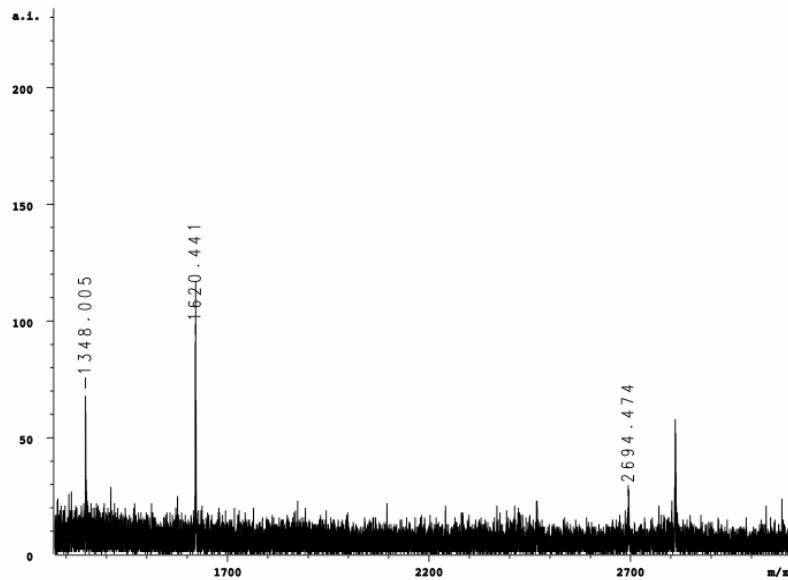


**Figure 63:** Tryptic digest from band 10P from the gel 2D\_9\_26\_03\_Phorbol. The uncalibrated m/z peaks for the standards substance P, bombesin, and ACTH clip 18-39 can be seen. When compared to the other spectra of this same spot (Figures 60 and 62), the shifts in the m/z values can be seen.

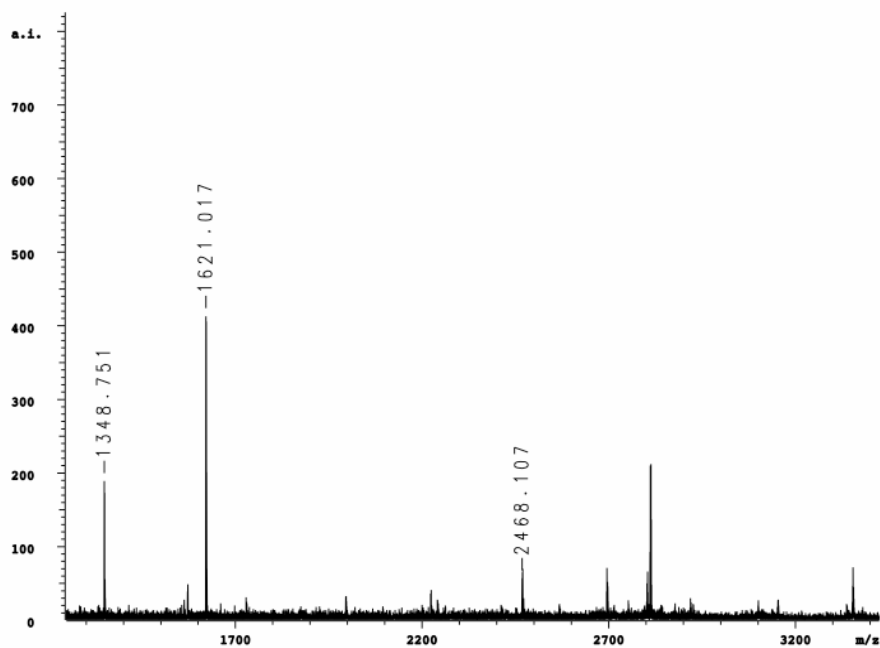


**Figure 64:** Tryptic digest from band 10P from the gel 2D\_9\_26\_03\_Phorbol. The uncalibrated m/z peaks for the standards substance P, bombesin, and ACTH clip 18-39 can be seen. When compared to the other spectra of this same spot (Figures 60 and 62), the shifts in the m/z values can be seen.

The following four spectra all contain standard peaks (Figures 65-68). They are from different sample spots acquired on the same day, listed chronologically in time. Again, none of the parameters of the instrument were changed. The ambiguity of the m/z values reported for the standard peaks can be seen.



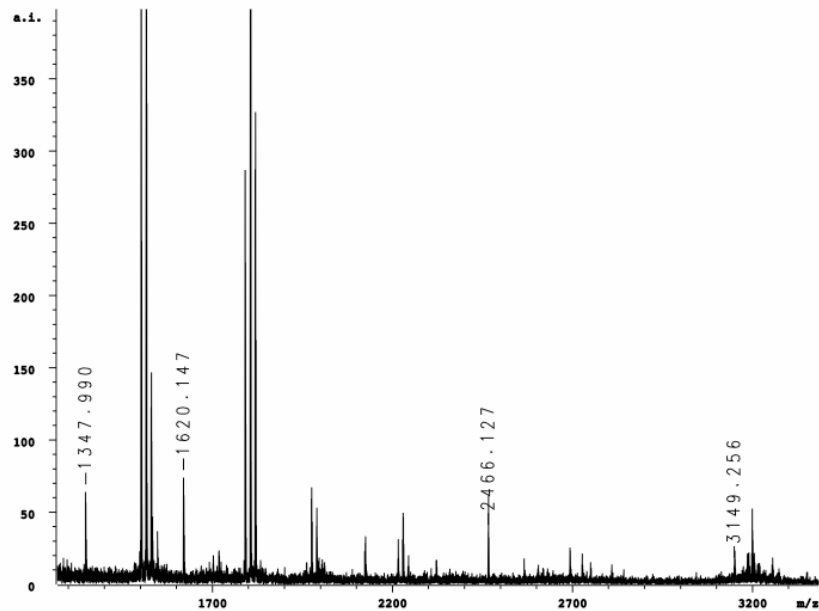


**Figure 65:** Tryptic digest from band 1P from the gel 2D\_9\_26\_03\_Phorbol. The uncalibrated m/z peaks for the standards substance P, bombesin, ACTH clip 18-39, and Somatostatin-28 can be seen. When compared to the other spectra acquired on the same day under the same instrumental parameters (Figures 65-68), the shifts in the m/z values can be seen.

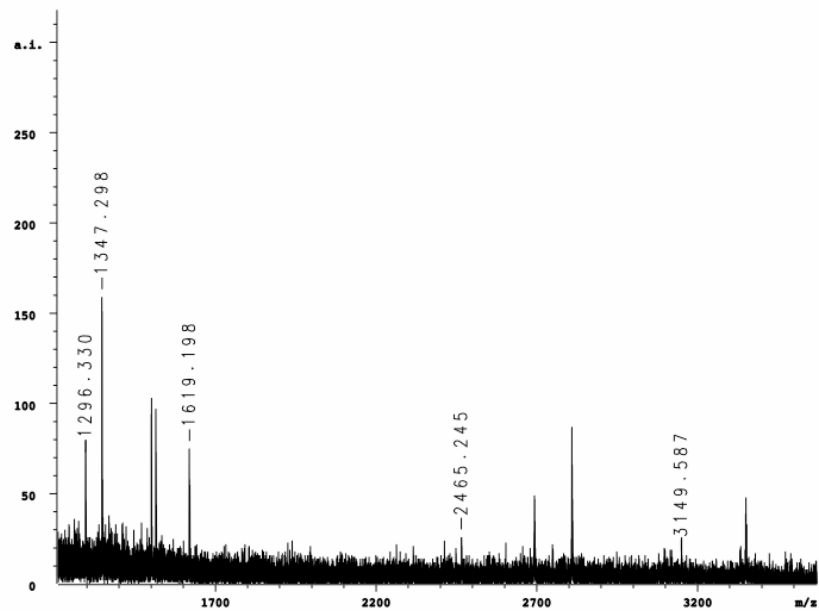


**Figure 66:** Tryptic digest from band 4P from the gel 2D\_9\_26\_03\_Phorbol. The uncalibrated m/z peaks for the standards substance P, bombesin, ACTH clip 18-39, and Somatostatin-28 can be seen. When compared to the other

spectra acquired on the same day under the same instrumental parameters (Figures 65,67-68), the shifts in the m/z values can be seen.

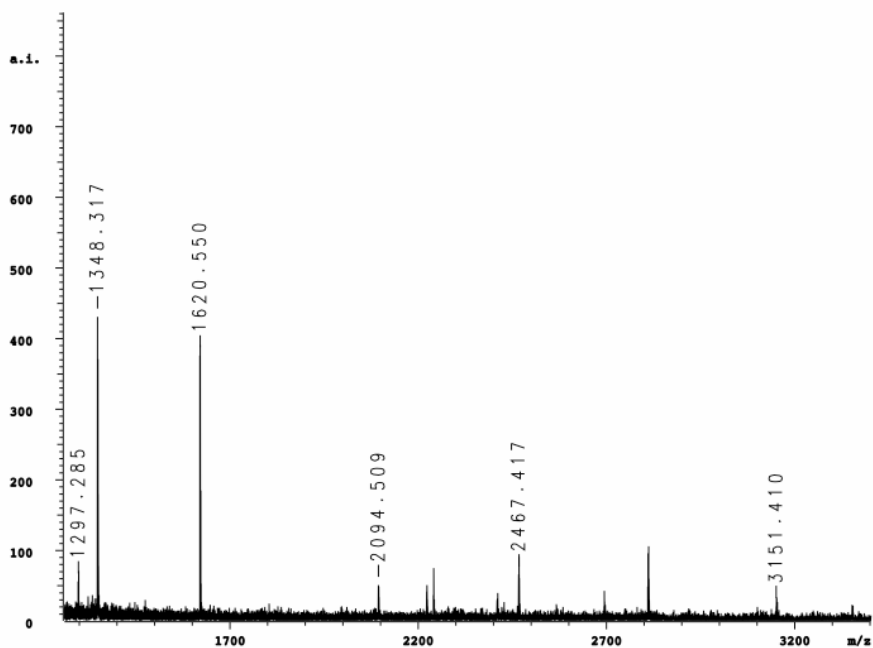


**Figure 67:** Tryptic digest from band 6P from the gel 2D\_9\_26\_03\_Phorbol. The uncalibrated m/z peaks for the standards substance P, bombesin, ACTH clip 18-39, and Somatostatin-28 can be seen. When compared to the other spectra acquired on the same day under the same instrumental parameters (Figures 65-66, 68), the shifts in the m/z values can be seen.

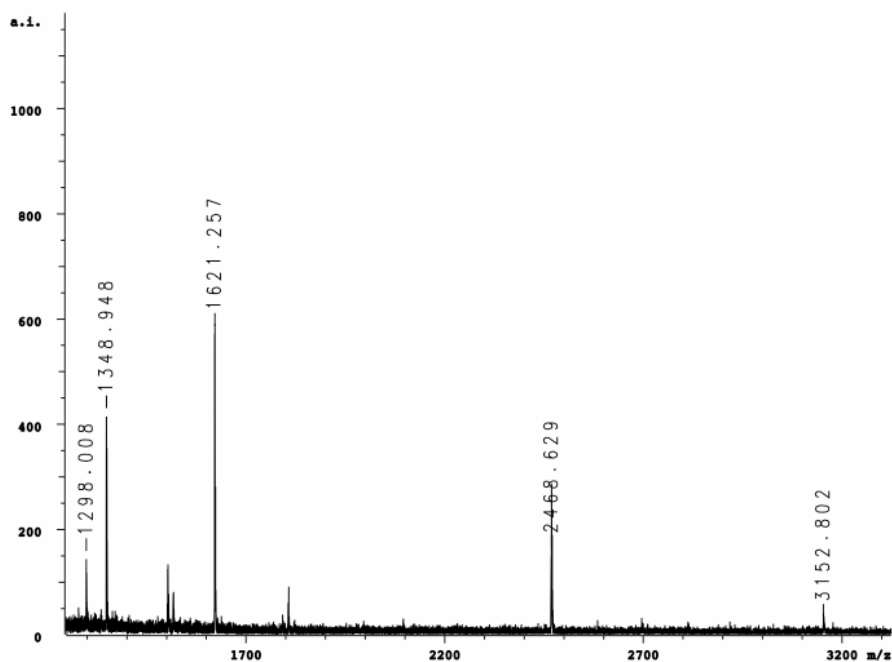


**Figure 68:** Tryptic digest from band 2P from the gel 2D\_9\_26\_03\_Phorbol. The uncalibrated m/z peaks for the standards substance P, bombesin, ACTH clip 18-39, and Somatostatin-28 can be seen. When compared to the other spectra acquired on the same day under the same instrumental parameters (Figures 65-67), the shifts in the m/z values can be seen.

Many adequate digest spectra, with a sufficient number of suitable S/N ratio peaks, were produced that could not be identified when peak lists were searched in the protein database. Some of these spectra can be seen in figures 69-74. Unfortunately, many protein candidates were found for each peptide fingerprint entered into the protein database search. Different search engines were used to determine whether the search engine was to blame for the lack of results. The same ambiguous results were furnished by the search engines. No two search engines produced the same results, either.

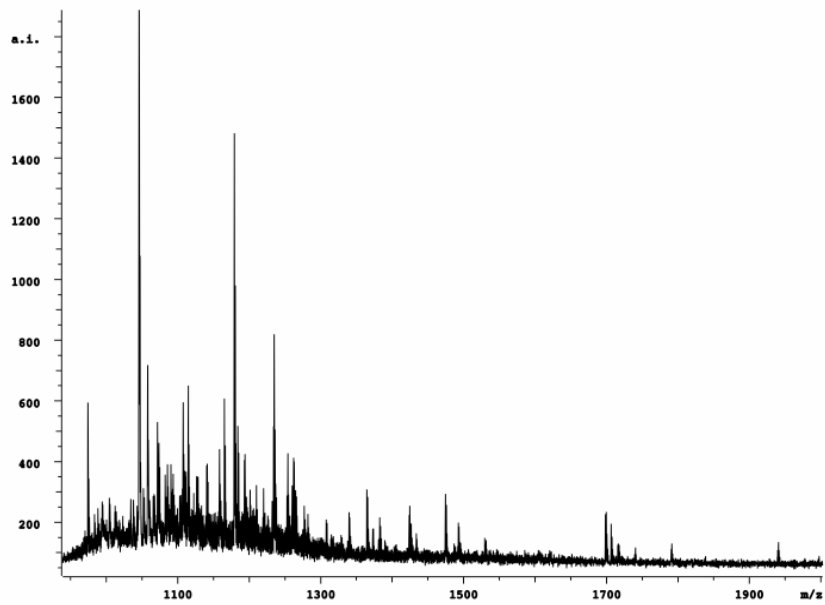


**Figure 69:** Example of a tryptic digest of band 14C from the gel 2D\_7\_30\_02\_Control. The spectrum has a sufficient number of adequate S/N peaks, but no identification could be made in the protein database.

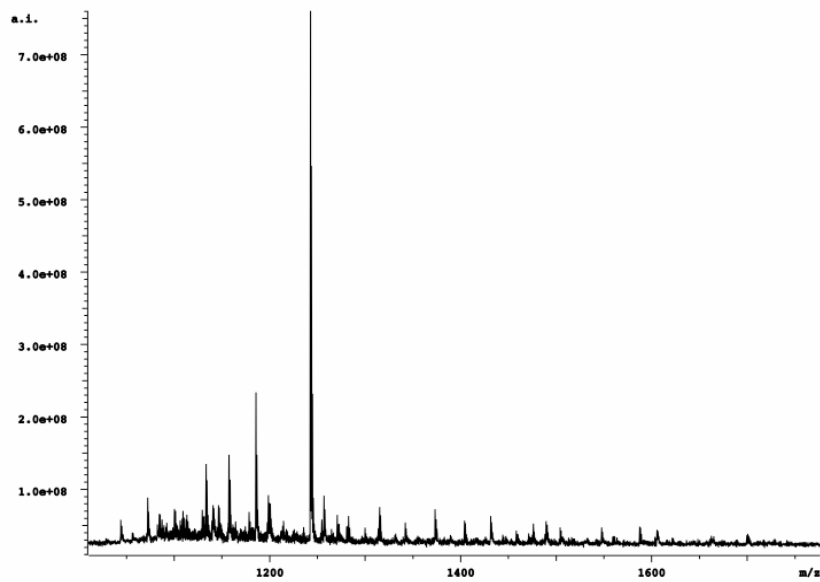


**Figure 70:** Example of a tryptic digest of band 11P from the gel 2D\_7\_30\_02\_Phorbol. The spectrum has a sufficient number of adequate S/N peaks, but no identification could be made in the protein database.

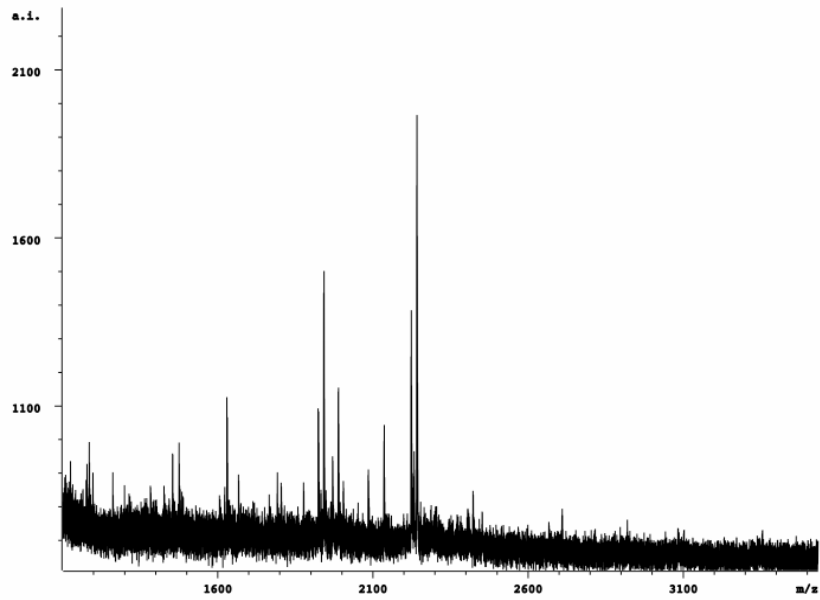


**Figure 71:** Example of a tryptic digest of band 16C from the gel 2D\_10\_09\_02\_Control. The spectrum has a sufficient number of adequate S/N peaks, but no identification could be made in the protein database. This spectrum was calibrated with internal standards, as well.

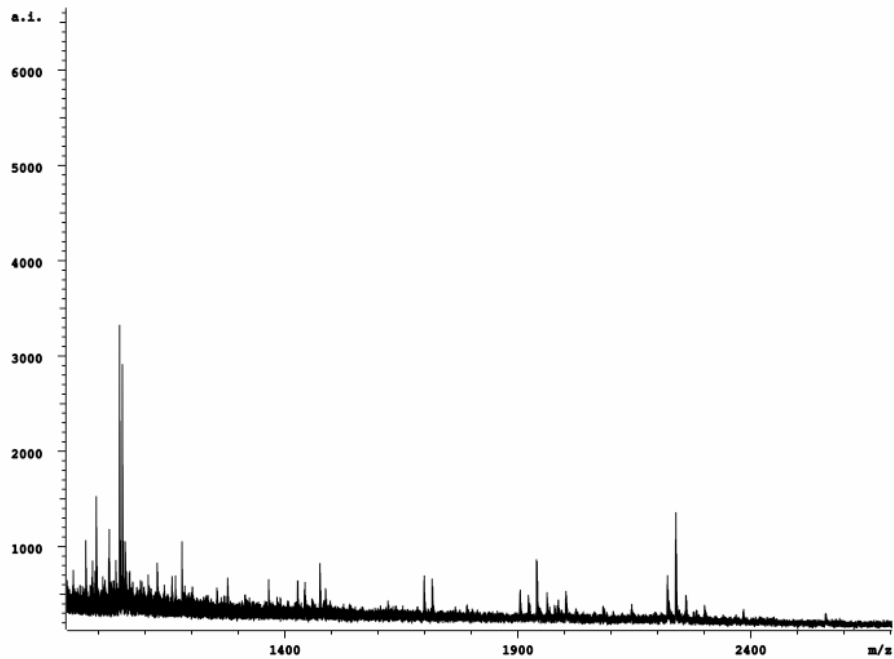


**Figure 72:** Example of a tryptic digest of band 26C from the gel 2D\_10\_09\_02\_Control. The spectrum has a sufficient number of adequate S/N peaks, but no identification could be made in the protein database.

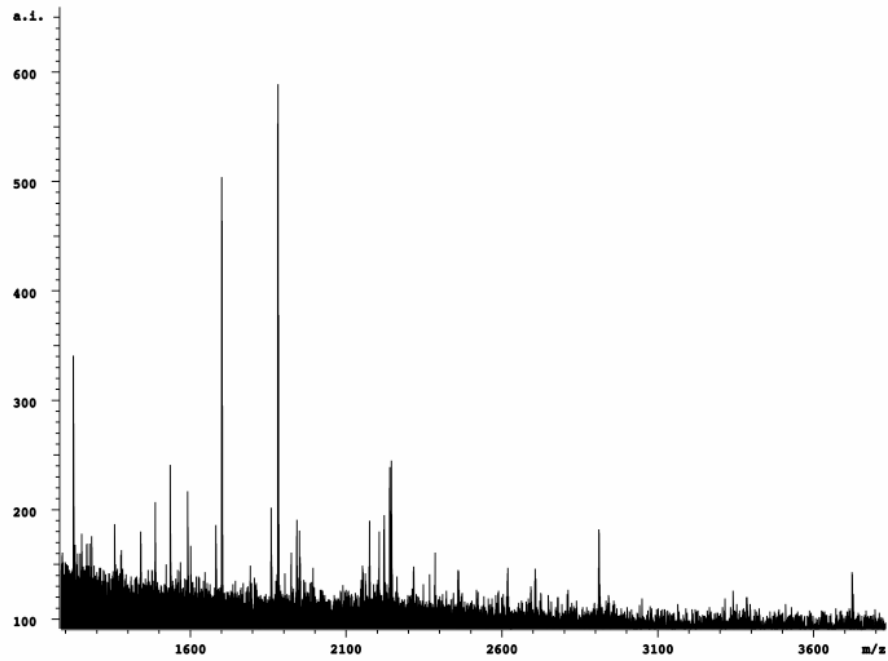


**Figure 73:** Example of a tryptic digest of band 9CP from the gel 2D\_10\_09\_02\_Control\_Pell. The spectrum has a sufficient number of adequate S/N peaks, but no identification could be made in the protein database.

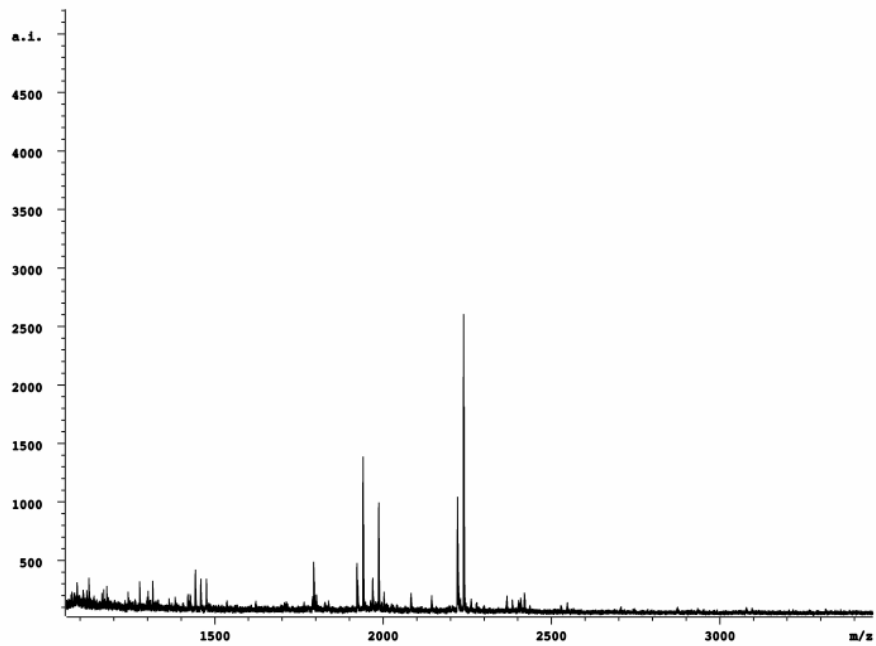


**Figure 74:** Example of a tryptic digest of band 17C from the gel 2D\_10\_09\_02\_Control. The spectrum has a sufficient number of adequate S/N peaks, but no identification could be made in the protein database.

A sufficient explanation as to why the instrument provides irregularly shifted  $m/z$  values has yet to be determined. Unintentional venting of the vacuum chambers may have allowed accumulation of water vapor, gases, dust, or other contaminants that would collide/interfere with the propagation of ions down the flight tube. Normal internal corrosion of the elements within the instrument due to the presence of such contaminants would also affect the performance of the instrument. The internal components should be thoroughly cleaned with a volatile solvent, such as methanol, to combat this problem. Software discrepancies may also contribute to the irregularity of generated data, in the computation of  $m/z$  values or the production of spectra, but it is difficult to pinpoint this as a problem unless the entire software were replaced, and data generated from the new software is tested.

In the cases where no identifications were made for digest spectra of good quality, it is always possible that the proteins were as yet uncharacterized/unidentified proteins, not in the database. However, this is unlikely, because the protein bands chosen were intense, they should be highly abundant and identified proteins in SM tissue.

In many digest spectra, what appeared to be contaminating polymer peaks were observed (Figures 75- 78). An experimental blank tryptic digest was performed on a small quantity of the latex gloves used regularly in the laboratory. The resultant spectrum is shown in figure 80. This may explain the source of the contaminating polymer peaks

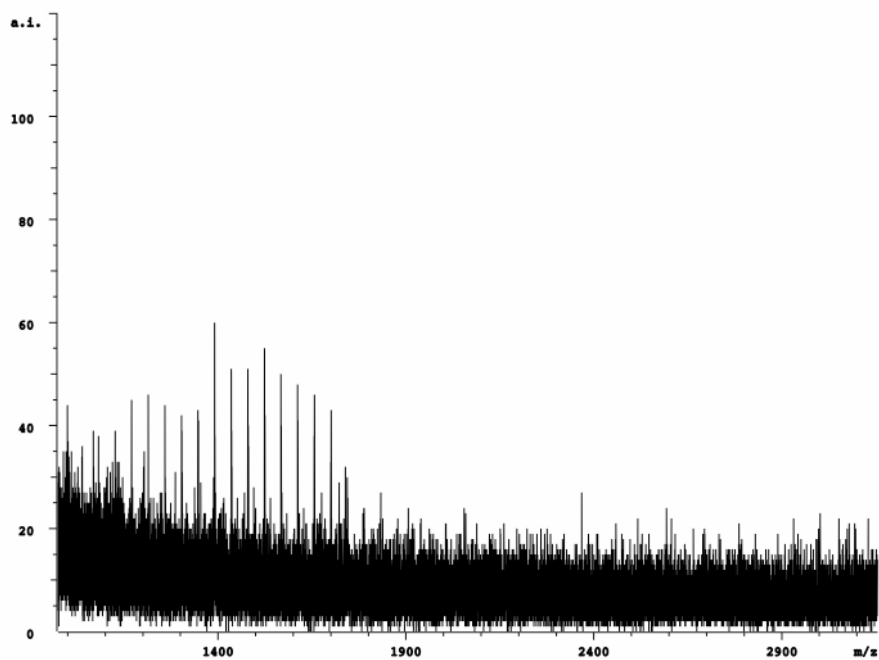


**Figure 75:** Tryptic digest averaged spectrum of protein band 6C from the 2D gel 2D\_7\_30\_02\_Control, revealing contaminating polymer peaks.

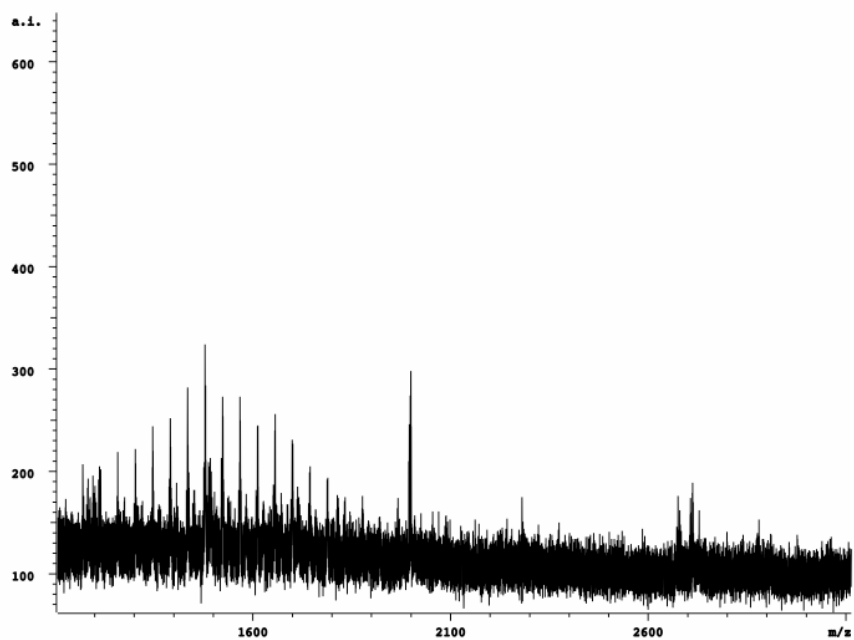


**Figure 76:** Tryptic digest averaged spectrum of protein band 1C from the 2D gel 2D\_7\_30\_02\_Control, revealing contaminating polymer peaks.



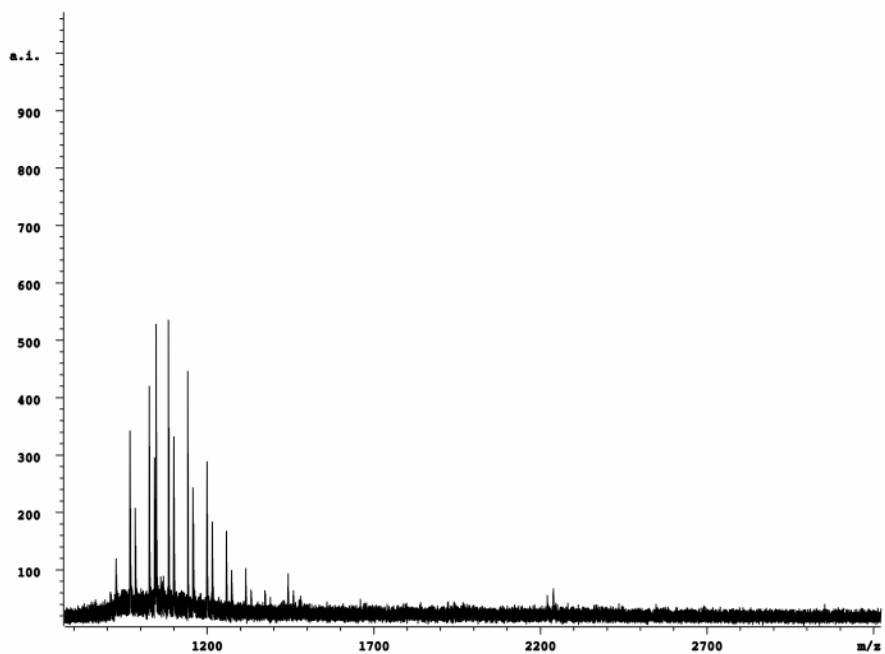


**Figure 77:** Tryptic digest averaged spectrum of protein band 23C from the 2D gel 2D\_10\_09\_02\_Control, revealing contaminating polymer peaks.

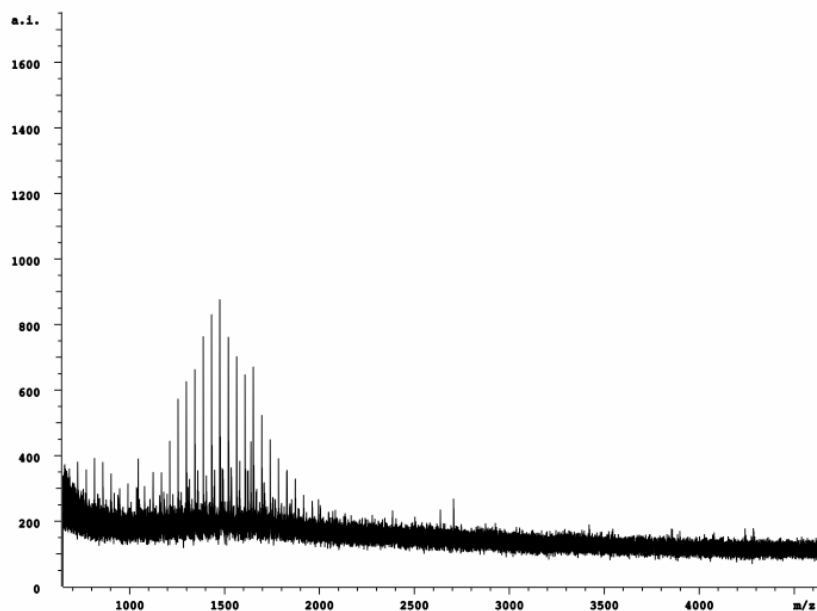


**Figure78:** Tryptic digest averaged spectrum of obtained when trypsin was added to a piece of the latex glove used in the laboratory, The spectrum reveals polymer peaks similar to those seen as contamination in many of the sample spectra, and may explain the source of such contamination.

Some observed phenomenon have yet to be explained. The modified and purified trypsin enzyme used for this analysis was purchased from Sigma-Aldrich. The trypsin was reportedly modified by dimethylation of lysine residues to prevent autolysis. The m/z peaks that would be obtained from autolysis of the modified trypsin are listed in table 6. An experimental blank was performed in which the trypsin was incubated with a blank piece of gel in attempt to allow autolysis. The spectra and peak list obtained from this blank may be seen in Figure 79 and Table 7, below.

The two sets of peaks for the theoretical and the experimental are incongruent with each other. The explanation for this is not known. It is suggested that the Sigma-Aldrich trypsin is modified in a different way or that instrument was malfunctioning as discussed earlier to produce m/z peaks of inaccurate value. The experimental blank was used to identify contaminating trypsin peaks in sample spectra.

1045.811	1744.266
1109.803	1849.249
1158.915	1888.293
1186.905	1893.404
1192.941	2048.456
1236.931	2055.453
1344.150	2067.366
1388.186	2209.504
1432.334	2224.469
1448.133	2237.546
1476.169	2351.598
1492.146	2510.736
1503.106	2633.923
1517.081	
1606.148	
1622.192	
1628.224	
1635.198	
1740.406	

**Table 6:** List of m/z peaks obtained from a theoretical digest of dimethylated trypsin.

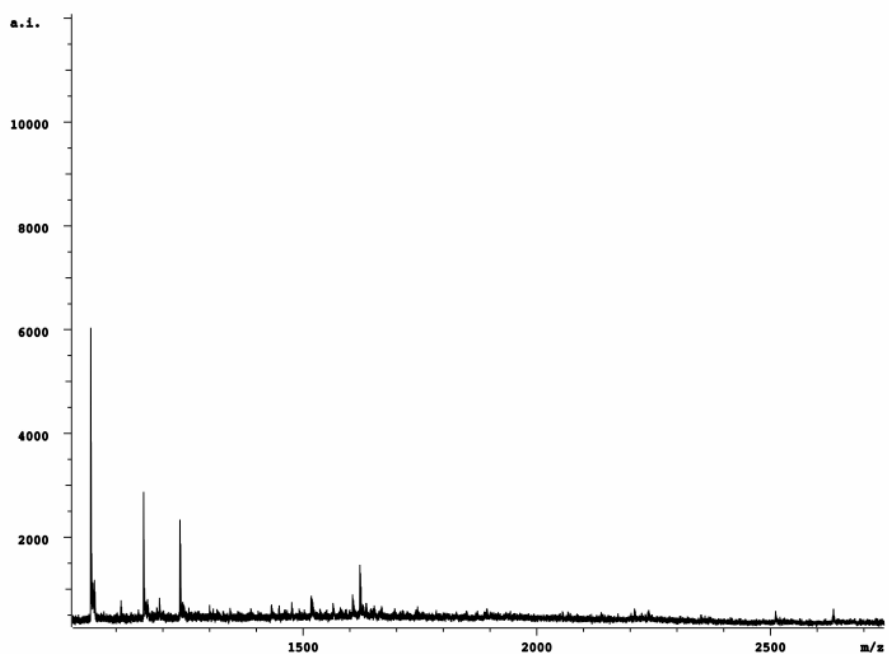


**Figure 79:** Averaged digest spectrum of self-digested, dimethylated trypsin purchased from Sigma-Aldrich performed in the laboratory at Marshall University to be referenced as an experimental blank for identification of contaminating trypsin peaks in sample spectra.

805.41	1999.04	2580.28
906.51	2027.08	2586.39
934.54	2055.11	2803.42
962.57	2083.14	2831.45
1020.20	2163.05	2910.31
1046.60	2191.08	2938.35
1048.54	2193.99	2966.38
1048.54	2209.98	3195.48
1074.63	2238.02	3211.47
1111.56	2273.16	3223.51
1139.57	2289.15	3239.50
1181.61	2301.19	3251.54
1364.69	2317.18	3267.53
1392.72	2321.20	3338.64
1420.75	2349.23	3366.67
1433.72	2377.27	3670.59
1461.75	2405.30	3686.58
1495.61	2514.33	3686.80
1497.76	2530.33	3698.62
1523.64	2542.37	3714.61

1525.79	2552.24	3714.83
1725.87	2558.36	3726.65
1753.89	2570.40	3742.64

**Table 7:** List of m/z peaks obtained from experimental autolysis of the dimethylated trypsin purchased from Sigma-Aldrich. These peaks are incongruent with those expected from the theoretical digest in table 5.

In many digest spectra, trypsin peaks were evident. This may be due to a concentration of trypsin that was too high for the amount of protein. Either the quantity of protein in the digested band was too low, as was often the case when the gels had to be silver stained, or too much trypsin was added. The abundance of trypsin peaks present in a sample spectrum could conceivably suppress actual peptide peaks, making protein identification and other analysis more difficult.

### ***PSD Analysis***

It was hoped that the employment of post source decay (PSD) analysis of peptide fragments within digested spectra would help facilitate a more positive identification of putative proteins. However, a good PSD spectrum was never obtained using the techniques described in this research. Preliminary spectra obtained in the acquisition of data during the stepwise voltage acclamations were of very poor resolution, especially those obtained from low reflector voltages which would deflect those fragments of lower MW. Naturally, if these are of poor quality, the subsequent fragmentation spectrum constructed from them will be of equally poor quality.

Manipulation of lens voltages to improve resolution of peaks proved unsuccessful. Because a good standard PSD fragmentation spectrum was never obtained, calibration of the instrument could not be performed, much less PSD analysis for an unknown sample spectrum. The instrumental software's peak picking parameters were found to be inadequate for choosing real m/z peaks, or else the calibration file was inaccurate. The m/z peaks chosen by the software were not real peaks, but noise spikes. Definite m/z peaks, though of poor resolution, were ignored by the software. It is probable that the ion gate that functions to preselect the peptide to be fragmented from the mixture of analytes was not working properly. This would inevitably cause difficulties in obtaining sufficient PSD data for sequencing the peptide.

## MASCOT Search Results

Unfortunately, many protein candidates were found for each peptide fingerprint entered into the protein database search—too many to report at full length in this collection.

An example of the possible candidates for one such spectra—band 1P from the 2D gel 7\_12\_02\_phorbol\_sup—is reported here (Figure 80). First, a list of the possible candidates was obtained from the MASCOT search engine, allowing for the indicated variable modifications. These candidates are listed in table 8, below.

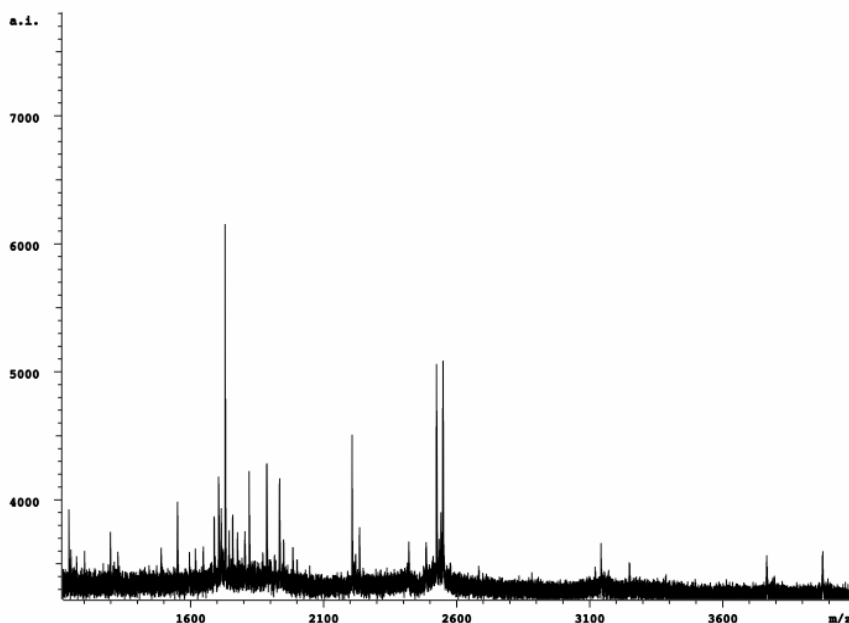


**Figure 80:** Tryptic digest spectra band 1P after from the 2D gel 2D\_7\_12\_02\_Phorbol. The peak list from this spectra was searched in the protein database by MASCOT to determine its identification.

### Possible IDs of Band 1P

Possible Candidates	# of Matching Peaks	MASCOT Score	Sequence coverage	Mass (Da)	Variable Modifications
$\alpha$ -actinin	30	28	48%	105176	Oxidized Met
Filamin C	29	42	34%	119496	Oxidized Met
Plectin 1	32	30	43%	95964	Oxidized Met
Vimentin	28	35	57%	53623	Oxidized Met
Vinculin	38	28	41%	117171	Oxidized Met
Integrin-linked PK	31	27	56%	51827	Oxidized Met Phos. Thr/Ser
PKA	26	25	47%	30322	Oxidized Met Phos. Thr/Ser

**Table 8:** List of the possible candidates for the identity of band 1P from the 2D gel 7\_12\_02\_phorbol\_sup.

Much information can be interpreted using the information in the database, and comparisons can be made between the characteristics of likely candidates and the experimentally determined parameters of a given protein digest, such as MW and pI. If these parameters do not match that of the unknown, it can be eliminated as a candidate. The protein  $\alpha$ -actinin is used as an example to show the comparison. In figure 81, the sequence of the protein covered by the peptide fingerprint spectra is shown. Table 9 compares the matching peaks in the sample spectra to the peptide fingerprint of the protein,  $\alpha$ -actinin.

1 MVMEKPSPLL VGREFVRQYY TLLNQAPDML HRFYGKNSSY AHGGLDSNGK  
51 PADAVYGQKE IHRKVMSQNF TNCHTKIRHV DAHATLNDGV VQVMGLLSN  
101 NNQALRRFMQ TFVLAPEGSV ANKFYVHNDI FRYQDEVFGG FVTEPQEERE  
151 EEVEEPEERQ QTPEVVPDDS GTFYDQTVSN DLEEHLEEPV VEPEPEPEPE  
201 PEPEPVDIQ EDKPEAALEE AAPDDVQKST SPAPADVAPA QEDLRTFSWA  
251 SVTSKNLPPS GAVPVTGTPP HVVKVPASQP RPESKPDSQI PPQRQRDQR  
301 VREQRINIPP QRGPRPIREA GEPGDVEPRR MVRHPDSHQL FIGNLPHEVD  
351 KSELKDFEQN FGNVELLRIN SGGKLPNFGF VVFDDSEPVQ KVLNSRPIMF  
401 RGAVRLNVEE KKTRAAREGD RRDNRLR GPG GPRGGPSGGM GPPRGGMVQ  
451 KPGFGVGRGI TTPRQ

**Figure 81:** Sequence coverage of the peptides matched for the band 1P from the 2D gel 7\_12\_02\_phorbol\_sup to  $\alpha$ -actinin, obtained from the MASCOT database search. Matching peptides are shown in red.

Amino acid Start - End	Observed M <sup>+</sup> Ion	Mass (expt) (Da)	Mass (calc) (Da)	Deviation (Da)	# of Missed Cleavages	Amino acid Sequence
41 - 50	1201.85	1200.84	1198.62	2.22	0	DLLLDPAWEK
51 - 65	1934.23	1933.22	1931.95	1.27	2	QQRKTFTAWCNSHLR
54 - 66	1647.73	1646.72	1647.83	-1.11	2	KTFTAWCNSHLRK
66 - 83	2047.83	2046.82	2048.02	-1.19	2	KAGTQIENIDEDFRDGL K
80 - 101	2524.39	2523.38	2521.43	1.95	2	DGLKLMLLLEVISGERL PKPER Oxidation (M)
109 - 125	1830.77	1829.76	1830.04	-0.27	2	INNVNKALDFIASKGVK
115 - 125	1150.06	1149.06	1147.66	1.40	1	ALDFIASKGVK
182 - 214	3974.08	3973.07	3973.05	0.02	2	NVNVQNPFHISWKDGLA FNALIHRRRPELIEYDK
205 - 214	1299.32	1298.31	1298.66	-0.35	0	HRPELIEYDK
218 - 233	1776.38	1775.37	1774.84	0.54	0	DDPVTNLNNAFEVAEK
234 - 255	2533.84	2532.83	2531.26	1.58	1	YLDIPKMLDAEDIVNTG RPDEK
234 - 255	2548.56	2547.55	2547.25	0.30	1	YLDIPKMLDAEDIVNTG RPDEK Oxidation (M)
240 - 255	1802.60	1801.59	1801.85	-0.26	0	MLDAEDIVNTGRPDEK
256 - 283	3120.72	3119.71	3121.51	-1.80	2	AIMTYVSSFYHAFSGAQ KAETAANRICK
312 - 331	2485.06	2484.05	2483.28	0.77	2	TIPWLEDRVPPQKTIQEM QQK Oxidation (M)
332 - 340	1272.09	1271.08	1268.63	2.46	2	LEDFRDYRR
364 - 378	1730.18	1729.18	1729.90	-0.72	1	LRLSNRPAFMPSEGR
396 - 410	1915.20	1914.19	1915.98	-1.79	1	GYEEWLLNEIPRLER
451 - 469	2206.65	2205.64	2206.12	-0.48	2	ALIRKHEAFESDLAAHQ DR
519 - 536	2215.74	2214.73	2214.16	0.57	2	TEKQLETIDQLHLEYAK R
605 - 632	3141.80	3140.79	3140.69	0.11	2	LSGSNPYTSVTPQIINSK WEKVQQLVPK
633 - 643	1327.51	1326.50	1324.67	1.83	1	RDHALLEEQSK
634 - 643	1171.73	1170.72	1168.57	2.15	0	DHALLEEQSK
653 - 668	1820.56	1819.55	1820.89	-1.34	0	QFASQANMVGPIQTK Oxidation (M)
761 - 779	2314.84	2313.83	2314.04	-0.21	1	GISQEQMQEFRASFNHF DK Oxidation (M)
780 - 813	3764.53	3763.52	3764.71	-1.19	2	DHGGALGPEEFKGLIS LGYDVENDRQGDAEFN R
814 - 837	2682.21	2681.20	2682.32	-1.12	0	IMSVVDPNHSGLVTFQA FIDFMSK
854 - 868	1706.05	1705.04	1702.93	2.12	1	VLAGDKNFITVEELR
869 - 882	1689.00	1687.99	1688.82	-0.83	1	KELPPDQAEYCIAR
900 - 911	1291.10	1290.09	1288.58	1.51	0	SFSTALYGESDL

**Table 9:** List of the matching monoisotopic m/z peaks of the sample band 1P from the 2D gel7\_12\_02\_phorbol\_sup compared to those of the candidate  $\alpha$ -actinin.

Variable phosphorylation of serine and threonine residues can also be tested in the database search. However, this comparison allows all possible serine and threonine residues to be phosphorylated, when matching theoretical peak masses. Phosphorylation at so many residues at once, or at all, is not likely. That makes this option of identifying phosphorylation sites tedious and most likely inaccurate. This option also provides more possible candidates for identification.

Only those candidates with significant MASCOT scores (>62) have been reported in depth. It was decided that a definitive positive identification should be concluded before time is spent, and likely wasted, investigating every possibility. Often, many likely candidates were produced with comparable, though insignificant, scores. There is simply not enough evidence to choose one candidate over another. The successfully identified proteins have been discussed, previously.

Only the MASCOT score, percentage of sequence coverage, and number of matched m/z peaks for each candidate are reported here. Of course, some spectra were very poor and did not have enough peaks to make any kind of characterization possible. Spectra with fewer than 8 peaks were not searched in the MASCOT database.

#### Unmatched Peaks

1143.59	1792.38
1309.17	1841.76
1313.44	1871.28
1444.90	1886.98
1489.97	1901.13
1551.34	1984.40
1596.36	2220.76
1618.66	2234.84
1715.49	2476.17
1722.11	2540.46
1758.34	2576.72

**Table 10:** List of the unmatched monoisotopic m/z peaks of the sample band 1P from the 2D gel 7\_12\_02\_phorbol\_sup when compared to the m/z peaks of  $\alpha$ -actinin.



Unmatched peaks may be molecules with salt adherents—such as sodium ( $\text{Na}^+$ ) or potassium ( $\text{K}^+$ )—, matrix peaks, trypsin peaks, or modified peaks (phosphorylated, glycosylated, etc). There is always the possibility that an incorrect identification has been made by the search engine. This probability is too high for candidates with MASCOT scores below the level of significance. Unmatched peaks may even be part of a second protein that migrated to a position on the gel near the band of interest, thus contaminating the sample analyte. Though this does not occur very often given the size of normal 2D gels.

Despite the limitations afforded by poor spectra, some general conclusions can be drawn from the lists of possible candidates. For example, it appears that the protein of band 1P, above, is at least a structural or filamentous protein involved in the cytoskeleton, because the majority of the likely candidates are structural proteins found in muscle tissue. The most rational options would be either vimentin or  $\alpha$ -actinin—structural proteins already known to exist in SM tissue. However, the possibility that the protein is an unknown structural protein still remains and cannot be ruled out.

Similar results were found for most of the protein spectra analyzed. Unfortunately, poor spectra prevented a positive identification for most of the spectra analyzed. Low MASCOT scores and a broad range of putative proteins inhibited any successful characterization. Such problems encountered in the development of this research have slowed its progress.

## **Phosphoproteomic Analysis**

Phosphoproteomic analysis was difficult given the methods use thus far and incorporating the setbacks imposed by encountered difficulties with the protocol. Sample enrichment,  $\beta$ -elimination, and other specific phosphoproteomic techniques have yet to be conducted, and should be attempted in the future. As mentioned in the introduction, analysis of phosphoproteins/peptides is more difficult because of their low stoichiometric abundance in digested peptide mixtures. Sample enrichment should improve their selective abundance. Phosphopeptides are also very hydrophilic and will not be selectively detained using the standard reverse-phase chromatography techniques used in this investigation. Purification of enriched sample using OligoR3 columns should instead be conducted in future work.

Two methods of detecting phosphorylated proteins were attempted in this research. The first utilized radioactive phosphorous-33 ( $^{33}\text{P}$ ) enrichment of tissue extracts coupled with autoradiographic detection to assay differential phosphorylation of proteins separated on 2D gels. This method was only attempted once with limited success. The autoradiographs produced from this protocol are shown in figures 82-85.

### **Autoradiograph Control**

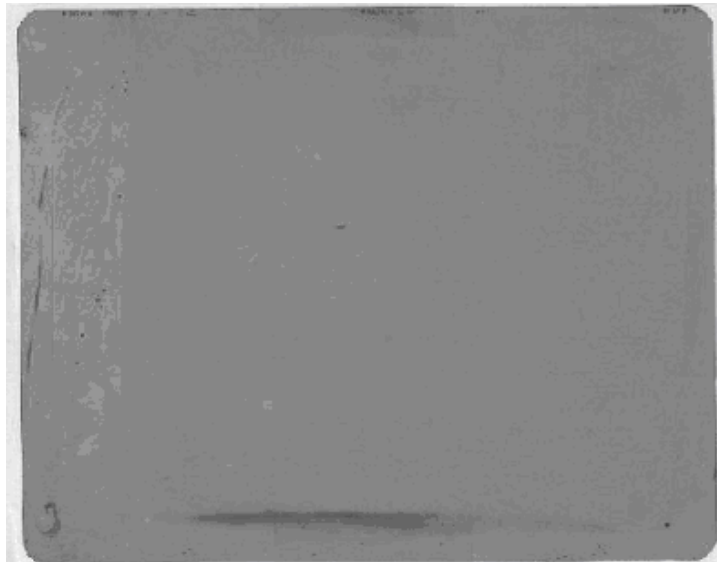


**Figure 82:** Autoradiograph obtained from a 2D gel produced from tube gel IEF separation with 12 hours of exposure. Aqueous proteins from resting SM tissue were used. The radiograph reveals no phosphorylated bands.

### **Autoradiograph Phorbol**

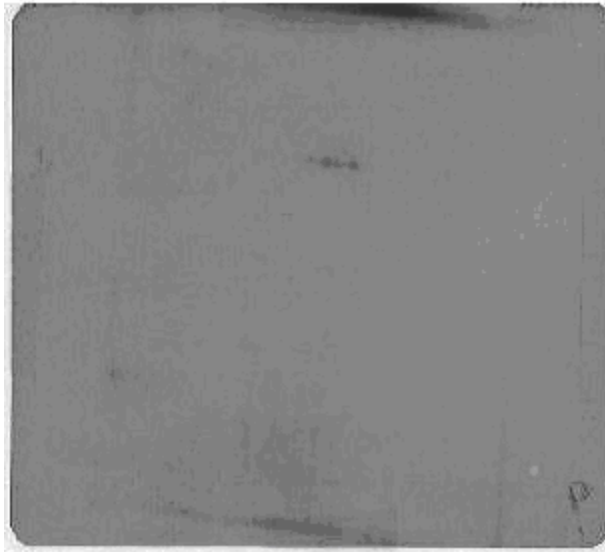


**Figure 83:** Autoradiograph obtained from a 2D gel produced from tube gel IEF separation with 12 hours of exposure. Aqueous proteins from phorbol-contracted SM tissue were used. The radiograph reveals phosphorylation on the band corresponding to tropomyosin.

#### **Autoradiograph Phorbol**

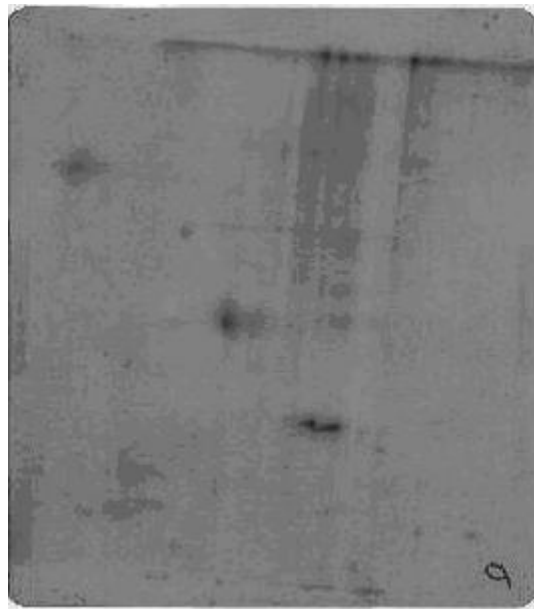


**Figure 84:** Autoradiograph obtained from a 2D gel produced from tube gel IEF separation with 36 hours of exposure. Aqueous proteins from phorbol-contracted SM tissue were used. More evidence of phosphorylated bands can be seen.

#### **Autoradiograph Phorbol-Membrane Proteins**

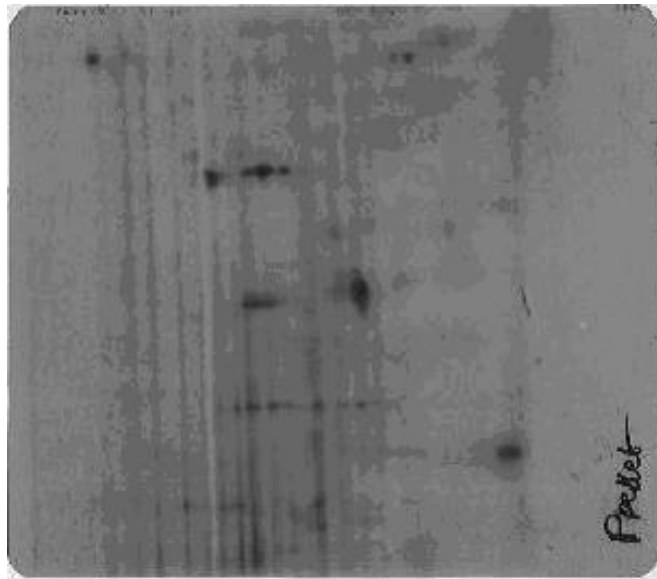


**Figure 85:** Autoradiograph obtained from a 2D gel produced from tube gel IEF separation with 36 hours of exposure. SDS-solubilized proteins from phorbol-contracted SM tissue were used. More evidence of phosphorylated bands can be seen.

For the first trial, evidence of phosphorylated proteins can be seen only for the protein band corresponding to tropomyosin on the phorbol-contracted gels (Figure 82). So, it can be concluded that the level of phosphorylation of tropomyosin increases during contraction. The enzyme that phosphorylates/dephosphorylates this protein is not known. This method was used in conjunction with tube gel IEF focusing. For this reason, the quantity of protein on the gel available for detection and subsequent analysis is low, as expected. The gels had to be silver stained to visualize any protein bands. This may explain the lack of evidence of phosphorylated proteins on the gel.

For the second trial, only gels corresponding to phorbol-contracted tissue were obtained. The corresponding silver stained gels can be seen in figures 32 and 46, respectively. These autoradiographs were subjected to a longer exposure time, so that phosphoprotein bands were more intense and better visualized. However, due to the lack of a corresponding control gel for resting tissue, differential analysis could not be conducted at this point. No protein identifications were made from these gels for the reasons discussed previously. Mainly, low protein concentration in the bands visualized by silver staining made analysis difficult, and thus

far, unsuccessful. Therefore, the identity of the phosphoproteins visualized on these gels is not known. However, improvement in this area promises better analysis for the future.

The second method for visualizing phosphoproteins makes use of the phosphospecific stain from Molecular Probes—ProQ Diamond Phosphoprotein stain, which binds more tightly to phosphorylated proteins than nonphosphorylated proteins due to charge interactions between the negatively-charged phosphate groups and the positively-charged stain molecules.

No bands were ever visualized using this stain, despite attempted modifications of lengthened staining and destaining periods. This method was attempted only in connection with the gels produced from IPG strips, so the total protein concentration should be high enough for detection. It is possible that the light source and camera used to excite and detect the stain were insufficient. The appropriate camera and filters may greatly enhance the sensitivity of the stain. These resources were not available. It is also possible that the stain is simply not sensitive enough to bind to and detect the low abundant phosphoproteins in biological samples.

Interference between the stain and free phosphate groups can occur if tissues are incubated in phosphate buffers. No such buffers were used during the lysis procedure conducted in preparation of the sample. Protein extracts should also be sufficiently purified during the acetone precipitation.

Because phosphoproteins were not sufficiently detected using the phosphoprotein stain, gels were stained with a total protein stain to look for deviations in the intensity of corresponding bands between the contracted and uncontracted gels. However, identification of proteins was not achieved, as was discussed earlier.

## **CONCLUSIONS**

Though some identifications of proteins in SM have been made given the results, thus far. Unexpected setbacks and other protocol adaptations have slowed research. So far, the localization of actin, tropomyosin, and MHC on a 2D gel has been discovered. It has also been concluded that tropomyosin is phosphorylated during contraction. As tropomyosin and actin bands can be seen in almost every gel, it may be concluded that they are present in abundance within aortic SM tissue. The heavy phosphorylation of this abundant protein implicate that this protein may play a larger role in contractile regulation than originally thought.

The primary objective of this research focused on the differential phosphorylation analysis between contracted and resting aortic SM tissue in order to better understand the mechanisms of signal transduction. Instead, the body of this work focused on the development of protocol for the analysis of phosphoproteins. Many problems were identified and solved. However, the largest obstacle of acquiring accurate, reproducible MS data to facilitate identification of proteins using the protein database still remains.

Future work in this investigation should include a Bradford assay for protein quantitation, use of the IPG strips for IEF separation of proteins to improve protein concentration on the 2D slab gels, and the use of phosphoproteomic techniques (sample enrichment of phosphoproteins, phosphatase inhibitors in cell lysis,  $\beta$ -elimination, Michael addition, etc.) for the selective analysis of phosphoproteins. Analysis of differential glycosylation in control and contracted SM tissue may be of interest for the future, as well.

Once a suitable protocol has been developed, the use of proteomic analysis should provide valuable information concerning the phosphorylation state of proteins in SM due to contraction, and from this information, conclusions made be drawn about signal transduction behind it. Once such goals have been accomplished, it should be followed by the use of different states of contraction (tonic/phasic), time dependent exposure of tissue to agonist, the effects of different agonists and/or relaxants on the state of phosphorylation, and perhaps different SM tissues. Ofcourse, analysis of signaling cascades in dysfunctional SM tissue should be explored, as well. There are many avenues of exploration that may be pursued, both biochemical at the molecular level and biophysical at the macroscopic level—mechanics/dynamics of contraction.

These preliminary results are just a small step in the process of understanding SM contraction. The need for its understanding becomes evident when the dominant and ever-

expanding threat of cardiovascular disease—the second leading cause of death in the United States, and number one in many countries (AHA 2002)—is considered. A thorough understanding of contraction in normal tissue will provide the base for which dysfunctions can be compared. Drug therapy, in particular, calls for the development of new, improved relaxants for the treatment of hypertension. Vascular SM contraction may also play a role in the development of atherosclerosis, which may be treated within SM tissue. Improvements in phosphoproteomic techniques and instrumentation capabilities will aid in the conquest.

**APPENDIX I:**  
**Mass Spectrometry**

The general principle behind mass spectrometry (MS) is the separation of gas phase ions based on their molecular weight (MW), or more specifically, the ratio of their mass to charge ( $m/z$ ). The advanced technology and specialization of mass spectrometry instrumentation and applications grows increasingly complex and sophisticated. Therefore, this appendix will cover only the general characteristics of MS.

The instrumentation of a mass spectrometer operates under three basic components: the source, the mass analyzer, and the detector. The choice of which type of each component is used depends on their suitability to the most desired qualities for sample analysis.

The source serves to vaporize and ionize—supply an electrical charge to—the sample analyte. Several different methods of ionization have evolved through avid research. In general, the ionization technique must transfer enough energy to the sample to cause it to vaporize.

In electron ionization (IE), the sample is bombarded with thermionic emission from a tungsten or rhenium filament (typically 70 eV). Fast atom bombardment (FAB) blasts a matrix-embedded sample with a fast beam of particles—usually an inert gas (Ar/Xe)—to facilitate ionization. Similarly, liquid secondary ion mass spectrometry (LSI-MS) uses an ion (usually  $CS^+$ ) to ionize the sample.

In electrospray ionization (ESI) makes use of the phenomenon of charged droplet evaporation. The sample solution is forced through a capillary to cause spraying or bubbling, producing minuscule charged droplets. A potential is then used to disperse the droplet into a fine spray of smaller droplets. The solvent evaporates away, shrinking the droplet, and causing the charged ions to get closer and closer together, until Coulombic repulsion causes the droplet to explode into smaller droplets. The process repeats itself until naked analytes are accomplished. The only problem with this technique lies in the statistical probability that analytes will be multiply-charged, which is not always desired. Smaller capillaries and slower flow rates decrease this probability, and, therefore, increase  $m/z$  ratios.

Matrix-assisted laser desorption/ionization (MALDI) couples a LASER pulse with a suitable matrix-embedded sample to produce molecular ions. The sample is embedded homogeneously in the matrix on a metal probe, facilitated by co-crystallization. The matrix, a small organic molecule, absorbs strongly at the wavelength of the LASER, and must itself be sublimable. It serves to donate its excitation energy to the sample, protects the sample



decomposition and/or aggregation of the analyte, and is also thought to donate protons to ionize the analyte (Figure 86).

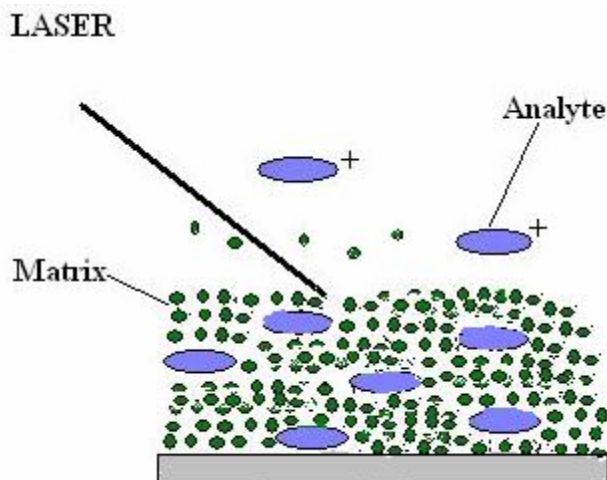


**Figure 86:** Illustration of a sample embedded in matrix on a metal probe.

This disadvantage of this technique is that the short duration of the ion burst produced by the laser desorption prevents association of the source with quadrupole analyzers, but makes it ideal for coupling with time of flight (TOF) analysis.

The mass analyzer is the component that separates the molecular ions. This can be accomplished based on the differential physical properties of the ions, done so in several ways.

In a double focusing sector mass analyzer, ions are accelerated through a potential into an electrostatic analyzer, which focuses ions of the same  $m/z$  to the same path, improving resolution. The ions then enter the magnetic sector, which produces a curved magnetic field—between 60 and 120°—whose strength can be varied to direct the flight path of different  $m/z$  ions toward the detector.

A time of flight mass analyzer accelerates molecular ions through a potential, supplying them with a characteristic kinetic energy (KE). The ions are then allowed to fly down a long chamber, or flight tube, under vacuum toward the detector. The ions will fly at a velocity characteristic of their KE, and that is a function of their molecular weight.

$$PE = eV = KE = \frac{1}{2} mv^2 \quad (2)$$

where PE = potential energy (Joules), V = voltage (volts), e = electron volts, m = mass (kg), and v = velocity (m/s).

A quadrupole mass analyzer is composed of four parallel rods, with static direct current (DC) through two, and alternating radio frequency (rF) applied to the other two. Ions are passed through the quad, and only those with the correct  $m/z$  values necessary to trajectory their path straight through the poles are detected, while all others deflected. The mathematics behind the physical event are complex, and will not be discussed.

In fourier transform ion cyclotron resonance (FT-ICR)—often referred to as FT-MS—, ions are first focused into a vacuum chamber. They then enter a cell housing a static magnetic field (B field), which causes the charged moieties to rotate in a circular orbit perpendicular to the field at a velocity characteristic of their  $m/z$ , and governed by the Lorentzian force.

$$F = zvB \quad (3)$$

where  $F$  = Lorentzian force.

An angular frequency ( $\omega$ ) is obtained because the ion is bent into the circular path.

$$\omega = zB/2\pi m \quad (4)$$

Ions are detected when an Rf pulse is used to excite ions at the correct  $m/z$  into a larger orbit.

The passing charge frequency is detected by two detectors located on either side of the cell, and a waveform is recorded. The waveform is computed back to the ion's  $m/z$ .

The ion trap is a system of three electrodes in a chamber that use varying voltages and Rf to trap ions in (Figure 87).

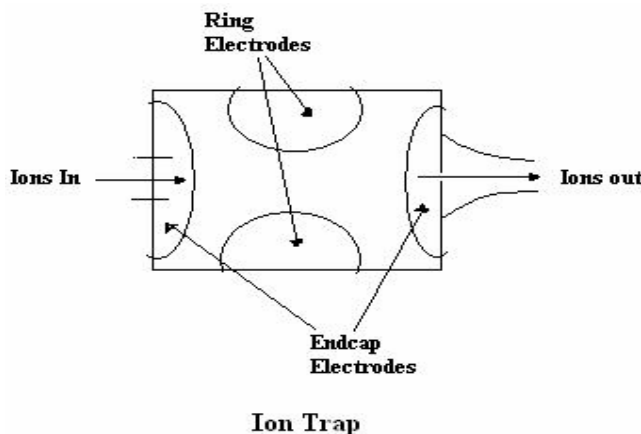


**Figure 87:** Diagram of the ion trap mass analyzer.

The ring electrode produces a three-dimensional electric field which causes ions to stay within the cell, with a trajectory dependent on their  $m/z$ .

The field is then changed to destabilize the ions' trajectories, so that the ions are ejected from the trap—smallest  $m/z$  to largest.

The third component is the detector which receives and processes the  $m/z$  signal. The detector transforms the electrical signal into a digital mass spectra, which is a plot of the ion intensity versus the  $m/z$  value.

Briefly, some general phenomenon associated with mass spectra, include the manifestation of isotopic peaks of a given ion. This is caused by the presence of multiple atomic isotopes that exist within a molecule, such as a deuterium ion (D) instead of a hydrogen. In peptides/proteins, frequent isotopes of hydrogen, nitrogen, carbon, and sulfur are usually seen. In a peptide spectra ( $\leq 5000$  Daltons (Da)), the result is a collection of peaks at the  $m/z$ , the first peak being the most abundant monoisotopic peak, except at higher mass values, where the probability of having to higher mass isotope atoms among the population of atoms increases. In a protein peak, isotope peaks are not clearly defined, but overlap each other (Figure 88).

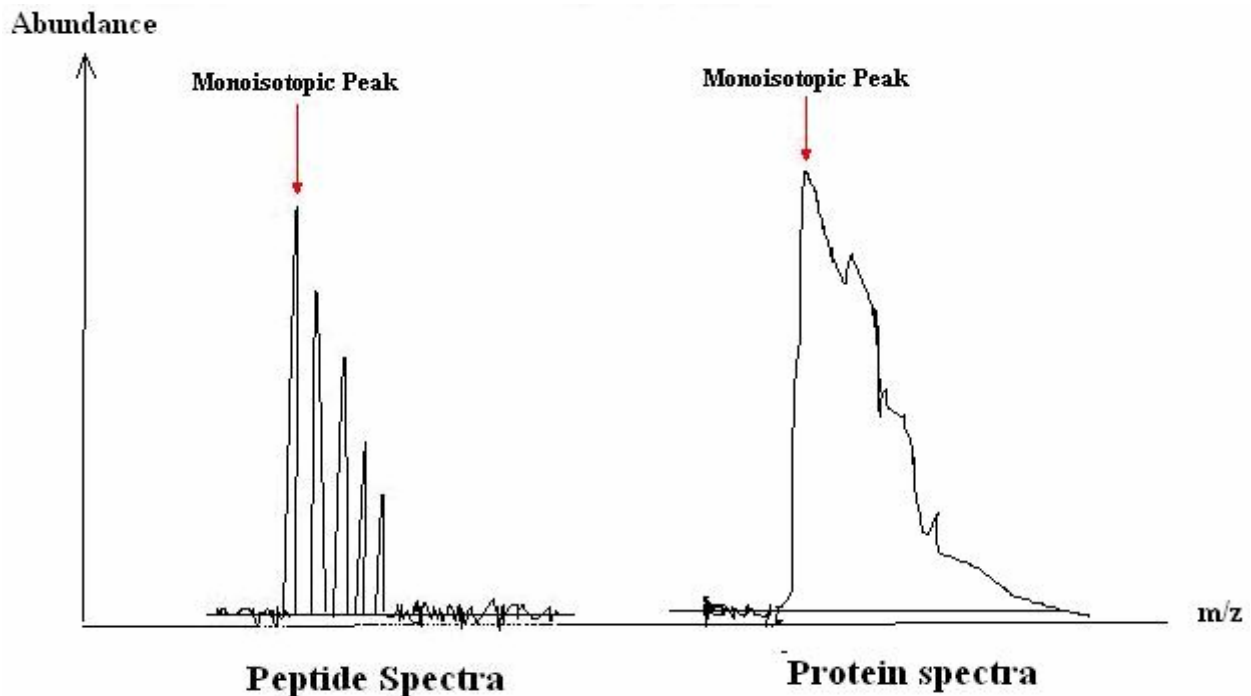


**Figure 88:** Illustration of a general peptide and protein mass spectrum, revealing the phenomenon of isotopic peaks.

Either the monoisotopic peak  $m/z$  can be used for analysis, or an average of the isotopic peaks can be used to characterize the molecular ion.

In biological samples, another frequently observed phenomenon is evidence of dimers, where two homogeneous or heterogeneous molecules are associated with each other and manifested in the same  $m/z$  peak. In the case of a homogeneous dimer, the  $m/z$  peak would appear at twice the normal mass  $[M^+]$  of the protein. A molecular ion can also be doubly-charged  $[M^{2+}]$ , which would result in an  $m/z$  peak at half the normal mass value (Figure 89).

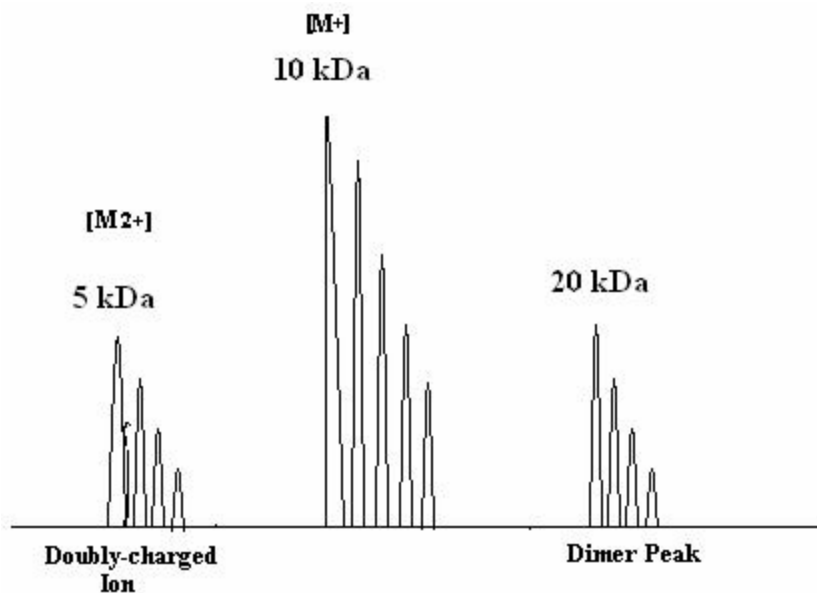


**Figure 89:** Simplified illustration showing the existence of a dimer peak and a doubly-charged peak  $[M^{2+}]$  in the same spectra as the normal molecular ion  $[M^+]$ .

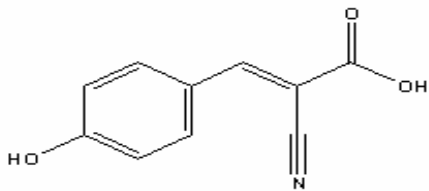
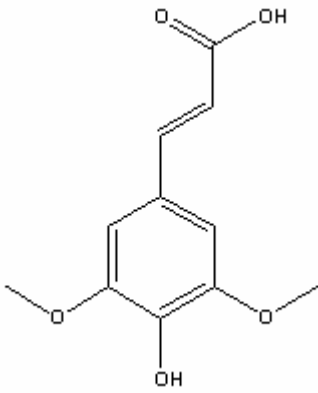
Applications of MS are numerous and exist in research, testing, and development practices of many areas; including industry, pharmaceuticals, academia, government, forensics and more. It is probably the most useful and widely-used technique, today. Advancements of instrumentation design continue to shape its influence and applicability in the progression of science.

## **APPENDIX II:**

### **MALDI-TOF MS and PSD**

MALDI-TOF MS uses a soft ionization technique coupled to a time of flight analyzer to provide quick  $m/z$  analysis of broad mass ranges with high sensitivity (see Appendix I). This method can detect picomolar (pm) quantities of analyte, and there is virtually no upper mass limit of detection.

For this research, a Bruker Biflex III MALDI-TOF was used. The Bruker Biflex III uses a nitrogen LASER source of 337.1 nm wavelength and 0.1 nm spectral bandwidth. The matrices used with this laser are sinapinic acid for proteins and  $\alpha$ -cyano-4-hydroxycinnamic acid (HCCA) for peptides (Table 11).

	<b>Other names</b>	<b>Use</b>	<b>Structure</b>
<b><math>\alpha</math>-cyano-4-hydroxycinnamic acid</b>	HCCA, $\alpha$ -cyano	Peptides	
<b>sinapinic acid</b>	3,5-Dimethoxy-4-hydroxycinnamic acid	Proteins	

**Table 11:** Matrices coupled with the nitrogen laser source for the Bruker Biflex III MALDI-TOF MS.

After desorption, ions are accelerated by a potential energy (PE) of 19 kV, which gives them a kinetic energy (KE), (equation 1). Ions are then allowed to travel down the time of flight tube at a velocity ( $v$ ) that is characteristic of their mass ( $m$ ).

$$PE = eV = KE = \frac{1}{2} mv^2 \quad (5)$$

where  $V$  = volts,  $e$  = electron volts. Smaller mass particles will travel faster and arrive at the detector first. Mass to charge ( $m/z$ ) values are computed based on the particles time of flight after acceleration (equation 2).

$$TOF = L \times \sqrt{(m/z)/2Ve} \quad (6)$$

where  $L$  = length of flight tube.

The instrument can activate in either positive or negative ion mode. Positive ion mode accelerates positively-charged ions toward the detector using a negative PE. Negative ion mode uses a positive voltage to accelerate negative ions.

The Bruker Biflex III design offers a delayed extraction function in which desorped and ionized particles are caught and focused by a set of focusing voltages/lenses (Figure 90). When the ions are blasted off the metal probe, they receive a KE. Each ion may have a different initial KE and starting position within the ionization chamber/source from which they may be accelerated (Figure 91).

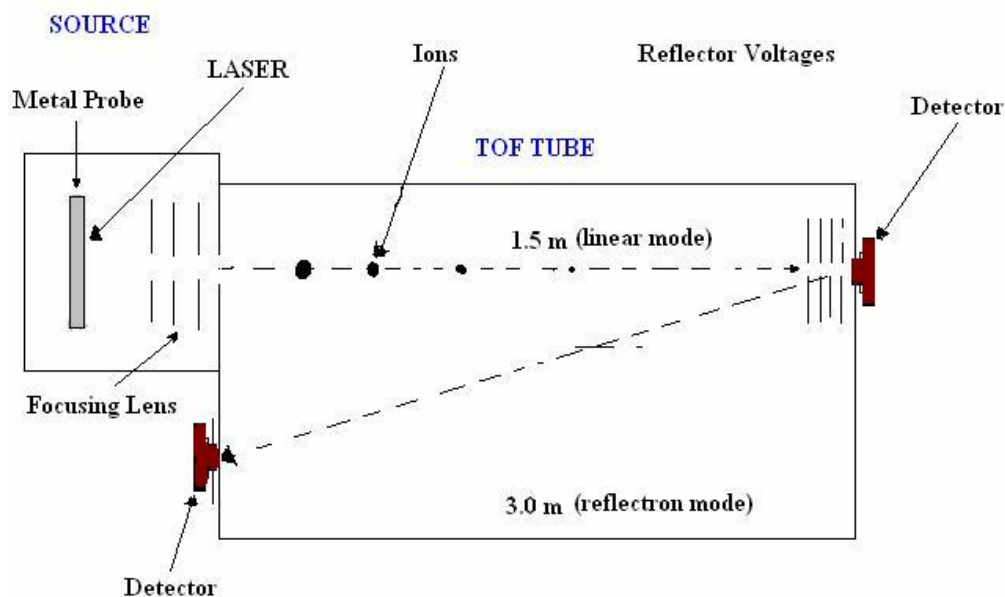


**Figure 90:** Diagram of the source (ionization chamber) and TOF tube of the Bruker Biflex III MALDI-TOF MS.

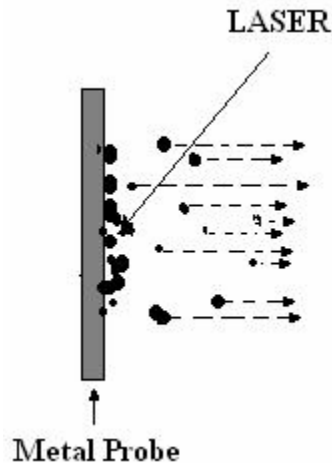


**Figure 91:** Illustration of the different starting positions of molecular ions in the ionization chamber prior to acceleration.

This will affect their time at which they will arrive at the detector and can cause broadening of peaks/loss of resolution. The focusing lenses help to equilibrate and concentrate the particles before they are accelerated by the 19 kV.

The Biflex III also offers a reflectron mode to further improve resolution and to allow post source decay (PSD) analysis. At the end of the flight tube are a series of reflector voltages which deflect oncoming particles back towards a detector at the other end of the tube, supplying a longer flight path and improved separation of ions (Figure 92). Reflectron mode is normally used for the analysis of peptides ( $\leq 5000$  Da). Linear mode is normally used for proteins.

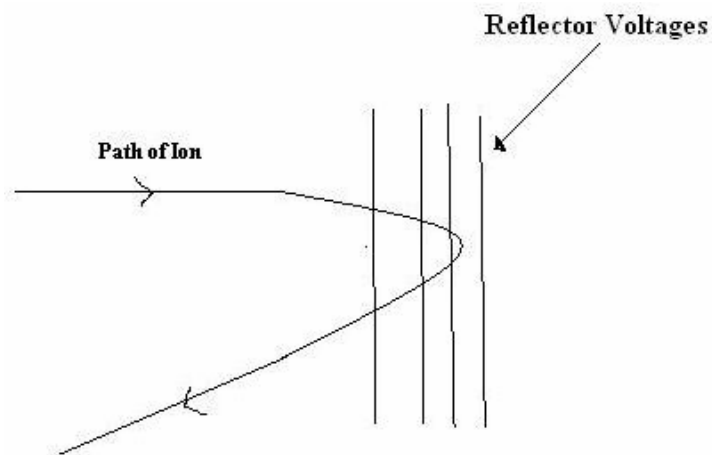


**Figure 92:** Diagram of the path of ions after reflection due to the reflector voltages in reflectron mode of the MALDI-TOF.

The reflectron feature also facilitates PSD, which can be used to devise structural information. A higher LASER power is used to supply more internal energy to the matrix and analyte. An ion gate (voltage) is used to select the molecular ion ( $m/z$  value) to be fragmented for PSD analysis. PSD theory makes use of the characteristic fragmentation of metastable molecular ions that occurs because of high internal energy and collisions that occur between the analyte, matrix ions, and/or residual gas in the flight tube (Kaufmann 1993). The molecular ion achieves its characteristic KE, and then fragments. The fragments will all have the same velocity, but the KE will be divided among the fragments (equation 3).

$$KE = \frac{1}{2} m_1 v^2 + \frac{1}{2} m_2 v^2 + \frac{1}{2} m_3 v^2 + \text{etc.} \quad (7)$$

The technique uses stepwise decreases in reflector voltages, collecting spectra at each voltage. Each reflector voltage focuses and deflects ions within a small KE range. This is known as a KE filter. High mass fragments are deflected first, and then increasingly lower mass fragments are deflected at each voltage. All the spectra are then computed and calibrated into a final fragmentation spectrum. Several properties such as LASER attenuation, focusing lens voltages, and reflector voltages can be adjusted to provide optimal resolution when collecting a spectrum.

A PSD spectrum reveals broken pieces of a peptide that can be put back together like a puzzle to reveal connectivity of composite amino acids. This can be used to devise structural information because fragmentation occurs along the weakest bond. In protein samples, this is usually the peptide bond (Figure 93).

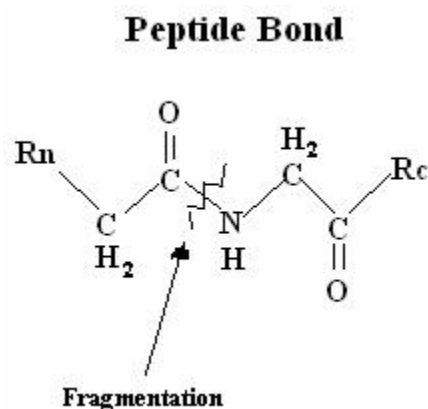


**Figure 93:** Illustration of the fragmentation of a peptide bond during PSD analysis.



Some limitations of PSD are that it is time-consuming to collect a spectrum at each reflector voltage, and then paste the spectra together. The technique is also less sensitive because it requires an increased amount of sample. A sample is depleted as a spectrum has to be collected at each voltage. There is also a loss of resolution associated with PSD that the reflector voltage normally supplies in normal analysis of peptides.

## **Appendix III:**

### **General Steps Involved in Proteomic Analysis of Biological Samples**

#### ***1. Isolation of Proteins***

Isolation is usually facilitated by SDS-PAGE (sodium dodecyl sulfate-polyacrylamide gel electrophoresis), in either one (1D) or two dimensions (2D). 1D electrophoresis separates a solubilized mixture of proteins by their molecular weight (MW), only. 2D electrophoresis also separates protein fractions by their isoelectric point (pI) in a pH gradient strip or gel. Isolation can also be accomplished by chromatography, in which various affinity reactions selectively retain desired products through antibody binding, enzyme-substrate association, or other specific chemical reactions (phosphorylation, glycosylation). A less efficient separation can be accomplished by centrifugation.

#### ***2. Purification***

Purification of samples can be achieved by dialysis prior to or after electrophoresis to filter lower MW contaminants such as salts from buffers or detergents, etc through a porous membrane in solution. Reverse-phase HPLC (high pressure liquid chromatography) or Ziptip concentration and desalting may be applied to protein/peptide mixtures, as well. In these methods, proteins or peptides mixtures are passed through and retained by tightly-packed columns of hydrophobic resin. They are then eluted off the column with a hydrophobic solvent, such as acetonitrile.

#### ***3. Analysis***

Analysis is usually performed using some form of mass spectrometry (MS), (see appendix I). Information that can be obtained by MS includes 1) MW, 2) amino acid (aa) sequence of peptides/proteins, 3) detection of post-translational modifications (phosphorylation sites, glycosylation sites), 4) detection of mutations, 5) isotopic abundance, 6) fragmentation patterns revealing structural information, 7) peptide fingerprints of proteolytically digested proteins, and 8) identification of unknown proteins when coupled with peptide maps in protein databases (facilitated to a large degree by the HGP).

**APPENDIX IV:**  
**Important Proteins in Smooth Muscle**

<b>Protein</b>	<b>MW (Da)</b>	<b>Theoretical pI</b>	<b>Function</b>	<b>Known P-Sites</b>
<b>α-Actin</b>	41,747	5.24	Composition of thin filaments.	UNKNOWN
<b>Myosin Heavy Chain (MHC)–SM1A fragment</b>	79,985	Undefined	Fragment of MHC that makes up the thick filaments.	UNKNOWN
<b>MHC—SM1B fragment</b>	80,736	Undefined	Fragment of MHC that make up the thick filaments.	UNKNOWN
<b>Myosin essential light chain (MLC<sub>essential</sub>)</b>	16,843.9	4.46	Part of the myosin head.	UNKNOWN
<b>Myosin regulatory light chain (MLC-20)</b>	19,764.1	4.67	Part of the myosin head. Regulates activity of actomyosin motor.	Thr-18 Ser-19
<b>Heavy meromyosin (HMM)</b>	-----	-----	Fragment of myosin formed by trypsin digestion—hinge region and ATPase.	UNKNOWN
<b>Light meromyosin (LMM)</b>	----- -	-----	Fragment of myosin formed during trypsin digestion—associates w/ other LMM to form filament.	UNKNOWN
<b>Tropomyosin (Tm)</b>	32,957.7	4.63	Thin-filament-associated protein-may help regulate contraction.	UNKNOWN
<b>Myosin light chain kinase (MLCK)</b>	113,993	5.48	Induces contraction by phosphorylating MLC-20.	UNKNOWN

<b>Myosin light chain phosphatase (MLCP)—cardiac isoform</b>	26,262	5.78	Inhibits contraction by dephosphorylating MLC-20.	UNKNOWN
<b>MYPT1—MLCP subunit</b>	8812	Undefined	Subunit of MLCP that targets myosin.	UNKNOWN
<b>PP1C—MLCP subunit</b>	36,983	6.12	Catalytic subunit of MLCP that dephosphorylates MLC-20	UNKNOWN
<b>20 kDa Fragment</b>	~20, 000	Undefined	Subunit of MLCP. Unknown function	UNKNOWN
<b>Tropomyosin (Tm)</b>	32,138.99	4.90	Associated with actin thin filaments. May help regulate contraction.	UNKNOWN
<b>Calmodulin (CaM)</b>	16,706.3	4.09	Binds Ca <sup>2+</sup> after influx; combines with MLCK to activate it.	Thr-44
<b>α-Actinin</b>	103,653.5	5.36	Found in the dense bodies of SM, analogous to z-discs in skeletal muscle—serve as attachments points for actin filaments.	UNKNOWN
<b>Desmin</b>	53,366.6	5.21	Found in the intermediate filaments of SM.	UNKNOWN
<b>Vimentin</b>	53,524.0	5.06	Found in the intermediate filaments of SM.	Ser-38 Ser-82
<b>Smoothelin</b>	100,135	9.01	Filamentous structural calponin-like protein present in the cytoplasm.	UNKNOWN

<b>Calreticulin</b>	46,319.8	4.33	Binds Ca <sup>2+</sup> in the SR.	UNKNOWN
<b>Calsequestrin</b>	41,662.9	3.96	Binds Ca <sup>2+</sup> in the SR.	UNKNOWN
<b>Phospholamban</b>			SR membrane protein that may regulate the Ca <sup>2+</sup> pump in the SR when phosphorylated.	Ser-16 Thr-17
<b>RhoA</b>	21,428.8	5.83	Regulatory protein in pathway of agonist-induced contraction.	UNKNOWN
<b>Rho-associated Kinase (ROK)</b>	159,526.6	5.72	Regulatory protein activated by RhoA. (See Appendix IIIf)	UNKNOWN
<b>cAMP-dependent protein kinase (PKA)</b>	40,462.9	8.71	Regulatory kinase activated by elevated [cAMP]. (See Appendix IIIe)	Ser-10 Ser-139 Ser-338 Thr-197 Lys-72 (ATP)
<b>cGMP-dependent protein kinase (PKG)</b>	Undefined	Undefined	Same as PKA.	UNKNOWN
<b>Protein Kinase C (PKC)</b>	76,742.9	6.61	Regulatory kinase activated by IP <sub>3</sub> . (See Appendix IIIId)	Thr-638 Thr-631 Lys-368 (ATP)
<b>Phospholipase C-β (PLC-β)</b>	138,257.5	5.86	Cleaves phosphoinositol into IP <sub>3</sub> and DAG.	Ser-887
<b>ZIP kinase</b>	51,3891.8	8.91	Phosphorylates MLCP and CPI-17. May be activated by ROK.	UNKNOWN
<b>Calmodulin kinase II (CaM KII)</b>	60,042.6	6.84	Regulatory kinase activated by elevated [Ca <sup>2+</sup> ]. (See	Lys-42 (ATP)

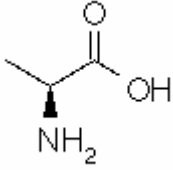
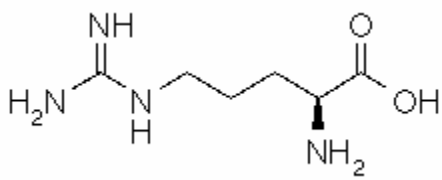
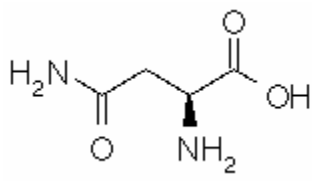
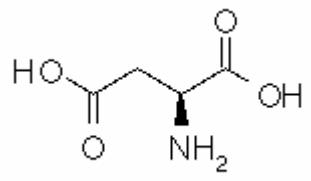
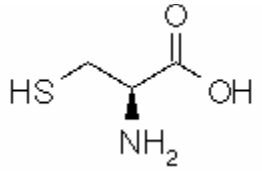
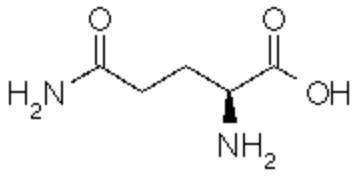
			Appendices IIIa and IIIb)	
<b>Integrin-linked kinase</b>	51313.9	8.30	Regulatory kinase that phosphorylates MLC-20.	Lys-220 (ATP)
<b>Mitogen-activated protein kinase (MAPK)</b>	42,023.8	8.67	Regulatory kinase in contraction. (See Appendix IIIg)	Thr-180 Tyr-182 Lys-54 (ATP)
<b>Mitogen-activated protein kinase kinase (MAPKK)</b>	43,306.3	6.20	Phosphorylates and activates MAPK.	Ser-217 Ser-221 Lys-96 (ATP)
<b>Raf</b>	67,508.37	9.27	Regulatory kinase involved in contraction. (See Appendix IIIg)	Lys-334 (ATP)
<b>Ras</b>	21,300.58	5.16	Regulatory GTPase protein involved in contraction. (See Appendix IIIg)	UNKNOWN
<b>Phospholipase A<sub>2</sub> (PLA<sub>2</sub>)</b>	13665.9	4.88	Calcium-dependent enzyme that cleaves arachidonic acid (AA) from phospholipids.	UNKNOWN
<b>Heat shock protein 20 (HSP-20)</b>	17.494.1	6.05	Inactivates the actomyosin MgATPase when phosphorylated by PKA/PKG	UNKNOWN
<b>Ryanodine receptor (RyaR)</b>			Ca <sup>2+</sup> ion channel in the SR. Allows Ca <sup>2+</sup> influx. (See Appendix IIIc)	UNKNOWN
<b>IP<sub>3</sub> receptor Ca<sup>2+</sup> channel</b>	Undefined	Undefined	Ca <sup>2+</sup> ion channel in the SR. Allows Ca <sup>2+</sup> influx. (See Appendix IIIc)	UNKNOWN
<b>Ca<sup>2+</sup>/Na<sup>+</sup> Exchanger</b>	Undefined	Undefined	Ca <sup>2+</sup> ion channel in the plasma membrane (PM).	UNKNOWN

			Removes Ca <sup>2+</sup> from the cytosol. (See Appendix IIIc)	
<b>Ca<sup>2+</sup>-ATPase pump</b>	Undefined	Undefined	Ca <sup>2+</sup> ion channel in the PM. Removes Ca <sup>2+</sup> from the cytosol. (See Appendix IIIc)	UNKNOWN

P-Sites = Phosphorylation Sites

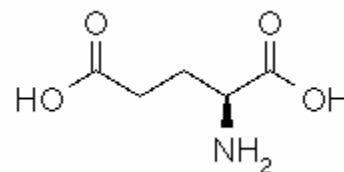
Information was obtained from the Swiss-Prot protein database.<sup>237</sup>

**APPENDIX V:**  
**20 Common Amino Acids**

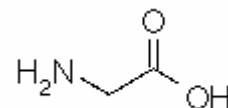
<u>Name</u>	<u>Abbrev.</u>	<u>Symbol</u>	<u>MW</u>	<u>pI</u>	<u>Structure</u>
1. Alanine	Ala	A	89.09	6.00	
2. Arginine	Arg	R	174.2	11.15	
3. Asparagine	Asn	N	132.12	5.41	
4. Aspartic Acid	Asp	D	133.10	2.77	
5. Cysteine	Cys	C	121.15	5.02	
6. Glutamine	Gln	Q	146.15	5.65	



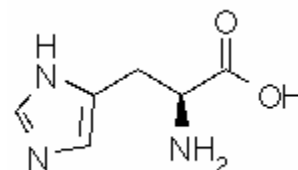
7. Glutamic Acid    Glu    E    147.13    3.22



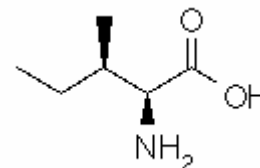
8. Glycine    Gly    G    75.07    5.97



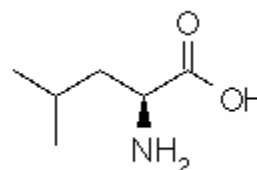
9. Histidine    His    H    155.16    7.47



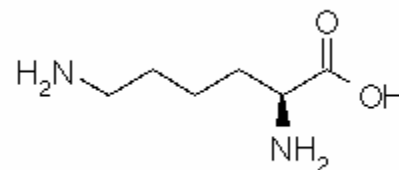
10. Isoleucine    Ile    I    131.17    5.94



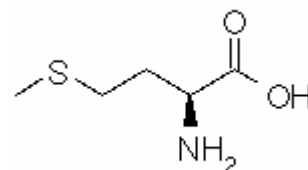
11. Leucine    Leu    L    131.17    5.98



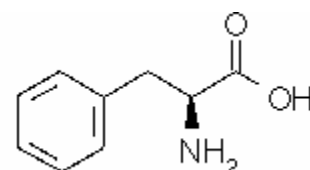
12. Lysine    Lys    K    146.19    9.59

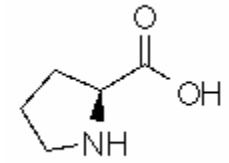
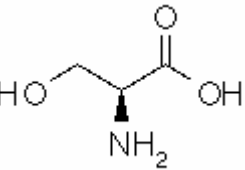
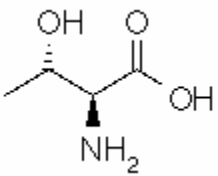
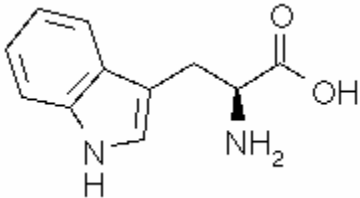
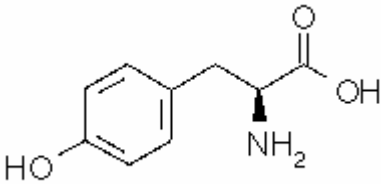
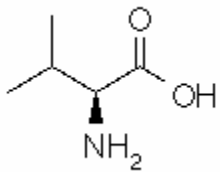


13. Methionine    Met    M    149.21    5.71



14. Phenylalanine    Phe    F    165.19    5.41



15. Proline	Pro	P	115.13	6.30	
16. Serine	Ser	S	105.09	5.68	
17. Threonine	Thr	T	119.12	5.64	
18. Tryptophan	Trp	W	204.23	5.89	
19. Tyrosine	Tyr	Y	181.19	5.66	
20. Valine	Val	V	117.15	5.96	

## REFERENCES

1. Aaronson P, van Breemen C. *J Physiol*, London. 319: 443-461, **1981**.
2. Abdel-Latif A. Cross talk between cyclic nucleotides and polyphosphoinositide hydrolysis, protein kinases, and contraction smooth muscle. *Exp Biol Med*. 226 (3): 153-163, **2001**.
3. Adam LP, Gapinski CJ, Hathaway DR. *FEBS Lett*. 302: 223-226, **1992**.
4. Adamczyk M, Gebler JC, Wu J. Selective analysis of phosphopeptides within a protein mixture by chemical modification, reversible biotinylation and mass spectrometry, *Rapid Commun Mass Spectrom*. 15(16):1481-8, **2001**.
5. Adelstein RS, Sellers JR, Conti MA, Pato MD, de Lanerolle P. Regulation of smooth muscle contractile proteins by calmodulin and cyclic AMP, *Fed Proc*. 41(12): 2873-2878, **1982**.
6. Alberts, Bray, Johnson, Lewis, Raff, Roberts, Walter. Myosin and actin model. Garland Publishing, **1998**. [http://www.accessexcellence.org/AB/GG/myosin\\_Actin.html](http://www.accessexcellence.org/AB/GG/myosin_Actin.html). 7/11/03.
7. Albrecht K, Schneider A, Liebetrau C, Ruegg JC, PfitzerG. Exogenous caldesmon promotes relaxation of guinea-pig skinned taenia coli smooth muscles: inhibition of cooperative reattachment of latch bridges? *Pflugers Arch*. 434:534-542, **1997**.
8. Alessi D, MacDougall LK, Sola MM, Ikebe M, Cohen P. The control of protein phosphatase-1 by targetin subunits: the major myosin phosphatase in avian smooth muscle is a novel form of protein phosphatase-1. *Euro J Biochem*. 219: 1023-1035, **1992**.
9. Amano M, Ito M, Kimura K, Fukata Y, Chihara K, Nakano T, Matsuura Y, Kaibuchi K. Phosphorylation and activation of myosin by Rho-associated kinase (Rho-kinase), *J Biol Chem*. 27(34): 20,246-20,249, **1996**.
10. American Heart Association, Heart Disease and Stroke Statistics-**2003 Update**. Dallas, TX: American Heart Association, 2002. <http://www.americanheart.org/>.
11. Arner A, Pfizer G. Regulation of cross-bridge cycling by Ca<sup>2+</sup> in smooth muscle, *Rev Physiol Biochem Pharmacol*. 134: 63-146, **1999**.
12. Arner A, Goody RS, Rapp G, Ruegg JC. Relaxation of chemically skinned guinea pig taenia coli smooth muscle from rigor by photolytic release of adenosine-5'-triphosphate, *J Muscle Res Cell Motil*. 8: 377-485, **1987**.
13. Bárány, M. and Bárány, K. Protein phosphorylation during contraction and relaxation. In *Biochemistry of Smooth Muscle Contraction* (M. Bárány, Ed.), pp. 321-339, Academic Press, **1996**.

14. Battistella-Patterson AS, Fultz ME, Li C, Geng W, Norton M, Wright GL. PKC $\alpha$  translocation is microtubule-dependent in passaged smooth muscle cells. *Acta Physiol Scand.* 170(2):87-97, **2000**.
15. Beall AC, Kato K, Goldenring JR, Rasmussen H, Brophy CM. Cyclic nucleotide-dependent vasorelaxation is associated with the phosphorylation of a small heat shock-related protein, *J Biol Chem.* 272: 11283-11287, **1997**.
16. Bolton TB, Imaizumi Y. Spontaneous transient outward currents in smooth muscle cells, *Cell Calcium.* 20(2): 141-152, **1996**.
17. Bond M, Shuman H, Somlyo AP, Somlyo AV. *J Physiol, London.* 357: 185-201, **1984**.
18. Bonev AD, Jaggar JH, Rubart M, Nelson MT. Activators of protein kinase Ca<sup>2+</sup> decrease C spark frequency in smooth muscle cells from cerebral arteries, *Am J Physiol.* 273(6 Pt 1): C2090-C2095, **1997**.
19. Bornfeldt KE, Krebs EG. Cross talk between protein kinase A and growth factor receptor signaling pathways in arterial smooth muscle, *Cell Signal.* 11: 465-477, **1999**.
20. Bradley AB, Morgan KG. Alterations in cytoplasmic calcium sensitivity during porcine coronary artery contractions as detected by aequorin, *J Physiol.* 385: 437-448, **1987**.
21. Brophy, C.M., Lamb, S., and Graham, A. The small heat shock-related protein-20 is an actin-associated protein. *J. Vasc. Surg.* 29, 326-333, **1999**.
22. Bulbring E, Tomita T. *Pharma Rev.* 39: 49-95, **1987**.
23. Byford MF. Rapid and selective modification of phosphoserine residues catalysed by Ba<sup>2+</sup> ions for their detection during peptide microsequencing. *Biochem J.* 280 ( Pt 1):261-5, **1991**.
24. Cao P, Stults JT. *Rapid Commun Mass Spectrom.* 14: 1600, **2000**.
25. Carafoli E, Guerini D. *Trends Cardiovasc Med.* 3: 177-184, **1993**.
26. Cardiovascular Diseases-Prevention and Control, WHO CVD Strategy, **2001/2002**.
27. Cherfils J, Chardin P. GEFs: structural basis for their activation of small GTP-binding proteins, *Trends Biol Sci.* 24: 306-311, **1999**.
28. Conti MA, Adelstein RS. The relationship between calmodulin binding and phosphorylation of smooth muscle kinase by the catalytic subunit of 3':5'-cAMP dependent protein kinase, *J Biol Chem.* 256: 3178-3181, **1981**.

29. Cospedal R, Lobo M, Zachary I. Differential regulation for extracellular signal-regulated protein kinases (ERKs) 1 and 2 by cAMP and dissociation of ERK inhibition from anti-mitogenic effects in rabbit vascular smooth muscle cells. *Biochem J.* 342: 407-414, **1999**.
30. Croxton TL, Lande B, Hirshman CA. Role of G proteins in agonist-induced  $Ca^{2+}$  sensitization of tracheal smooth muscle, *Amer J Physiol.* 275: L748-755, **1998**.
31. Dai Y, Whittall RM, Li L. Two-layer sample preparation: a method for MALDI-MS analysis of complex peptide and protein mixtures, *Anal Chem.* 71(5):1087-1091, **1999**.
32. De Alencar Cunha KM, Paiva IA, Santos FA, Gramosa NV, Silveira Er, Rao VS. Smooth muscle relaxant effect of kaurenoic acid, a diterpene from *Copaifera langsdorffii* on rat uterus in vitro, *Phytother Res.* 17(4): 320-324, **2003**.
33. De Lanerolle P, Nishikawa M, Yost DA, Adelstein RS. Increased phosphorylation of myosin light chain kinase after an increase in cyclic AMP in intact smooth muscle, *Science* (Washington, DC). 223: 1415-1417, **1984**.
34. Dechert M, Holder F., Gerhoffer W. p21-activated kinase 1 participates in tracheal smooth muscle cell migration by signaling to p38 MAPK, *Am Physiol Soc.* C123-C132, **2001**.
35. Deng JT, Van Lierop JE, Sutherland C, Walsh MP.  $Ca^{2+}$ -independent smooth muscle contraction. A novel function for integrin-linked kinase, *J Biol Chem.* 276(19): 16,365-16,373, **2001**.
36. Dessy C, Kim I, Sougnez, CL, Laporte R, Morgan KG. A role for MAP kinase in differentiated smooth muscle contraction evoked by  $\alpha$ -adrenoreceptor stimulation. *Am J Physiol.* 275 (*Cell Physiol* 44): C1081-C1086, **1998**.
37. Dhanikoti SN, Gao Y, Nguyen MQ, Raj JU. Involvement of cGMP-dependent protein kinase in the relaxation of ovine pulmonary arteries to cGMP and cAMP, *Appl Physiol.* 88: 1637-1642, **2000**.
38. Di Blasi P, Van Riper D, Kaiser R, Rembold CM, Murphy RA. Steady-state dependence of stress on cross-bridge phosphorylation in the swine carotid media, *Am J Physiol Cell Physiol.* 262: C1388-C1391, **1992**.
39. Dodge KL, Carr DW, Sanborn BM. Protein kinase A anchoring to the myomerial plasma membrane is required for cAMP regulation of phosphoinositide turnover, *Endocrinology.* 140: 5165-5170, **1999**.
40. Drab M, Verkade P, Wlger M, Kasper M, Lohn M, Lauterback B, Menne J, Lindschau C, Mende f, Luft FC, Schedl A, Haller H, Kurzchalia TV. Loss of caveolae, vascular

- dysfunction, and pulmonary defects in caveolin-1 gene-disrupted mice, *Science*. 293(5539): 2449-2452, **2001**.
41. Dykes AC, Fultz ME, Norton ML, Wright GL. Microtubule-dependent PKC-alpha localization in A7r5 smooth muscle cells. *Am J Physiol Cell Physiol*. 285(1):C76-87, **2003**.
  42. Ebashi S. *A Rev Physiol*. 53: 1-16, **1991**.
  43. Eto M, Ohmori T, Suzuke M, Furuya K, Morita F. A novel protein phosphatase-1 inhibitory protein potentiated by protein kinase C. Isolation from porcine aorta media and characterization, *J Biochem (Tokyo)*. 118: 1104-1107, **1995**.
  44. Feng J, Ito M, Kureishi Y, Ichikawa K, Isaka N, Nishikawa M, Hartshorne DJ, Nakano T. Inhibitory phosphorylation site for Rho-associated kinase on the smooth muscle myosin phosphatase target, *J Biol Chem*. 274: 3744-3752, **2000**.
  45. Feng J, Ito M, Kureishi Y, Ichikawa K, Amano M, Isaka N, Okawa K, Iwamatsu A, Kaibuchi K, Hartshorne DJ, Nakano T. Rho-associated kinase of chicken gizzard smooth muscle, *J Biol Chem*. 274: 3744-3752, **1999**.
  46. Fernandes DJ, Mitchell RW, Lakser O, Dowell M, Stewart AG, Solway J. Invited Review: Do inflammatory mediators influence the contribution of airway smooth muscle contraction to airway hyperresponsiveness in asthma? *J Appl Physiol*. 95(2):844-53, **2003**.
  47. Ficarro SB, McClelland ML, Stukenberg PT, Vurke DJ, Ross MM, Shabanowitz J, Hunt DF, White FM. Phosphoproteome analysis by mass spectrometry and its application *Saccharomyces cerevisiae* *Nature Biotechnol*. 20: 301, **2002**.
  48. Filo RS, Bohr DF, Ruegg JC. *Science*. 147:1581-1583, **1965**.
  49. Fischer W, Pfitzer G. Rapid myosin phosphorylation transients in phasic contraction in chicken gizzard smooth muscle, *FEBS Lett*. 258: 59-62, **1989**.
  50. Fleischer S, Inui M. *A Rev Biophys Acta*. 882: 258-265, **1986**.
  51. Fu X, Gong MC, Jia T, Somlyo AV, Somlyo AP. The effects of the Rho-kinase inhibitor Y-27632 on arachidonic-acid-GTPγS-, and phorbol ester-induced Ca<sup>2+</sup>-sensitization of smooth muscle, *FEBS Lett*. 440: 183-187, **1998**.
  52. Fuglsang A, Kromov A, Torok K, Somlyo AV, Somlyo AP. *J Musc Res Cell Motil*. 15: 666-673, **1993**.

53. Fujihara H, Walker LA, Gong MC, Lemichez E, Boquet P, Somlyo AV, Somlyo AP. Inhibition of RhoA translocation, and calcium sensitization by in vivo ADP-ribosylation with the chimeric toxin DC3B, *Mol Biol Cell*. 8: 2437-2447, **1997**.
54. Fultz ME, Wright GL. Myosin remodelling in the contracting A7r5 smooth muscle cell. *Acta Physiol Scand*. 177(2):197-205, **2003**.
55. Fultz ME, Li C, Geng W, Wright GL. Remodeling of the actin cytoskeleton in the contracting A7r5 smooth muscle cell. *J Muscle Res Cell Motil*.21(8):775-87, **2000**.
56. Fung ET, Wright GL Jr, Dalmaso EA. Proteomic strategies for biomarker identification: progress and challenges. *Curr Opin Mol Ther*. 2(6):643-50, **2000**.
57. Gailly P, Gong MC, Somlyo AV, Somlyo AP. Possible role of a typical protein kinase C activated by arachidonic acid in Ca<sup>2+</sup> sensitization of rabbit smooth muscle, *J Physiol (Lond)*. 500: 95-109, **1997**.
58. Gailley P, Gong MC, Somlyo AP, Cohen PTW, Cohen P, Somlyo AV. Regions of the 100-kDa regulatory subunit M<sub>110</sub> required for regulation of myosin-light-chain-phosphatase activity in smooth muscle, *Euro J Biochem*. 239: 326-332, **1996**.
59. Ganitkevich V, Hasse V, Pfitzer G. Ca<sup>2+</sup>-dependent and Ca<sup>2+</sup>-independent regulation of smooth muscle contraction, *J Musc Res Cell Motil*. 23: 47-52, **2002**.
60. Ganitkevich VY, Isenber G. *J Physiol, London*. 470: 35-44, **1993**.
61. Gao Y, Kawano K, Yoshiyama S, Kawamichi H, Wang X, Nakamura A, Kohama K. Myosin light chain kinase stimulates smooth muscle myosin ATPase activity by binding to the myosin heads without phosphorylating the myosin light chain. *Biochem Biophys Res Commun* .305(1):16-21, **2003**.
62. Genomic Solutions, Inc. *Investigator 2-D Electrophoresis System*; Ann Arbor, MI, **1997**.
63. Gong MC, Fujihara H, Somlyo AV, Somlyo AP. Translocation of rhoA associated with Ca<sup>2+</sup>-sensitization of smooth muscle, *J Biol Chem*. 272: 10704-10709, **1997**.
64. Gong MC, Kinter MT, Somlyo AV, Somlyo AP. Arachidonic acid and diacylglycerol release associated with inhibition of myosin light chain dephosphorylation in rabbit smooth muscle, *J Physiol*. 486: 113-122, **1995**.
65. Gong MC, Fuglsang A, Alessi D, Kobayashi S, Cohen P, Somlyo AV, Somlyo AP. Arachidonic acid inhibits myosin light chain phosphatase and sensitizes smooth muscle to calcium, *J Biol Chem*. 267: 21492-21498, **1992**.

66. Goshe MB, Conrads TP, Panisko EA, Angell NH, Veenstra TD, Smith RD. Phosphoprotein isotope-coded affinity tag approach for isolating and quantitating phosphopeptides in proteome-wide analyses, *Anal Chem.* 73(11):2578-86, **2001**.
67. Gosser YQ, Nomanbhoy TK, Aghazadeh B, Manor D, Combs C, Cerione RA, Rosen MK. C-terminal domain of Rho GDP-dissociation inhibitor directs N-terminal inhibitory peptide to GTPase, *Nature.* 387: 814-819, **1997**.
68. Hart MJ, Jiang X, Kozawa T, Roscoe W, Singer WD, Gilman AG, Sternweis PC, Bollag G. Direct stimulation of the guanine nucleotide exchange activity of p115 RhoGEF by G<sub>α13</sub>, *Science.* 280: 2112-2114, **1998**.
69. Hart C, Schulenberg B, Steinberg TH, Leung WY, Patton WF. Detection of glycoproteins in polyacrylamide gels and on electroblots using Pro-Q Emerald 488 dye, a fluorescent periodate Schiff-base stain, *Electrophoresis.* 24: 588-598, **2003**.
70. Hartshorne DJ. Biochemistry of the contractile proteins in smooth muscle. In Physiology of the Gastrointestinal Tract, 2<sup>nd</sup> ed, edited by Johnson LR, pp. 423-482. Raven Press, New York, **1987**.
71. Hartshorne DJ, Ito M, Erdodi F. Myosin light chain phosphatase: subunit composition, interactions, and regulation, *J Muscle Res Cell Motil.* 19: 325-341, **1998**.
72. Hashimoto T, Hirata M, Itoh T, Kanmura Y, Kuriyama H, *J Physiol*, London. 370: 605-618, **1986**.
73. Haystead CMM, Gailly P, Somlyo AP, Somlyo AV, Haystead TAF. Molecular cloning and functional expression of a recombinant 72.5 kDa fragment of the 110 kDa regulatory subunit of smooth muscle protein phosphatase 1M, *FEBS Lett.* 377: 123-127, **1995**.
74. Herrman-Frank A, Darlin E, Meissner G. *Pflugers Arch ges Physiol.* 418: 353-359, **1991**.
75. Himpins B, Kitazawa T, Somlyo AP. Agonist dependent modulation of the Ca<sup>2+</sup> sensitivity in rabbit pulmonary artery smooth muscle, *Pflugers Archiv.* 417: 21-28, **1990**.
76. Himpins B, Somlyo AP. Free-calcium and force transients during depolarization and pharmacomechanical coupling in guinea-pig smooth muscle, *J Physiol.* 495: 507-530, **1988**.
77. Hirschman CA, Emala CW. Actin reorganization in airway smooth muscle cells involves G<sub>q</sub> and G<sub>1-2</sub> activation of Rho, *Amer J Physiol.* 277: L653-L661, **1999**.
78. Hibberd MG, Trentham DR. *A Rev Biophysio biophysio Chem.* 15: 119-161, **1989**.
79. Ho AK, Hashimoto K, Chik CL. CGMP activates mitogen-activated protein kinase in rat pinealocytes, *J Neurochem.* 73: 598-604, **1999**.



80. Horiutu K, Somlyo AV, Goldman YE, Somlyo AP. *J Gen Physiol.* 94: 769-781, **1989**.
81. Husain S, Abdel-Latif AA. Endothelin-1 activated protein kinase and cytosolic phospholipase A<sub>2</sub> in cat iris sphincter smooth muscle cells, *Biochem J.* 342: 87-96, **1999**.
82. Husain S, Abdel-Latif AA. Role of protein kinase C<sub>α</sub> in endothelin-1 stimulation of cytosolic phospholipase A<sub>2</sub> and arachidonic acid release in cultured cat iris sphincter smooth muscle cells, *Biochim Biophys Acta.* 1392: 127-144, **1998**.
83. Huxley AF. *Prog Biophys biophys Chem.* 7: 255-318, **1957**.
84. Ichikawa K, Heirano K, Ito M, Tanaka J, Nakano T, Hartshorne DJ, Interactions and properties of smooth muscle myosin phosphatase, *Biochemistry.* 35(20): 6313-6320, **1996a**.
85. Ichikawa K, Ito M, Hartshorne DJ. Phosphorylation of the large subunit of myosin phosphatase and inhibition of phosphatase activity, *J Biol Chem.* 271: 4733-4740, **1996b**.
86. Iino M. Dynamic regulation of intracellular calcium signals through calcium release channels, *Mol Cell Biochem.* 190(1-2):185-190, **1989**.
87. Iizuka K, Yoshi A, Samizo K, Tsukagoshi H, Ishizuka T, Dobashi K, Nakazawa T, Mori M. A major role for the Rho-associated coiled coil forming protein kinase in G-protein-mediated Ca<sup>2+</sup>-sensitization through inhibition of myosin phosphatase in rabbit trachea, *Brit J Pharmacol.* 128: 925-933, **1999**.
88. Itoh H, Shimomura A, Okubo S, Ichikawa K, Ito M, Konishi T, Nakano T. Inhibition of myosin light chain phosphatase during Ca<sup>2+</sup>-independent vasoconstriction, *Am Physiol Soc.* C1319-C1324, **1993**.
89. Itoh T et al. *J Physiol*, London. 451: 307-328, **1992**.
90. Jaggar JH, Nelson MT. Differential regulation of Ca<sup>2+</sup> sparks and Ca<sup>2+</sup> waves by UTP in rat cerebral artery smooth muscle cells, *Am J Physiol Cell Physiol.* 278(2): C235-C256. **2000**.
91. Jensen PE, Gong MC, Somly AV, Somlyo AP. Separate upstream and convergent downstream pathways of G-protein and phorbol ester-mediated Ca<sup>2+</sup>-sensitization of myosin light chain phosphorylation in smooth muscle, *Biolcem J.* 318: 469-475, **1996**.
92. Johansson B, Somlyo AP. The Handbook of Physiology: The Cardiovascular System, Vol. II (ed. Bohr DF, Somlyo AP, Sparks HV), pgs. 301-324. Am Physiol Soc, Bethesda, **1980**.

93. Juhaszova M, Ambesi A, Lindenmayer GE, Block RJ, Blaustein MP. *Am J Physiol.* 266: C234-C242, **1993**.
94. Kamm KE, Stull JT. The function of myosin and myosin light chain kinase phosphorylation in smooth muscle, *Annu Rev Pharmacol Toxicol.* **25**: 593-620, **1985**.
95. Kaneko T, Amano M, Maeda A, Got H, Takahashi K, Ito M, Kaibuchi K. Identification of calponin as a novel substrate of Rho-kinase, *Biochem Biophys Res Commun.* **273**: 110-116, **2000**.
96. Karaki H, Sato K, Ozaki H, Murakami K. Effects of sodium nitroprusside on cytosolic calcium level in vascular smooth muscle, *Eur J Pharmacol.* **156**: 259-266, **1988**.
97. Kargacin GJ. Calcium signaling in restricted diffusion spaces, *Biophys J.* **67**(1): 262-272, **1994**.
98. Katoch SS, Su X, Moreland RS. Ca<sup>2+</sup>-and protein kinase C-dependent stimulation of mitogen-activated protein kinase in detergent-skinned vascular smooth muscle. *J Cell Physiol.* **179**: 208-217, **1999**.
99. Katoch SS, Ruegg JC, Pfitzer G. Differential effects of a K<sup>+</sup> channel agonist and Ca<sup>2+</sup> antagonists on myosin light chain phosphorylation in relaxation of endothelin-1-contracted tracheal smooth muscle, *Pflugers Arch.* **433**: 472-477, **1997**.
100. Katoh H, Aoki J, Yamaguchi Y, Kitano Y, Ichikawa A, Negishi M. Constitutively active G $\alpha_{12}$ , G $\alpha_{13}$  and G $\alpha_q$  induce Rho-dependent neurite retraction through different signaling pathways, *J Biol Chem.* **273**: 28700-28707, **1998**.
101. Kaufmann R, Spengler B, Lutzenkirchen F. Mass spectrometric sequencing of linear peptides by product-ion analysis in a reflectron time-of-flight mass spectrometer using matrix-assisted laser desorption ionization. *Rapid Commun Mass Spectrom.* **7**(10):902-10, **1993**.
102. Kerrick WG, Hoar PE. Inhibition of smooth muscle tension by cyclic AMP-dependent protein kinase, *Nature.* **202**: 253-255, **1981**.
103. Khromov A, Somlyo AV, Trentham DR, Zimmermann B, Somlyo AP. The role of MgADP in force maintenance by dephosphorylated cross-bridges in smooth muscle: a flash photolysis study, *Biophys J.* **69**: 2611-2622, **1995**.
104. Kim SO, Xu Y-J, Katz S, Pelech S. cGMP-dependent and -independent regulation of MAP kinases by sodium nitroprusside in isolated cardiomyocytes, *Biochim Biophys Acta.* **1496**: 277-284, **2000**.
105. Kimura K, Ito M, Amano M, Chihara K, Fukata Y, Nakafuku M, Yamamori B, Feng J, Nakano T, Okawa K, Iwamatsu A, Kaibuchi K. Regulation of myosin phosphatase by Rho and Rho-associated kinase (Rho-kinase), *Science.* **273**: 245-248, **1996**.

106. Kitazawa T, Khalequzzaman Md, Woodsmoe TP, Eto M. Evaluation of signaling pathways for C sensitization in smooth muscle, *Biophys J*. 82(1): 421a, **2002**.
107. Kitazawa T, Takizawa Nk, Ikebe M, Eto M. Reconstitution of protien kinase C-induced contractile C sensitization in Triton-X-100-demembranated rabbit arterial smooth muscle, *J Physiol (Lond)*. 520: 139-152, **1999**.
108. Klages B, Brandt U, Simon MI, Schultz G, Offermanns S. Activation of G<sub>12</sub>/G<sub>13</sub> results in shape change and Rho/Rho-kinase-mediated myosin light chain phophorylation in mouse platelets, *J Cellular Biol*. 14: 745-754, **1999**.
109. Klemke RL, Cai S, Giannini AL, Gallahger PJ, de Lanerolle P, Cheresch DA. Regulation of cell motility by mitogen-activated protein kinase, *J Cell Biol*. 137: 481-492, **1997**.
110. Kobayashi S, Kitazawa T, Somlyo AV, Somlyo AP. *J Biol Chem*. 264: 17997-18004, **1989**.
111. Kocher T, Allmaier G, Wilm M. Nanoelectrospray-based detection and sequencing of substoichiometric amounts of phosphopeptides in complex mixtures, *J Mass Spectrom*. 38: 131-137, **2003**.
112. Koshimizu T, Tanoue A, Hirasawa A, Yamauchi J, Tsujimoto G. Recent advances in alpha(1)-adrenoceptor pharmacology. *Pharmacol Ther*. 98(2):235-44, **2003**.
113. Kotlikoff MI, Herrera G, Nelson MT. Calcium permeant ion channels in smooth muscle, *Rev Physiol Biochem Pharmacol*. 134: 147-199, **1999**.
114. Kotlikoff MI, Kamm KE. Molecular mecanisms of  $\beta$ -adrenergic relaxation of airway smooth muscle, *Annu Rev Physiol*. 58: 115-141, **1996**.
115. Komalavilas P, Shah PK, Jo H, Lincoln TM. Activation of mitogen-activated protein kinase in contractile vascular smooth muscle cells, *J Biol Chem*. 274: 34301-34309, **1999**.
116. Koyama M, Ito M, Feng J, Seko T, Shiraki K, Takase k, Hartshorne DJ, Nakano T. Phosphorylation of CPI17, an inhibitory phosphoprotein of smooth muscle myosin phosphatase, by Rho-kinase, *FEBS Lett*. 475: 197-200, **2000**.
117. Kozasa T, Jiang X, Hart MJ, Sternweis PM, Singer WD, Gilman AG, Bollag G, Sternweis PC. P115 RhoGEF, a GTPase activating protein for G <sub>$\alpha$ 12</sub> and G <sub>$\alpha$ 13</sub>, *Science*. 280: 2109-2111, **1998**.
118. Kureishi Y, Ita M, Feng J, Okinaka T, Isaka N, Nakano T. Regulation of Ca<sup>2+</sup>-independent smooth muscle contraction by alternative saurosporine-sensitive kinase, *Euro J Pharmacol*. 376: 315-320, **1999**.

119. Kuriyama H (ed.) Proc Int Symp Smooth Muscle Jpn. *J Pharmacol.* 58, **1992**.
120. Lee YH, Kim I, Laporte R, Walsh MP, Morgan KG. Isozyme-specific inhibitors of protein kinase C translocation: effects on contractility of single permeabilized vascular muscle cells of the fernet. *J Physiol.* 517: 709-720, **1999**.
121. Lee MR, Li L, Kitazawa T. Cyclic GMP causes Ca<sup>2+</sup> desensitization in vascular smooth muscle by activating the myosin light chain phosphatase, *J Biol Chem.* 272(8) 5963-5968, **1997**.
122. Leung T, Manser E, Tan L, Lim L. A novel serine-threonine kinase binding the Ras-related RhoA GTPase which translocates the kinase to peripheral membranes, *J Biol Chem.* 270: 29051-29054, **1995**.
123. Li C, Fultz ME, Wright GL. PKC-alpha shows variable patterns of translocation in response to different stimulatory agents. *Acta Physiol Scand.* 174(3):237-46, **2002**.
124. Li C, Fultz ME, Geng W, Ohno S, Norton M, Wright GL. Concentration-dependent phorbol stimulation of PKCalpha localization at the nucleus or subplasmalemma in A7r5 cells. *Pflugers Arch.* 443(1):38-47, **2001a**.
125. Li C, Fultz ME, Parkash J, Rhoten WB, Wright GL. Ca<sup>2+</sup>-dependent actin remodeling in the contracting A7r5 cell. *J Muscle Res Cell Motil.* 22(6):521-34, **2001b**.
126. Lincoln TM, Cornwell TL, Komalazilas P, MacMilan-Crow LA, Boerth N. The nitric oxide-cGMP signaling system. In: Barany M, Ed. Biochemistry of Smooth Muscle Contraction. San Diego: Academic Press, pp 257-268, **1996**.
127. Liu M, Simon MI. Regulation by cAMP-dependent protein kinase of a G-porein-mediated phospholipase C, *Nature.* 382: 83-87, **1996**.
128. Loirand G, Cario-Toumaniantz C, Chardin P, Pacaud P. The Rho-related protein Rnd1 inhibits Ca<sup>2+</sup> sensitization of rat smooth muscle, *J Physiol.* 516: 825-834, **1999**.
129. Longenecker K, Read P, Derewenda U, Dauter Z, Liu X, Garrard S, Walker L, Somlyo AV, Nakamoto RK, Somlyo AP, Derewenda ZS. How RhoGDI binds Rho, *Acta Crystallographica.* D55: 1503-1515, **1999**.
130. MacDonald JA, Borman MA, Muranyi A, Somlyo AV, Hartshorne DH, Haystead TA. Identification of the endogenous smooth muscle myosin phosphatase-associated kinase, *Proc Natl Acad Sci USA.* 98: 2419-2424, **2001a**.
131. MacDonald JA, Eto M, Borman MA, Brautigam DL, Haystead TA. Dual Ser and Thr phosphorylation of CPI-17, an inhibitor of myosin phosphatase, MYPT-associated kinase, *FEBS Lett.* 493(2-2): 91-94, **2001b**.

132. Malmqvist U, Arner A, Uvelius B. Mechanics and Ca(2+)-sensitivity of human detrusor muscle bundles studied in vitro. *Acta Physiol Scand.* 143: 373-380, **1991**.
133. Marks AR et al. *Proc natn Acad Sci USA.* 86: 8683-8687, **1989**.
134. Martin K, Steinberg TH, Goodman T, Schulenberg B, Kilgore JA, Gee KR, Beechem JM, Patton WF. Strategies and solid-phase formats for the analysis of protein and Peptide phosphorylation employing a novel fluorescent phosphorylation sensor dye. *Comb Chem High Throughput Screen.* 6: 331-9, **2003**, PN50101.
135. Marsten SB, Redwood CS. *Biochem J.* 279: 1-16, **1991**.
136. Matsui T, Amano M, Yamamoto T, Chihara K, Nakafuku M, Ito M, Nakano T, Okawa K, Iwamatsu A, Kaibuchi K. Rho-associated kinase, a novel serine-threonine kinase, as a putative target for small GTP binding protein Rho, *EMBO J.* 15(9): 2208-2216, **1996**.
137. McDaniel NL, Chen XL, Singer HA, Murphy RA, Rembold CM. Nitrovasodilators relax arterial smooth muscle by decreasing  $[Ca^{2+}]$  and uncoupling stress from myosin phosphorylation, *Am J Physiol Cell Physiol.* **263**: C461-C467, **1992**.
138. McDonald TF, Pelzer S, Trautwein W, Pelzer D. *J Physiol Rev.* 74: 365-507, **1994**.
- 139.** Mega T, Nakamura N, Ikenaka T. Modifications of substituted seryl and threonyl residues in phosphopeptides and a polysialoglycoprotein by beta-elimination and nucleophile additions. *J Biochem (Tokyo).* 107(1):68-72, **1990**.
140. Mega T, Hamazume Y, Hong YM, Ikenaka T, Nong YM. Studies on the methods for the determination of phosphorylation sites in highly phosphorylated peptides or proteins: phosphorylation sites of hen egg white riboflavin binding protein, *J Biochem (Tokyo).* 100(5):1109-16, **1986**.
141. Miller-Hnce WC, Miller JR, Wells JN, Stull FT, Kamm KE. *J Biol Chem.* 263: 13979-13982, **1988**.
142. Minekus J, van Magstrigt R. Length dependence of the contractility of pig detrusor smooth muscle fibres. *Urol Res.* 29: 126-133, **2001**.
143. Miyazaki K, Yano T, Schmidt DJ, Tokui T, Shibata M, Liftshitz LM, Kimura S, Tuft RA, Ikebe M. Rho-dependent agonist-induced spatio-temporal change in myosin phosphorylation in smooth muscle cells, *J Biol Chem.* 277(1): 725-734, **2002**.
144. Morgan JP, Morgan KG. Alteration of cytoplasmic ionized calcium levels in smooth muscle by vasodilators in the ferret, *J Physiol (Lond).* 357: 539-551, **1984**.
145. Moriya M, Miyazaki E. Force-velocity characteristics of stomach muscle: a comparison between longitudinal and circular muscle strips. *Comp Biochem Physiol A.* 81(3): 531-

537, **1985**.

146. Murphy RA. What is special about smooth muscle? The significance of covalent crossbridge regulation, *FASEB J.* 8: 311-318, **1994**.
147. Murthy LS, Zhou H, Grider JR, Brautigan DL, Eto M, MaKLOUF gm. Differential signaling by muscarinic receptors in smooth muscle: m2-mediated inactivation of MLCK via Gi33, Cdc42/Rac1, and PAK1, and m3-mediated MLC 20 phosphorylation via Rho kinase/ MYPT1 and PKC/CPI-17 pathways, *Biochem J*, **2003**.
148. Nakahara T, Moriuchi H, Yunoki M, Sakamoto K, Ishii K. Y-27632 potentiates relaxant effects of 2-adrenoreceptor agonists in bovine tracheal smooth muscle, *Eur J Pharmacol.* 389: 103-106, **2000**.
149. Neal LB. THESIS: Methods development for the identification of unknown proteins, Marshall University, **2001**.
150. Neary JT. MAPk cascades cell growth and death, *News Physiol Sci.* 12: 286-293, **1997**.
151. Nelson Mt, Cheng H, Rubart M, Santana LF, Bonev AD, Knot HJ, Lederer WJ. Relaxation of arterial smooth muscle by calcium sparks, *Science.* 270(5326): 622-637, **1995**.
152. Neubauber G, Mann M. *Anal Chem.* 71: 235, **1999**.
153. Niuro N, Ikebe M. Zipper-interacting protein kinase induces Ca<sup>2+</sup>-free smooth muscle contraction via myosin light chain phosphorylation, *J Biol Chem.* 276(31): 29,567-29,574, **2001**.
154. Nixon G, Mignery GA, Sudhof TC, Somlyo AV. *J Musc Res Cell Motil.* 15: 682-700, **1994**.
155. Ohmichi M, Koike K, Kimura A, Masuhara K, Ikegami H, Ikebuchi Y, Kanzaki T, Touhara K, Sakaue M, Kobayash Y, Akabane M, Miyake A, Murata Y. Role of mitogen-activated protein kinase pathway in prostaglandin F<sub>2α</sub> -induced rat puerperal uterine contraction, *Endocrinology.* 138: 3103-3111, **1997**.
156. Packer NH, Ball MS, Devine PL, Patton WF. Detection of glycoproteins in gels and blots, The Protein Protocols Handbook, 2nd Ed., Walker JM, Ed. pp. 761-772, **2002**.
157. Pape PC, Konishi M, Baylor SM, Somlyo AP. *FEBS Lett.* 235: 57-62, **1988**.
158. Patel S, Joseph SK, Thomas AP. Molecular properties of inositol 1,4,5-triphosphate receptors, *Cell Calcium.* 25: 247-264, **1999**.

159. Pearce W, Williams J, Chang M, Gerhoffer W. ERK inhibition attenuates 5-HT-induced contractions in fetal and adult ovine carotid arteries, *Arch Physiol Biochem.* 111(1): 36-44, **2003**.
160. Pfitzer, G. Signal Transduction in Smooth Muscle. Invited Review: Regulation of myosin phosphorylation in smooth muscle, *J Appl Physiol.* 91: 497-503, **2001**.
161. Pfitzer G, Merkel L, Ruegg JC, Hofmann F. Cyclic GMP-dependent protein kinase relaxes skinned fibers from guinea pig taenia coli but not from chicken gizzard, *Pflugers Arch.* 407: 87-91, **1986**.
162. Pfitzer G, Hofmann F, DiSalvo J, Ruegg JC, *Pflugers Arch ges Physiol.* 401: 270-280, **1984**.
163. Porter VA, Bonev AD, Knot HJ, Heppner TJ, Stevenson AS, Klepisch T, Lederer WJ, Nelson MT. Frequency modulation of Ca<sup>2+</sup> sparks is involved in regulation of arterial diameter by cyclic nucleotides, *Am J Physiol.* 274(5 Pt 1): C1345-C1355, **1998**.
164. Posewitz MC, Tempst P. *Anal Chem.* 71: 2883, **1999**.
165. Prosser CL. *News Physiol Sci.* 7: 100-105, **1992**.
166. Raska CS, Parker CE, Dominski Z, Marzluff WF, Glish GL, Pope RM, Borchers CH. *Anal Chem.* 74: 3429, **2002**
167. Read, PW, Liu X, Longenecker K, DiPierro CG, Walker LA, Somlyo AV, Somlyo AP, Nakamoto RK. Human RhoA/RhoGDI complex expressed in yeast: GTP exchange in sufficient for translocation of RhoA to liposome, *Protein Science.* **2000**.
168. Rembold CM, Foster DB, Strauss JD, Wingard CJ, Van Eyck JE. cGMP-mediated phosphorylation of heat shock protein 20 may cause smooth muscle relaxation without myosin light chain dephosphorylation in swine carotid artery, *J Physiol (Lond).* 524: 865-878, **2000**.
169. Rembold CM, Murphy RA. *J Musc Res Cell Motil.* 14: 325-333, **1993**.
170. Sah VP, Seasholtz TM, Sagi SA, Brown JH. The role of Rho in G protein-coupled signal transduction, *Ann Rev Pharmacol Toxicol.* 40: 459-489, **2000**.
171. Sakurada S, Okamoto H, Takuwa N, Sugimoto N, Takuwa Y. Rho activation in excitatory agonist-stimulated vascular smooth muscle, *Am J Physiol Cell Physiol.* 28(21): C571-C578, **2001**.
172. Sanders LC, Matsumura F, Bokoch GM, de Lanerolle P. Inhibition of myosin light chain kinase by p21-activated kinase, *Science.* 283(5410): 2083-2085, **1999**.

173. Sauzeau V, Le Jeune H, Cario-Toumaniantz C, Smolenski A, Lohmann SM, Beroglio J, Chardin P, Pacaud P, Loirand G. Cyclic CMP-dependent protein kinase signaling pathway inhibits RhoA-induced  $Ca^{2+}$  sensitization of contraction in vascular smooth muscle, *J Biol Chem.* 275(28): 21,722-21,729, **2000**.
174. Seguchi H, Nishimura J, Toyofuku K, Kobayashi S, Kumazawa J, Kanaide H. The mechanism of relaxation induced by atrial natriuretic peptide in the porcine renal artery, *Br J Pharmacol.* 118: 343-351, **1996**.
175. Shimizu H, Ito M, Miyahara M, Ichikawa K, Okubo S, Koshih T, Naka M, Tanaka T, Hirano K, Harshorne DJ, Nakano T. Characterization of the myosin-binding subunit of smooth muscle myosin phosphatase, *J Biol Chem.* 269: 30407-304011, **1994**.
176. Shirazi A, Iizuka K, Fadden P, Mosse C, Somlyo AP, Somlyo AV, Haystead TAJ. Purification and characterization of the mammalian myosin light chain phosphatase holoenzyme: The differential effects of the holoenzyme and its subunits on smooth muscle, *J Biol Chem.* 269: 31598-31606, **1994**.
177. Siegman MJ, Butler TM, Mooers SU, Davies RE. *J Gen Physiol.* 76: 609-617, **1980**.
178. Sigma-Aldrich, Inc. *Product Information-ProteoPrep Universal Extraction Kit*; St Louis, **2003**.
179. Sobue K, Sellers JR. *J Biol Chem.* 266: 12115-12118, **1991**.
180. Somlyo AP, Somlyo AV. Signal transduction by G-proteins, rho-kinase, and protein phosphatase to smooth muscle and non-muscle myosin II, *J Physiol (Lond).* 522: 177-185, **2000**.
181. Somlyo AP. Kinases, myosin phosphatase and Rho proteins: curiouser and curiouser, *J Physiol.* 516, 630, **1999**.
182. Somlyo AP. Rhomantic interludes raise blood pressure, *Nature.* 389: 908-911, **1997**.
183. Somlyo AP, Somlyo AV. Signal transduction and regulation in smooth muscle, *Nature.* 372: 231-236, **1994**.
184. Somlyo AP. *J Musc Res Cell Motil.* 15: 557-663, **1993**.
185. Somlyo AV, Horiuti K, Trentham DR, Kitazawa T, Somlyo AP, *J Biol Chem.* 267: 22316-22322, **1992**.
186. Somlyo AP, Somlyo AV. *The Heart and Cardiovascular System*, 2<sup>nd</sup> edition (eds Fozzard HA, Haber E, Jennings RB, Katzand AM, Morgan HE). pgs 845-864. Raven, New York, **1991**.



187. Somlyo AP, Somlyo AV. Flash photolysis studies of excitation-contraction coupling, regulation, and contraction in smooth muscle, *Annu Rev Physiol.* 52: 857-887, **1990**.
188. Somlyo AP. *Adv Prot Phosphatases.* 5: 181-195, **1989**.
189. Somlyo AP, Somlyo AV. Cross-bridge kinetics, cooperativity, and negatively strained cross-bridges in vertebrate smooth muscle, A laser-flash photolysis study, *J Gen Physiol.* 91: 165-192, **1988**.
190. Somlyo AV, Somlyo AP. *J Pharma Exp Ther.* 159: 129-145, **1968**.
191. Somlyo AV, Somlyo AP. *J Gen Physiol.* 50: 168-169, **1967**.
192. Steen H, Mann M. A new derivatization strategy for the analysis of phosphopeptides by precursor ion scanning in positive ion mode, *J Am Soc Mass Spectrom.* (8):996-1003, **2002**.
193. Steinberg TH, Pretty On Top K, Berggren KN, Kemper C, Jones L, Diwu Z, Haugland RP, Patton WF. Rapid and simple single nanogram detection of glycoproteins in polyacrylamide gels on electroblots, *Proteomics* 1: 841, **2001**.
194. Stensballe A, Andersen S, Jensen ON. *Proteomics.* 1: 207, **2001**.
195. Stephens NL. Force-velocity constants in smooth muscle: afterloaded isotonic and quick-release methods. *Can J Physiol Pharmacol.* 63(1): 48-51, **1985**.
196. Suematsu E, Resnick M, Morgan KG. Change of Ca<sup>2+</sup> requirement for myosin phosphorylation by prostaglandin F<sub>2α</sub>, *Am J Physiol Cell Physiol.* 261: C253-C258, **1991**.
197. Sward K, Dreja K, Susnjar M, Hellstrand P, Hartshorne DJ, Walsh MP. Inhibition of Rho-associated kinase blocks agonist-induced Ca<sup>2+</sup> sensitization of myosin phosphorylation and force in guinea-pig ileum, *J Physiol (Lond).* 522: 33-49, **2000**.
198. Sweeny HL, Yang Z, Zhi G, Stull JT, Trybus KM. *Proc Natn Acad Sci USA.* 91: 1490-1494, **1994**.
199. Taggart MJ. Smooth muscle excitation-contraction coupling: a role for caveolae and caeolins? *News Physiol Sci.* 16: 61-65, **2001**.
200. Taggart MJ, Lee YH, Morgan KG. Cellular redistribution of RKCα, rhoA, and ROKα following smooth muscle agonist stimulation, *Exper Cell Res.* 251: 92-101, **1999**.
201. Takahashi E, Berk BC. MAP kinases and vascular smooth muscle function. *Acta Physiol Scand.* 164: 611-621, **1998**.
202. Takuwa Y, Kelley G, Takuwa N, Rasmussen H. Protein phosphorylation changes in bovine carotid artery smooth muscle during contraction and relaxation. *Mol Cell*

- Endocrinol.* 60(1):71-86, **1988**.
203. Tansey MG, Luby-Phelps K, Kamm KE, Stull JT.  $Ca^{2+}$  dependent phosphorylation of myosin light chain kinase decreases the  $Ca^{2+}$ -sensitivity of light chain phosphorylation within smooth muscle cells, *J Biol Chem.* 259: 9912-9920, **1994**.
204. Tansey MG, Word RA, Hidaka H, Singer HA, Schworer CM, Kamm KE, Stull JT. Phosphorylation of myosin light chain kinase by the multifunctional calmodulin-dependent protein kinase II in smooth muscle cells, *J Biol Chem.* 267(18): 12,511-12,516, **1992**.
205. Tansey MG, Hori M, Karachi K, Kamm KE, Stull JT. Okadaic acid uncouples myosin light chain phosphorylation and tension in smooth muscle cells. *J Biol Chem.* 269: 9912-9920, **1990**.
206. Trinkle-Mulcahy L, Ichikawa K, Hartshorne DJ, Siegman MJ, Butler TM. Thiophosphorylation of the 130-kDa subunit is associated with a decreased activity of myosin light chain phosphatase in alpha-toxin-permeabilized smooth muscle, *J Biol Chem.* 270: 18191-18194, **1995**.
207. Uehata M, Ishizaki T, Satoh H, Onon T, Kawahara T, Morishita T, Tamakawa H, Yamagami K, Inui J, Maekawa M, Narumiya S. Calcium sensitization of smooth muscle mediated by a Rho-associated protein kinase in hypertension, *Nature.* 389: 990-994, **1997**.
208. Uvelius B, Hellstrandt P. Effects of phasic and tonic activation on contraction dynamics in smooth muscle. *Acta Physiol Scand.* 109: 399-406, **1980**.
209. Uvelius B. Shortening velocity, active force and homogeneity of contraction during electrically evoked twitches in smooth muscle from rabbit urinary bladder. *Acta Physiol Scand.* 106: 481-486, **1979**.
210. Uvelius B. Influence of muscle length on the force-velocity relation of  $K^{+}$ -contractures in smooth muscle from rabbit urinary bladder. *Acta Physiol Scand.* 101(3): 270-277, **1977**.
211. Van Koevringe GA. Dynamics of smooth muscle. Thesis Erasmus University Rotterdam, **1997**.
212. Van Mastrigt R. Mechanical properties of (urinary bladder) smooth muscle, *J Muscle Res Cell Motil.* 23(1): 53-57, **2002**.
213. Van Riper DA, Weaver BA, Stull JT, Rembold CM. Myosin light chain kinase phosphorylation in swine carotid artery contraction and relaxation, *Am J Physiol Hear Circ Physiol.* 268: H2466-H2475, **1995**.

214. Velarde V, Ullan ME, Morinelli TA, Mayfield RK, Jaff AA. Mechanisms of MAPK activation by bradykinin in vascular smooth muscle cells, *Am J Physiol* 277 (*Cell Physiol* 46): C253-C261, **1999**.
215. Villa et al. *J Cell Biol.* 221: 1041-1051, **1993**
216. Vyas TB, Mooers SU, Narayan,SR, Witherell JC, Siegman MJ, Butler TM. Cooperative activation of myosin by light chain phosphorylation in permeabilized smooth muscle, *Am J Physiol.* 263: C210-C219, **1992**.
217. Walker LA, Gailly P, Jensen PE, Somlyo AV, Somlyo AP. The unimportance of being (protein kinase C) epsilon, *FASEB J.* 12: 813-821, **1998**.
218. Wang S, Wright G, Harrah J, Touchon R, McCumbee W, Geng W, Fultz ME, Abdul-Jalil MN, Wright GL. Short-term exposure to homocysteine depresses rat aortic contractility by an endothelium-dependent mechanism. *Can J Physiol Pharmacol.* 78(6):500-6, **2000**.
219. Wellmann GC, Santana LF, Bonev AD, Nelson MT. Role of phospholamban in the modulation of arterial Ca<sup>2+</sup> sparks and Ca<sup>2+</sup>-activated K<sup>+</sup> channels by cAMP, *Am J Physiol Cell Physiol.* 281(3): C1029-C1037, **2001**.
220. Geng WD, Boskovic G, Fultz ME, Li C, Niles RM, Ohno S, Wright GL. Regulation of expression and activity of four PKC isozymes in confluent and mechanically stimulated UMR-108 osteoblastic cells. *J Cell Physiol.* 189(2):216-28, **2001a**.
221. Geng W, Wright GL. Skeletal sensitivity to dietary calcium deficiency is increased in the female compared with the male rat. *Can J Physiol Pharmacol.* 79(5):379-85, **2001b**.
222. Winder SJ, Walsh MP. *Cell Signaling.* 5: 677-686, **1993**.
223. Wilm M, Neubauer G, Mann M. *Anal Chem.* 68: 527, **1996**.
224. Word RA, Tang DC, aKamm KE. Activation properties of myosin light chain kinase during contraction/relaxation cycles of tonic and phasic smooth muscles, *J Biol Chem.* 269: 21596-21602, **1994**.
225. Wright GL, Wang S, Fultz ME, Arif I, Matthews K, Chertow BS. Effect of vitamin A deficiency on cardiovascular function in the rat. *Can J Physiol Pharmacol.* 80(1):1-7, **2002**.
226. The World Health Report, **2002**.
227. Wu H, Bruley DF. Chelator, metal ion and buffer studies for protein C separation, *Comp Biochem Physiol A Mol Integr Physiol.* 132(1):213-220, **2002**.

228. Wu X, Haystead TA, Nakamoto RK, Somlyo AV, Somlyo AP. Acceleration of myosin lights chain dephosphorylation and relaxation of smooth muscles, *J Biol Chem.* 273: 11362-11369, **1998**.
229. Yoshii A, Iizuka K, Dobashi K, Horie T, Harada T, Nakazawa T, Mori M. Relaxation of contracted rabbit tracheal and human bronchial smooth muscle by Y-27632 through inhibition of  $Ca^{2+}$  sensitization, *Am J Respir Cell Mol Biol.* 20: 1190-1200, **1999**.
230. Yousufzai SY, Gao G, Abdel-Latif AA. Mitogen-activated protein kinase inhibitors suppress prostaglandin  $F_{2\alpha}$ -induced myosin light chain phosphorylation and contraction, but not phosphoinositide hydrolysis, in iris sphincter smooth muscle. *Eur J Pharmacol.* 407: 17-25, **2000**.
231. Yousuzai SYK, Abdel-Latif AA. Tyrosine kinase inhibitors suppress prostaglandin  $F_{2\alpha}$ -induced phosphoinositide hydrolysis,  $Ca^{2+}$  elevation and contraction in iris sphincter smooth muscle, *Eur J Pharmacol.* 360: 15-193, **1998**.
232. Zhou CJ, Akhtar RA, Abdel-Latif AA. *Biochem J.* 289: 401-409, **1993**.
233. ZhuGe R, Fogarty KE, Tuft RA, Liftshitz LM, Sayar K, Walsh JV Jr. Dynamics of signaling between  $Ca^{2+}$  sparks and  $Ca^{2+}$ -activated  $K^+$  channels studied with a novel image-based method for direct intracellular measurement of ryanodine receptors  $Ca^{2+}$  current. *J Gen Physiol.* 116(6): 845-864, **2000**.
234. ZhuGe R, Sims SM, Tuft RA, Fogarty KE, Walsh JV Jr.  $Ca^{2+}$  sparks activate  $K^+$  and  $Cl^-$  channels, resulting in spontaneous transient currents in guinea-pig tracheal myocytes, *J Physiol.* 513(Pt 3): 711-718, **1998**.
235. <http://nurseweek.com/news/99-8/42e.html>. 7/08/03.
236. <http://musom.marshall.edu/phys/WRIGHT.HTM>.
237. <http://www.appliedbiosystems.com/>
238. <http://www.matrixscience.com/>
239. <http://webpages.marshall.edu/~pricew/index.html>
240. <http://us.expasy.org/sprot/>